SALT MINERALS AND WATERS FROM SOILS IN KONYA AND KENYA

CENTRALE LANDBOUWCATALOGUS
0000 0086 7032

ISN= 136084-02

Promotor: dr. L. van der Plas, persoonlijk hoogleraar

NN 8201 845 C

Lideke Vergouwen

SALT MINERALS AND WATERS FROM SOILS IN KONYA AND KENYA

Proefschrift
ter verkrijging van de graad van
doctor in de landbouwwetenschappen,
op gezag van de rector magnificus,
dr. H.C. van der Plas,
hoogleraar in de organische scheikunde,
in het openbaar te verdedigen
op vrijdag 22 mei 1981
des namiddags te vier uur
in de aula
van de Landbouwhogeschool te Wageningen

BN:13 6084

BIBLIOTHEEK L.H.
0 6 MEI 1981
ONTV. TIJDSCHR. ADM.

NN08201,845

STELLINGEN

1. Ten onrechte concluderen Hallam en Eugster dat in de aardkorst de fugaciteit van NH_3 enkele ordes groter is dan de fugaciteit van stikstof; dit geldt alleen bij onwaarschijnlijk lage totaalspanningen van stikstof + ammoniak in metamorfe en magmatische vloeistoffen.

Hallam, M., and Eugster, H.P., 1976. Contrib. Mineral. Petrol., 57, p.227-244

2. Skarns in contact-halo's van intrusies zijn niet altijd metasomatisch veranderde carbonaatgesteentes. Skarnvorming kan eveneens plaatsvinden ten koste van hoornrotsen.

3. Zoutuitbloeiingen op Nederlandse bakstenen bestaan grotendeels uit de sulfaten eugsteriet, syngeniet en gips.

4. Kittrick bestrijdt de conclusie van Giltrap en Churchman dat bij de oplosexperimenten met de Colony montmorilloniet de oplossing na verloop van tijd in evenwicht is met een vaste fase, op grond van het onjuist citeren van hun resultaten.

Kittrick, J.A., 1978. Soil Sci. Soc. Am. J., 42, p.524-528.
Giltrap, D.J., and Churchman, G.J., 1977. Geochim. Cosmochim. Acta, 41, p.387-392.

5. Lateritisatie en ferralitisatie zijn geochemisch twee geheel verschillende processen die vaak verward worden.

Maignien, R., 1966. Review of research on laterites. UNESCO.
Jenny, H., 1980. The Soil Resource. Springer Verlag.

6. Het heeft slechts dan zin om fijnkorrelige mineraal associaties met een scanning electronen microscoop te bekijken, wanneer deze uitgerust is met een systeem waarmee de individuele mineralen chemisch onderzocht kunnen worden. Vergissingen als gemaakt door Driessen en Schoorl en Eswaran en Carrera kunnen zo vermeden worden.

Driessen, P.m., and Schoorl, R., 1973. J. Soil Sci., 24, p.436-442.
Eswaran, H., and Carrera, M., 1980. International symposium on salt affected soils, Karnal. p. 237-293.

7. De methode waarbij door vereenvoudiging van de chemische samenstelling Gibbs energieën van chemisch gecompliceerde natuurlijke mineralen worden geschat of vergeleken, leidt tot ongeoorloofde conclusies.

Huang, W.H., and Keller, W.D., 1972. Am. Min., 57, p.1152-1162.
Reesman, A.L., 1978. Clays Clay Min., p. 217-225.

8. Bij theoretische voorspellingen over de zoutsequentie die bij verdamping van een waterige oplossing zal neerslaan, moet terdege rekening gehouden worden met de vorming van metastabiele zoutmineralen.

Dit proefschrift.

9. Wanneer bij verdamping van een waterige oplossing magnesium neerslaat niet als een carbonaat maar als een silicaat, impliceert toename van de $Ca^{2+} + Mg^{2+}$-concentratie bij verdere verdamping niet noodzakelijkerwijs afname van de alkaliniteit.

Dit proefschrift.

10. Vrouwen in de zogenaamde "hogere functies" vormen nog steeds een te grote uitzondering.

11. Er lijkt een inverse relatie te bestaan tussen wetenschapsbeleid en wetenschapsbeoefening in Nederland.

zie ook Sperna Weiland, J., 1981. Universiteit en Hogeschool, p.311-322.

12. De laatste stelling van de mens is in moeder aarde.

Lideke Vergouwen
Salt minerals and waters from soils in Konya and Kenya.
Wageningen, 22 mei 1981.

CONTENTS

1. *Introduction* 1

2. *General information about salt-affected soils* 3
   2.1 Introduction 3
   2.2 Some concepts 4
   2.3 Soil classification 7
   2.4 Problems arising with irrigation and cropping in arid regions 9
   2.5 Reclamation of salt-affected soils 10
   2.6 Reclamation of sodic soils 10
   2.7 Prevention of resalinisation 12
   2.8 Cropping 13

3. *Salt-affected soils in the Great Konya Basin in Turkey* 14
   3.1 Physiography 14
   3.2 Geology 15
   3.3 Soil Types 17
   3.4 Correlation of occurrence of salts with soil type 20
   3.5 Sampling and analytical procedure 21
   3.6 Correlation between the fabric and mineralogy of the salt associations 21
   3.7 Methods of water analysis 23

4. *Salt-affected soils in Kenya* 27
   4.1 Physiography and climate 27
   4.2 Geology 27
   4.3 Amboseli Basin 30
   4.4 Lake Victoria 32
   4.5 East of Lake Turkana and the Chalbi Desert 33
   4.6 Sampling and analytical procedure 35
   4.7 Correlation between the fabric and mineralogy of the salt associations 35

5. Brine evolution in closed basins 91
5.1 Introduction 41
5.2 Chemical evolution 42
5.3 Acquisition of solutes 43
5.4 Evaporation 43
5.5 Application to irrigation of salt-affected soils 55

6. Application of the model of brine evolution to Konya and Kenya 56
6.1 Salts 56
6.2 Water composition in the system (Na+K)-Ca-Mg-Cl-SO_4-(HCO_3+CO_3) 57
6.3 Water composition in the system MgO-SiO_2-CaO 58
6.4 Concentration of individual ions versus chlorine concentration 61
6.5 Conclusions 66

7. Mineralogy 67
7.1 Identification of minerals 67
7.2 Crystallographic properties 67
7.3 Eugsterite, a new salt mineral 69
7.4 Konyaite, a new salt mineral 75
7.5 Two new occurrences and the Gibbs energy of burkeite 79
7.6 Scanning electron microscopy applied to saline soils from the Konya Basin in Turkey and from Kenya 84

8. Salt assemblages and evaporation experiments 91
8.1 Introduction 91
8.2 Evaporation experiments 91
8.3 Phase diagrams in the system Na-Ca-SO_4-CO_2-H_2O 97
8.4 Solubility calculations in the system Na-K-Mg-Ca-Cl-SO_4-H_2O 109

9. Stable isotopes in waters from the Konya- and Amboseli Basins; a reconnaissance study 119
9.1 Introduction 119
9.2 Stable isotopes of hydrogen and oxygen 119
9.3 Factors affecting the isotopic composition of natural waters 120
9.4 Analytical procedures and data 123
9.5 Discussions 125

10. Summary 129

11. Samenvatting 131

12. References 134

VOORWOORD

Het hangt van een veelheid van invloeden af welk zout uitkristalliseert en welke vorm het aanneemt. Zo werden ook vorm en inhoud van dit proefschrift extern beïnvloed. Van hen die tot de uitkristallisatie hiervan bijdroegen wil ik noemen:

Prof. Dr. L. van der Plas, mijn promotor, wiens deur in ruime zin altijd voor mij openstond,

Drs. E.L. Meijer, mijn kamergenoot, die zijn thermodynamisch inzicht belangeloos met mij deelde en altijd bereid was mee te denken,

Prof. Dr. Ir. P. Buringh, Prof. Dr. R.D. Schuiling, Dr. Ir. N. van Breemen, Drs. N.M. de Rooij, Drs. B.W. Zuurdeeg, met wie ik verhelderende discussies voerde,

Prof. H.P. Eugster, Dr. Y. Gat, Dr. C.E. Harvie, Mrs. Nancy Möller-Weare, Dr. Y. Tardy, Prof. J.H. Weare, who kindly supplied necessary information,

Ing. H.W. Boxem, Dr. Ir. P.M. Driessen, Dr. A. Mermut, Drs. L. Touber, Dr. Ir. W.G. Sombroek, Drs. R.F. van den Weg en Ir. W.G. Wielemaker, die mij begeleidden op mijn verzamelreizen in Kenya en Turkije,

Dr. R. Kreulen en J. Meesterburrie, die de isotoop-analyses uitvoerden,

Drs. J.M.A.R. Wevers, die de precessieopnames verzorgde,

Mevr. A.M.A. Baas, L.Th. Begheijn, J.D.J. van Doesburg, A.J. Kuijper en E.J. Velthorst vanwege hun analytische inspanningen,

Dr. M. Barton, die deskundig en snel mijn Engelse tekst zuiverde,

G. Buurman en O.D. Jeronimus voor het tekenwerk,

Z. van Druuten voor de fotografie,

Mevr. A. Bouter en Mevr. C.B. Beemster die het type-werk verzorgden

en Olaf en Elleke.

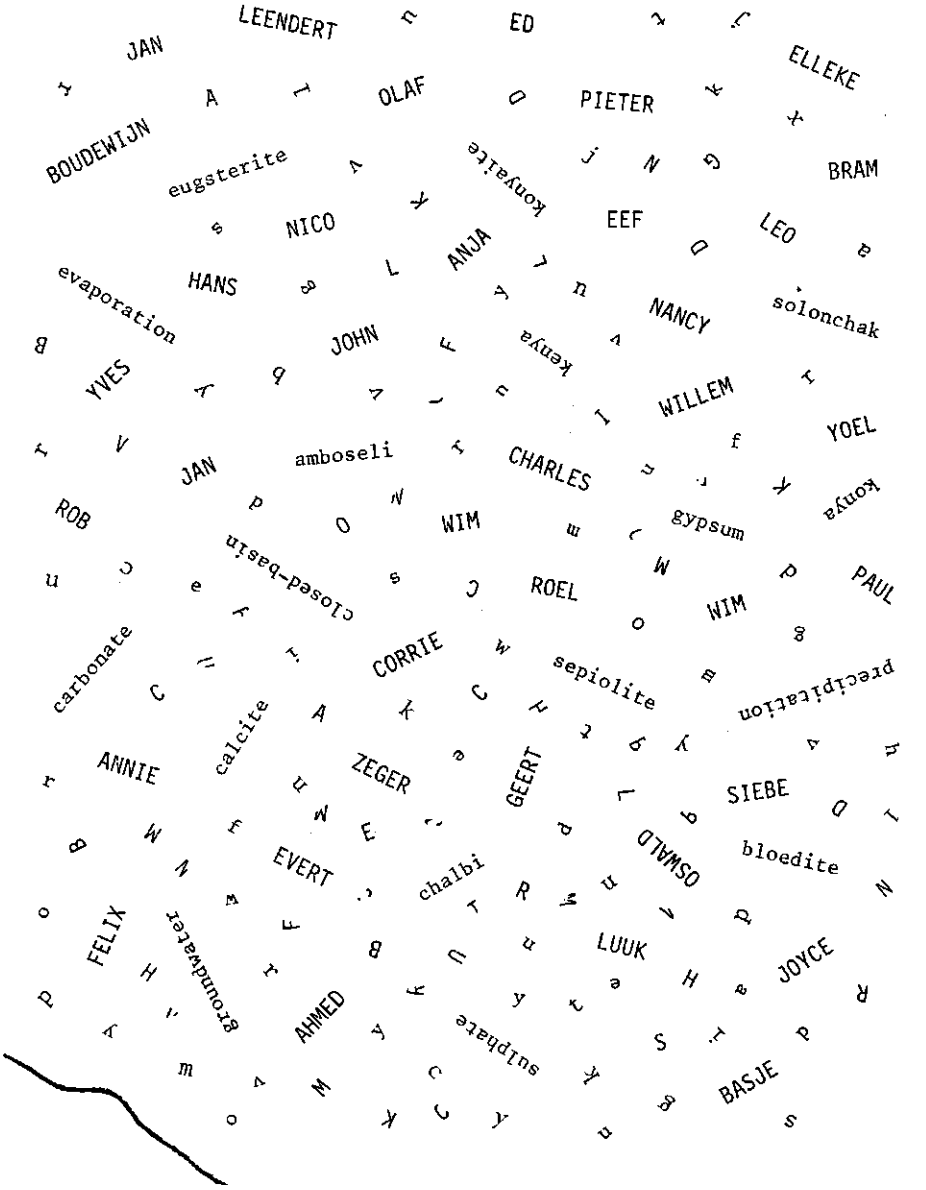

SALT MINERALS AND WATERS FROM SOILS IN KONYA AND KENYA

1. INTRODUCTION

Salt-affected soils are characterized by the presence of highly soluble salts, mainly chlorides, sulphates and carbonates, which influence plant growth. Such salts increase the osmotic pressure in the soil moisture and consequently plants cannot take up enough water. This results in physiological drought, a typical phenomenon for plants growing on saline land. How much plants suffer depends on the quantity of salts and on the type of salts present in the soil solution.

Salt-affected soils occur in many parts of the world, mainly in warm arid and semi-arid regions, where precipitation is too low to leach the salts. Soil salinisation is a normal process in those regions were groundwater is saline and at a shallow depth. Irrigated land in rather arid regions often becomes saline, because soluble salts accumulate in the soils, particularly if insufficient provisions are made for leaching and drainage.

The reclamation of salt-affected soils in order to make them suitable for agricultural production is a subject that has been studied for many years. There are several books and articles dealing with salt-affected soils and in particular with salts at the soil surface, in the soil profile and in the groundwater. In studies of salt-affected soils the soluble salts are usually dissolved and the total amount of salts and/or the concentration of various ions in the solution are determined. Only little attention is paid to the mineralogical composition of these salts.

Most salts in salt-affected soils originate by evaporation of groundwater or irrigation water. Slight differences in the composition of the dilute waters give rise to different types of salt assemblages and accordingly to different types of salt provinces. Conversely, the evolution of the groundwater composition during further evaporation is linked to the minerals which form from these waters.

This study treats the relation between the mineralogical composition of the salt assemblages and the groundwater composition.
Samples were taken from three different regions in Kenya during the autumn of 1977 and from the Great Konya Basin in Turkey during the summer of 1978. In addition to samples of salt efflorescences, samples of the groundwaters were taken at the same localities.

These two countries were chosen for two reasons:

1. The salts in Kenya consist mainly of sodium carbonates whereas those in the Great Konya Basin consist mainly of sodium-magnesium sulphates.
2. Regions in both countries have previously been studied by soil scientists from the Department of Soil Science of the Agricultural University in Wageningen. Special reference is made to the studies of de Meester (1970) and Driessen (1970). The latter also started the study of salt minerals in the Great Konya Basin in Turkey. Soil scientists working at a training project in Kisii, Kenya, from the same department, and Dutch soil scientists working at the Kenya Soil Survey in Nairobi provided the necessary pedological information for the sampling program in Kenya.

The crystallographic and morphological properties of many salt minerals are not well described. Some of these minerals, occurring in one or more of the sampling areas, were selected to investigate these properties in detail. Moreover, two new minerals have been discovered and described.

2. GENERAL INFORMATION ABOUT SALT-AFFECTED SOILS

2.1 INTRODUCTION

Salt-affected soils (Halomorphic soils) are indicated on the new Soil Map of the World (1 : 5.000.000) by FAO/Unesco (1974-1980) by two major soil units: Solonchaks and Solonetz.

Solonchaks are soils with a high salinity (EC_e^* > 15 ms/cm) within 125 cm of the soil surface.

The Solonchaks are subdivided into four mapping units:

Orthic Solonchaks, the most common Solonchaks,
Gleyic " , Solonchaks with ground water influence in the upper 50 cm,
Takyric " , Solonchaks in cracking clay soils,
Mollic " , Solonchaks with a dark-coloured surface layer, often high in organic matter.

Soils with lower salinity than Solonchaks are mapped as a "Saline phase" of other soil units.

Solonetz are sodium-rich soils with accumulation of clay in the subsurface soil. This clay has an ESP* > 15% and the structure is columnar or prismatic.

The Solonetz are subdivided into three mapping units:

Orthic Solonetz, the most common Solonetz,
Gleyic " , those with ground water influence in the upper 50 cm,
Mollic " , those with a dark-coloured surface layer, often high in organic matter.

Soils with a lower percentage of exchangeable sodium than Solonetz are mapped as "Sodic phase" of other soil units.

Reference is made to FAO/Unesco (1974) for precise definitions. It is evident from these short descriptions that salt-affected soils which are characterized by the presence of highly soluble chlorides and sulphates (Solonchaks) are distinguished from those with highly soluble carbonates and bicarbonates (Solonetz) in which the structure of the soils is deteriorated and consequently there is a poor medium for root growth.

* These abbreviations will be explained in Section 2.2.

Besides the real Solonchaks and Solonetz there are also soils having intermediate characteristics, which are often called Solonchak-Solonetz or saline-sodic soils (Richards, ed., 1954; the so-called "Handbook 60"). The term "sodic" is rather new; in older publications the name "alkali soils" was often used, but this name is now abandoned.

There is not much confusion about the characteristics, properties and agricultural evaluation of the various salt-affected soils. However, there is much confusion on how such soils should be classified or presented as mapping units on soil maps. In section 2.3 the classification of salt-affected soils will be dealt with in a general manner; specific and often complicated definitions and details will be avoided.

2.2 SOME CONCEPTS

In section 2.1 some abbreviations have been introduced. These terms, commonly used in soil science, and some other relevant facts, which are not familiar to non-pedologists, will be explained before dealing with the classification of salt-affected soils.

In some clay minerals cations are replaced by other cations with a lower valency, for example Si^{4+} by Al^{3+} or Al^{3+} by Mg^{2+}. This produces a negative charge at the mineral surfaces which enables them to adsorb positively charged ions from the soil solution.
Organic matter can also adsorb cations at the surface and exchange these ions with others.
The adsorbed ions distribute themselves over the negatively charged surface of the clay minerals according to a Boltzmann-type distribution (fig. 2.1a and 2.1b). This is the result of an equilibrium between the attractive forces of the surface and the tendency of the ions to diffuse away. The layer of liquid which extends from the mineral surface to the point where the concentration of the ions has dropped to the concentration of the soil solution is called the diffuse double layer (DDL).
The thickness of the diffuse double layer is dependent on the charge of the adsorbed ions; divalent ions are attracted more strongly to the surface and their DDL is thinner than in the case of monovalent ions. The thickness of the DDL is also dependent on the concentration of the soil solution; the thickness decreases when the concentration of the ions in the soil solution increases.

When water is introduced into a dry soil, the ions exert a swelling pressure,

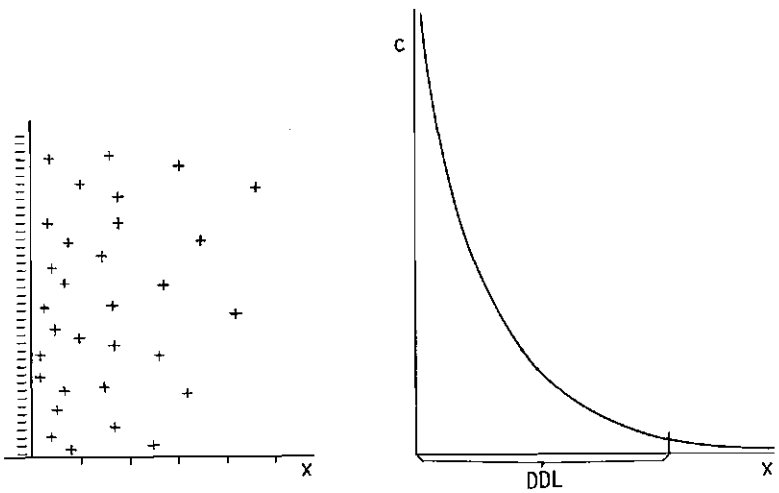

Fig. 2.1a and 2.1b Distribution of cations against the surface of a clay mineral: c = concentration; x = distance from the surface; DDL = diffuse double layer. (modified after Bolt & Bruggenwert, 1976)

the clay particles are driven away from each other, the soil swells and the permeability decreases. This swelling is most pronounced when much sodium, a monovalent ion, is adsorbed and when little salt is dissolved in the water, as is the case with rain water, because under such conditions the DDL is at its maximum. When abundant water is available, the soil peptises, the water and the clay particles form a kind of concentrated suspension and there are no aggregates any more and the soil structure disappears completely.
The physical properties of a soil are thus dependent upon the adsorption of sodium on the adsorbing complex and upon the concentration of the solutes in the soil solution. The dependence on these two is presented in fig. 2.2.

The amount of cations which a soil can adsorb by cation exchange is called the cation-exchange-capacity or *CEC*, expressed as mmol $\frac{1}{z}M^{z+}$. kg^{-1} of soil in which M denotes the cation and z is its charge. These units conform to SI, the Système International d'Unités (Brinkman, 1979). Before the introduction of SI, the CEC of a soil was expressed as milliequivalent . kg^{-1} of soil. The milliequivalent is not recognized in SI.

The exchangeable sodium percentage or *ESP* is the percentage of the exchange-

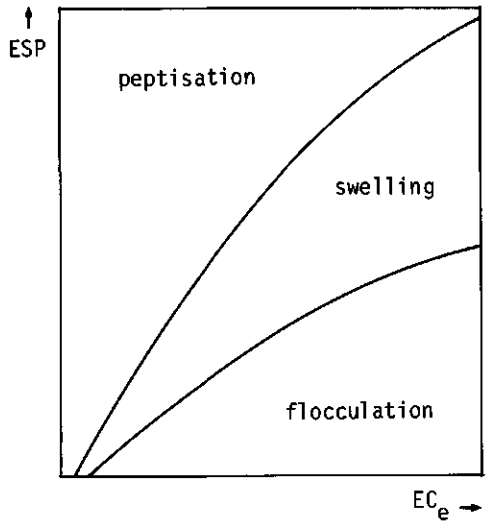

Fig. 2.2 Dependence of the soil structure on the electroconductivity (Ec) of the soil solution and the exchangeable sodium percentage (ESP) in the soil. For explanation of Ec and ESP, see text. (after Bolt & Bruggenwert, 1976)

able cations on the adsorption complex which consist of sodium.

$$ESP = \frac{\text{exchangeable sodium mmol } Na^+ \text{ . } kg^{-1} \text{ of soil}}{CEC \qquad \text{mmol } \frac{1}{z}M^{z+} \text{ . } kg^{-1} \text{ of soil}} \times 100$$

The sodium adsorption ratio or *SAR* is another term which is commonly used. This ratio expresses the relative activity of sodium in soil- and irrigation waters and is expressed as

$$SAR = \frac{Na}{\sqrt{(Ca^{2+} + Mg^{2+})/2}}$$

with all concentrations expressed as mol $\frac{1}{z}M^{z+}$. m^{-3}

A *saturated soil paste* is a soil sample to which so much water has been added that all of the voids are filled with water. The paste starts to glisten and is able to flow. The moisture extracted from this paste is called the saturation extract.

The electrical conductivity or *Ec* is the reciprocal of electrical resistivity expressed as millisiemens per cm (ms/cm). Before introduction of the SI system, the Ec was expressed as mmho/cm.

2.3 SOIL CLASSIFICATION

All soil classification systems have hierarchies of groups of soils (taxa). This means that there are different levels of classification. At the highest levels soils are classified according to certain characteristics which are considered to be more important than other characteristics which are used to distinguish soils at the lower levels. In some soil classification systems salt-affected soils are separated from other soils on the highest levels of classification. In other systems soils are first classified according to other criteria and at lower levels of classification the presence of soluble salts is indicated. The last procedure is, for example, followed in the new American system of soil classification "Soil Taxonomy" (Soil Survey Staff, 1975). Here the real salt-affected soils belong to the soil order of the Aridisols. There are two sub-orders viz. the *Argids* (soils with clay accumulation in the subsurface horizon) and the *Orthids* (soils without such a clay accumulation). At the third level of classification there is a great group named *"Natrargids"*, which are Argids with a high sodium percentage at the adsorption complex, and are indicated as the Solonetz on the Soil Map of the World (FAO/Unesco, 1974-1980). At this third level of classification (great groups) there are the *"Salorthids"* in the sub-order of Orthids, which are the Solonchaks on the Soil Map of the World. In the old American system of soil classification (1938) the names Solonchak soils and Solonetz soils were used.

In the French system of soil classification (CPSS, 1967) the salt-affected soils are separated from all other soils on the highest level of classification. There is a "Classe des sols sodiques" with a "Sous-classe des sols sodiques à structure non dégradé" to which belong the "Groupe des sols salins" (Solonchak). To the other "Sous-classe des sols sodiques à structure dégradé" belongs a "Groupe des sols salins à alcalins" (Solonchak-Solonetz) and a "Groupe des sols sodiques à horizon B" (Solonetz). In the provisional new French system (Fauck et al, 1979) there are at the highest level "Les Selsols". One of the great subclasses is called "Halisols" or "Selsols haliques" and this is subdivided according to the dominant salts present in the soil, for example "halisols à chlorure de sodium". Another subclass of the "Halisols" refers to the "halisols carboxiques" or "carboxihalisols", the former Solonetz.

In the Russian classification of soils, Solonchaks and Solonetz are distinguished at a high level of classification. The origin of both names is Russian.

The Solonchaks can be subdivided into *external Solonchaks* with soluble salts throughout the whole soil, and *internal Solonchaks* with soluble salts in the subsoil or substratum. The Solonchaks can be subdivided according to the composition of the salts. The following types exist: nitrate-, nitrate-chloride-, chloride-, sulphate-chloride-, chloride-sulphate-, sulphate-, sulphate-soda-, soda-, borate-solonchaks.
External Solonchaks can also be subdivided according to their morphological features. The following types of external Solonchaks may occur:

1. Flooded Solonchaks
These soils are periodically under water. Evaporation of the surface water produces a coherent white crust, sometimes of several centimeters thickness. This crust seals the subsurface thereby preventing further evaporation. Therefore, the soil under the crust is rather wet.
2. Puffed Solonchaks (puffy or fluffy Solonchaks)
The upper part of the soil is very loose and puffy because of the presence of sodium sulphate needles which push the soil particles apart. The uppermost layer is sometimes a little bit crusty (sodium chloride) which holds the soil together and counteracts evaporation. This type of soil forms by evaporation of groundwater.
3. Sabbakh soils (or wet mineral soils)
These soils contain magnesium and calcium chlorides which are extremely hygroscopic. They attract moisture from the air and are, therefore, darker in colour than the surroundings, especially in the morning (Sabbakh is Arabic for morning).

There are many other ways in which salt-affected soils have been subdivided, although most of these classifications are not official systems of soil classification. Sometimes a subdivision is made according to the origin of the salt. The following types exist:

1. Closed basin saline soils
Weathering products from the hinterland are transported by surface and subsurface waters into the basin, they accumulate and cannot be removed from the basin. Evaporation of the water causes salts to be deposited in and on top of the soil profile. These soils will be treated in detail in chapter 5.
2. Marine saline soils
These soils occur along coasts either by flooding, seepage of seawater or by seaspray.

3. Allochthonous airblown saline soils
Salts from other localities are transported by the wind and form new saline soils at the places of deposition.
4. Anthropogenic saline soils
Saline soils caused by the influence of man by means of irrigation and flooding without concomittant drainage to remove the dissolved salt. The irrigation water evaporates and salts are formed.

This short introduction indicates that there are many criteria by which salt-affected soils may be classified. It depends on the purpose of investigation which classification system will be chosen. The classification from the point of view of soil systematics is quite different from one that is set up to characterize the productive capacity for agricultural purposes. For the latter it is necessary not only to know the EC_e and ESP values, but also which salts are present in the soil, the soil solution and in the ground water. A simple EC measurement alone gives only a very rough idea of the total amount of salts because divalent ions have a different contribution to the electroconductivity than monovalent ions. Moreover the EC measurements are carried out on a saturation extract and the water content of different soils under field conditions is extremely variable. Therefore, the osmotic pressure of the soil solution, which this EC measurement is meant to indicate, may be incorrect.

In this study the terms *salt-affected soils* and *Solonchaks* will be used.

2.4 PROBLEMS ARISING WITH IRRIGATION AND CROPPING IN ARID REGIONS

In arid regions irrigation is applied for two different purposes:
1. water supply for plants
2. improvement of chemical and physical properties of the soil.

Before soils which show a poor natural vegetation are used for agriculture, it must be ascertained whether they are chemically and physically suitable for growing crops.
Salts must be removed from soils which are too saline, and if too much sodium is adsorbed on the adsorption complex in the soil, the sodium must be exchanged with other cations. In the following sections the reclamation of such soils will be dealt with.

2.5 RECLAMATION OF SALT AFFECTED SOILS

Irrigation is the method whereby water is supplied for crop growth in arid regions. If the soils are salt-affected, the salts must first be removed.

Usually, salts are removed by leaching; so much water is added to the soil that all salts are dissolved and transported downwards in the profile.

The dependence of the solubilities of most naturally occurring binary salts on temperature is shown in fig. 2.3 and fig. 2.4. The solubilities are expressed in g/kg water and in mole/kg water respectively.
The gypsum and anhydrite data are the mean curves of the ranges given by Hardie (1967). The other solubility data are from Linke (1965). Sodium salts are present in most salt efflorescences, at least in the case of saline soils which originated by evaporation of ground water. When the sodium salts are dissolved in the irrigation water, care must be taken that the SAR value of the irrigation water remains low in order to prevent the soil from becoming sodic.
Leaching in summer has the advantage that the solubility of most salts increases with temperature (fig. 2.3 and fig. 2.4), but it has the disadvantage that evaporation is high.
If there is a hard layer of calcite or gypsum present in the soil, which is impermeable and impenetrable to roots, this layer must be broken mechanically, for example by subsoiling. Such a natural gypsum supply is very favourable when the soil is sodic as well (see section 2.6).

2.6 RECLAMATION OF SODIC SOILS

If too much sodium is adsorbed at the adsorption complex, which makes the soil unsuitable for growing crops, the first irrigation water is used for improvement of the physical properties of the soil. The sodium must be replaced by double-charged cations such as calcium and magnesium because sodium causes the soil to swell and to become impermeable when it becomes wet and further irrigation is useless.
The conductivity of the first irrigation water must be high, because the dispersion of the clay particles depends not only on the ESP of the soil, but also on the salt content of the water (see fig. 2.2). Usually gypsum ($CaSO_4.2H_2O$) is added to the irrigation water. The electroconductivity increases and calcium ions become available to replace the sodium ions.

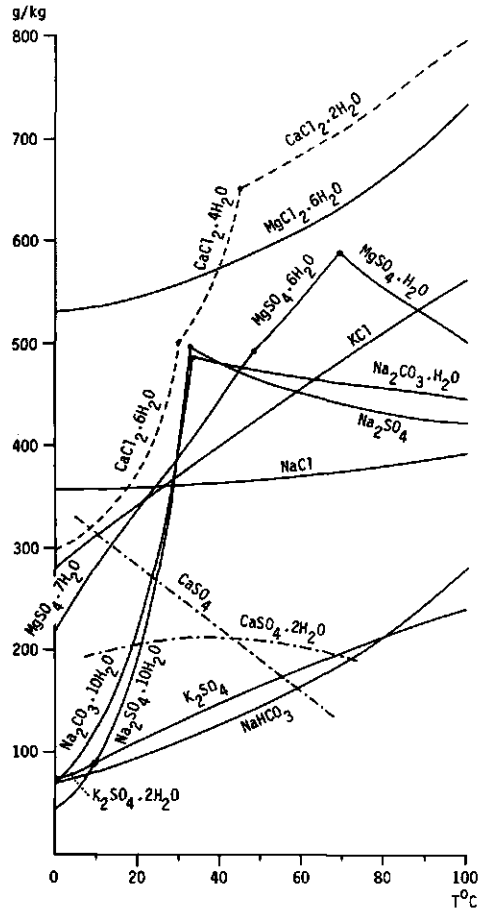

Fig. 2.3 Dependence of the solubility of some binary salts with temperature expressed in g anhydrous salt/kg H_2O.

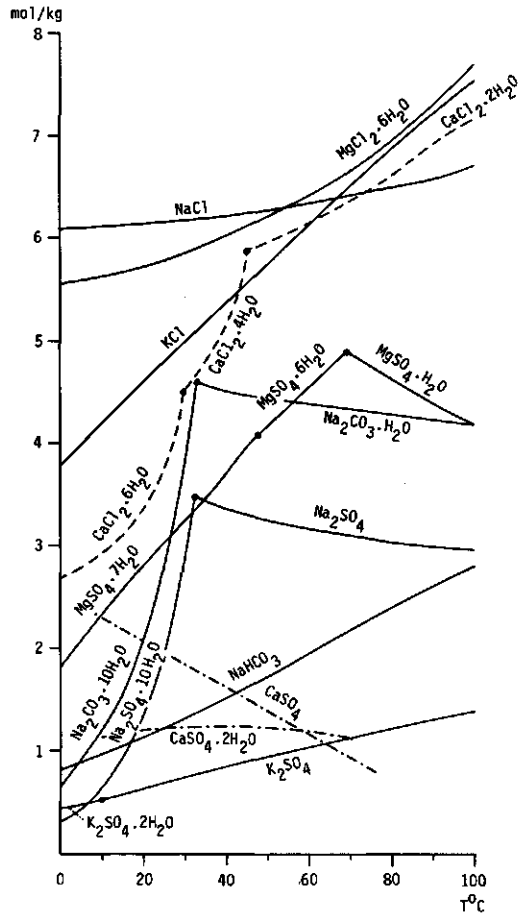

Fig. 2.4 Dependence of the solubility of some binary salts with temperature expressed in mole anhydrous salt/kg H_2O.

For $CaCl_2$ (dashed line) the concentrations must be multiplied by two. For $CaSO_4$ (dashed-dotted line) the concentrations must be divided by hundred.

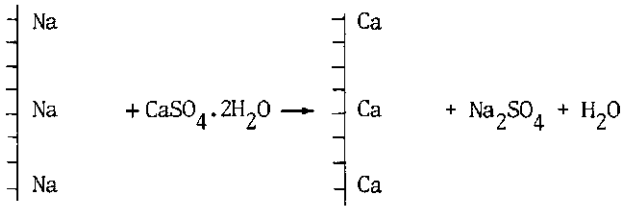

If the clay content of the soil is very high and much sodium is adsorbed at this clay, the maximum electroconductivity reached with the addition of gypsum may not be high enough to avoid peptisation of the clay particles. This is because gypsum has a low solubility (2.1 g/kg water at 25° C). In such cases a more soluble salt such as calcium chloride, which has a solubility of 828 g/kg water at 25° C, is added. However, this salt is much more expensive than gypsum. Sometimes sodium salts are added in addition to gypsum in order to increase the electroconductivity of the irrigation water. In this particular case the process of replacing sodium by calcium is obviously slower.
Sodium must be removed from the adsorption complex, especially in regions where the composition of the irrigation water cannot be kept under control, such as in regions with intermittent rainfall. Rainwater contains few dissolved salts and a rainshower causes the clay particles to disperse immediately, if the ESP is too high.

2.7 PREVENTION OF RESALINISATION

In arid regions reclamation and irrigation of soils is useless without drainage. Irrigation causes the water level to rise and both capillary rise and evaporation will cause the harmful constituents to reach the root zone and the surface again.
If natural drainage is absent, an artificial drainage system must be built to keep the water level at a critical depth. Evaporation must be reduced as much as possible. This can be achieved by a dense vegetation cover, e.g. lucerne in times of fallow or after harvesting. The plants provide shade, the roots increase the permeability and they add organic matter to the soil. This organic matter increases the dissolution of calcium-carbonate because of the released carbonic acid and in addition nitrogen is added to the soil.

In general, enough water must be added to the soil to prevent the upward movement of the salts. This is more water than is required to balance the consumption by the crops plus the water which evaporates.

2.8 CROPPING

Once the soil has been reclaimed, crops can be grown. There is an intimate relation between the soil condition, the quality of the irrigation water which is available, and the type of crops which can be grown. If the irrigation water is rather mineralised, the soil cannot be reclaimed completely and only salt tolerant crops can be grown. On the other hand, the choice of crops determines the degree to which the soil must be reclaimed.

Saline solutions are harmful to plants because of the osmotic pressure the solution exerts on the plant, which suppresses the absorption of water by the plant, and because of the toxic effects of the individual ions present in the solutions. These two effects will act simultaneously.

The concentration of the constituents in the soil solution will increase by evaporation. This leads to an increase of the osmotic pressure, but also the soil moisture tension increases. Both limit the availability of water to the plants.

In arid regions, many factors, which are sometimes difficult to consider simultaneously, must be accounted before a choice can be made about the type of crop to grow under those specific circumstances and about the degree of soil reclamation which is required.

3. SALT-AFFECTED SOILS IN THE GREAT KONYA BASIN IN TURKEY

3.1 PHYSIOGRAPHY

The Great Konya Basin is situated about 300 km south of Ankara on the Central Anatolian Plateau on which several basins of varying size occur. The inset in fig. 3.2 shows the location of the Konya Basin in Turkey.
The altitude is about 1000 m above sea level. The highest peak in the Basin is the Karadağ, a volcanic and limestone massif, 2390 m high. The area of the Basin is about 10,000 km^2. There are some perennial lakes such as Hotamiş Göl and Akgöl. The Basin has no natural hydrographic outlet.

The climate in the Konya Basin is semi-arid with cold, moist winters and hot, dry summers. Temperatures of -25^{o}C are common in winter whereas in the summer temperatures reach 35^{o}C. The average temperature in winter is about 0^{o}C and in summer about 20^{o}C. There is a frost-free period of only 165 days. Precipitation is restricted to autumn, winter and spring. In winter precipitation is in the form of snow; for at least three months per annum the basin is covered with snow. The summers are normally dry. The average precipitation is about 300 mm/year although it can vary between 250 mm and 350 mm depending upon geographic location. Evaporation exceeds precipitation; the average evaporation is about 930 mm/year.

There is much evidence that the basin was once a lake. Abandoned shore lines can be found at the rims of the basin and sand barriers run parallel to the former shoreline. Furthermore there are deposits of limestone containing freshwater fauna. Terra rossa layers, which occur 100 - 200 m below the soil surface indicate that this lake must have periodically dried up.
There is archeological evidence that the basin has been dry from at least 6500 B.C. because from that time the basin has been inhabited (Mellaart, 1964). At about that time the climate must have changed; in the Pleistocene the temperature was a little lower so that precipitation exceeded evaporation whereas evaporation now exceeds precipitation and the basin is dry most of the time.

3.2 GEOLOGY

The Basin originated when, during the Tertiary upfolding of the Anatolian belt, the inner Anatolian dome collapsed and subsidence took place. Throughout most of the Tertiary and the Pleistocene the large depressions so formed were filled with water, forming inland seas.

The Basin is bordered by two alpine orogens. The Taurus orogen forms the border in the south and west, whereas the Anatolides border the Basin to the north and east. These two mountain chains consist of Paleozoic sediments and upper Miocene limestones. Ultrabasic rocks occur on a large scale in the Taurus mountains.

From the Eocene-Oligocene onwards clastic material (clay, marl, sand, gravel and conglomerate) was deposited in the Basin. During the Mio-Pliocene non-clastic freshwater limestone was deposited and in many places this forms intercalations between marl and clay. In some places rather thick freshwater limestone beds can be found. The formation of limestone terminated abruptly and the upper parts of the sediments are formed of clastic material.

The Konya basin shows many features of volcanic origin. The volcanic activity started in the Upper-Miocene when the Central Anatolian Plateau was still rising and the basins originated, which became filled with sediments. Volcanic activity reached a maximum in Pliocene time. During the Quaternary, volcanic activity started again. The volcanic products of these two periods differ as follows (Jung & Keller, 1972):

1. The main part of the volcanic material from the *Upper Miocene* period consists of intermediate to basic volcanics such as andesites, latites, and andesitic basalts. These volcanics belong to the so-called andesitic belt which ranges from the south of Italy to Pakistan. Examples of this type of volcanism are the Erenler Dağ-Alaça Dağ-complex west of the town of Konya, the Kara Dağ in the centre of the Basin, the Karaça Dağ NE of the village of Karapinar and the Hasan Dağ-Melendiz Dağ-massif near the town of Niğde NE of the Basin. Some acid lavas such as dacites and rhyolites also occur.
2. The *Quaternary* volcanic activity produced on the one hand extremely acid obsidians and vitrophyres and on the other hand isolated cinder cones, made up of basaltic scoriae, and maars. The cinder cones form a chain from the Kara Dağ Massif towards the town of Bor in the NE of the Basin which suggests a correlation between this type of volcanism and young fault tectonics.

Nowadays volcanic activity is manifest by saline springs near Akhüyük and the ancient city of Tiana (localities T16 and T25 respectively, see fig. 3.2).

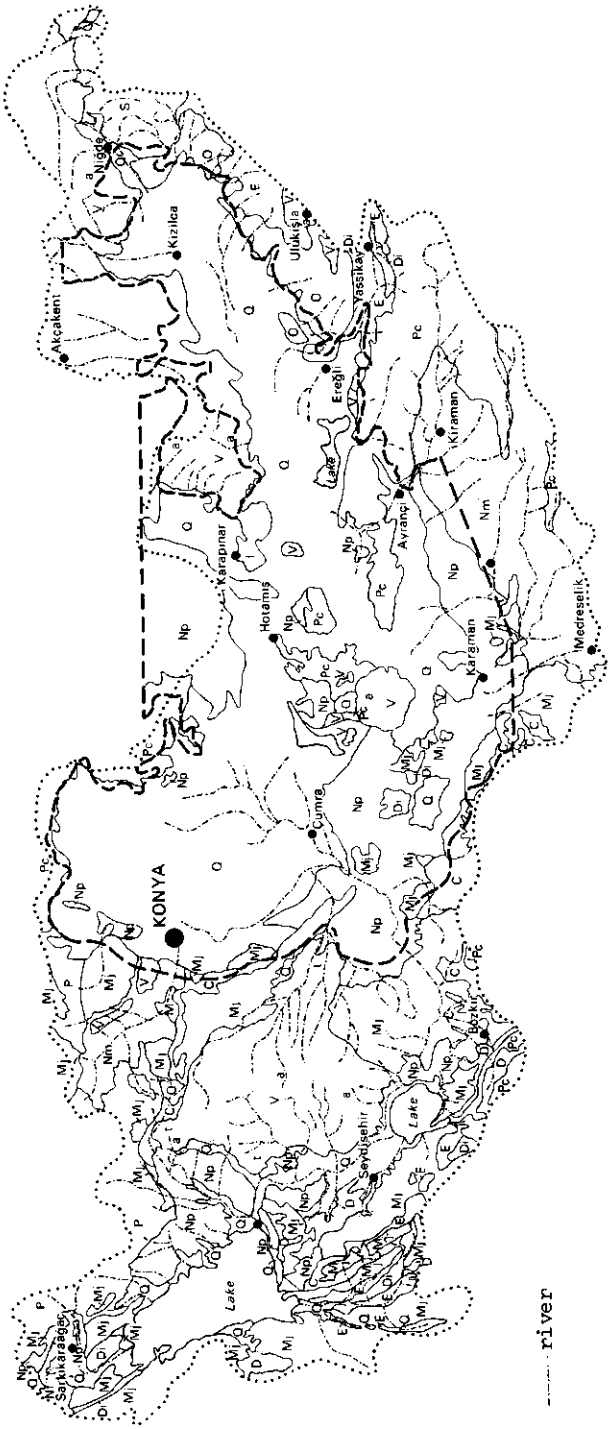

Fig. 3.1 Geology of the Basin's catchment area. (from de Meester, 1970)

Legend to fig. 3.1

Q Quarternary (mainly alluvial and lacustrine calcareous clays)
Np Neogene (mainly Pliocene horizontally stratified freshwater limestone)
Nm Neogene (mainly Miocene marine limestone)
O Oligocene (mainly gypsum or soluble salts)
E Eocene (mainly calcareous Flysch deposits)
Mj Mesozoic (mainly Jurassic and Triassic limestone)
C Cretaceous (mainly marls with Serpentine and radiolaries)
P Palaeozoic (mainly marmor)
PC Permocarboniferic (mainly limestone and marmor)
D Devonic (mainly stratified limestone)
S Chrystalline Schist
DI Diorites
V Volcanic deposits
a mainly Andesit and Dacit
b mainly Basalt
t mainly Tuff
ll mainly Quarternary lava

The springs near Tiana are still visited by patients suffering from internal diseases.
Fig. 3.1 shows the geology of the Great Konya Basin's catchment area.

3.3 SOIL TYPES

Fig. 3.2 presents a simplified soil map of the Konya Basin (de Meester, 1971). For a detailed map reference is made to "Soil map of the Great Konya Basin" (de Meester, 1971). Fig. 3.3 shows the cross sections. The soil associations on the map of fig. 3.2 were defined by their physiographic features. The following associations are distinguished on the map (de Meester, 1970):

The Uplands (U). These represent the surrounding mountains which consist of limestone and volcanics and the volcanoes in the basin itself.

The Colluvial Slopes (C). These form steep taluses at the base of the uplands and consist of rock debris from the mountains.

The Bajadas (B). These are gently sloping piedmont plains consisting of fine grained material from the uplands.

The Terraces (T). These are remnants of Neogene terraces; the higher terraces are cut by erosion gullies, the lower terraces are flat.

The Alluvial Plains (A). These consist of sediments transported by the rivers into the basin. They range from coarse sand to heavy clay.

The Lacustrine Plains (L). These are very flat marl soils which cover the floor of the Ancient Lake in the centre of the basin. They include the old sandy beach ridges.

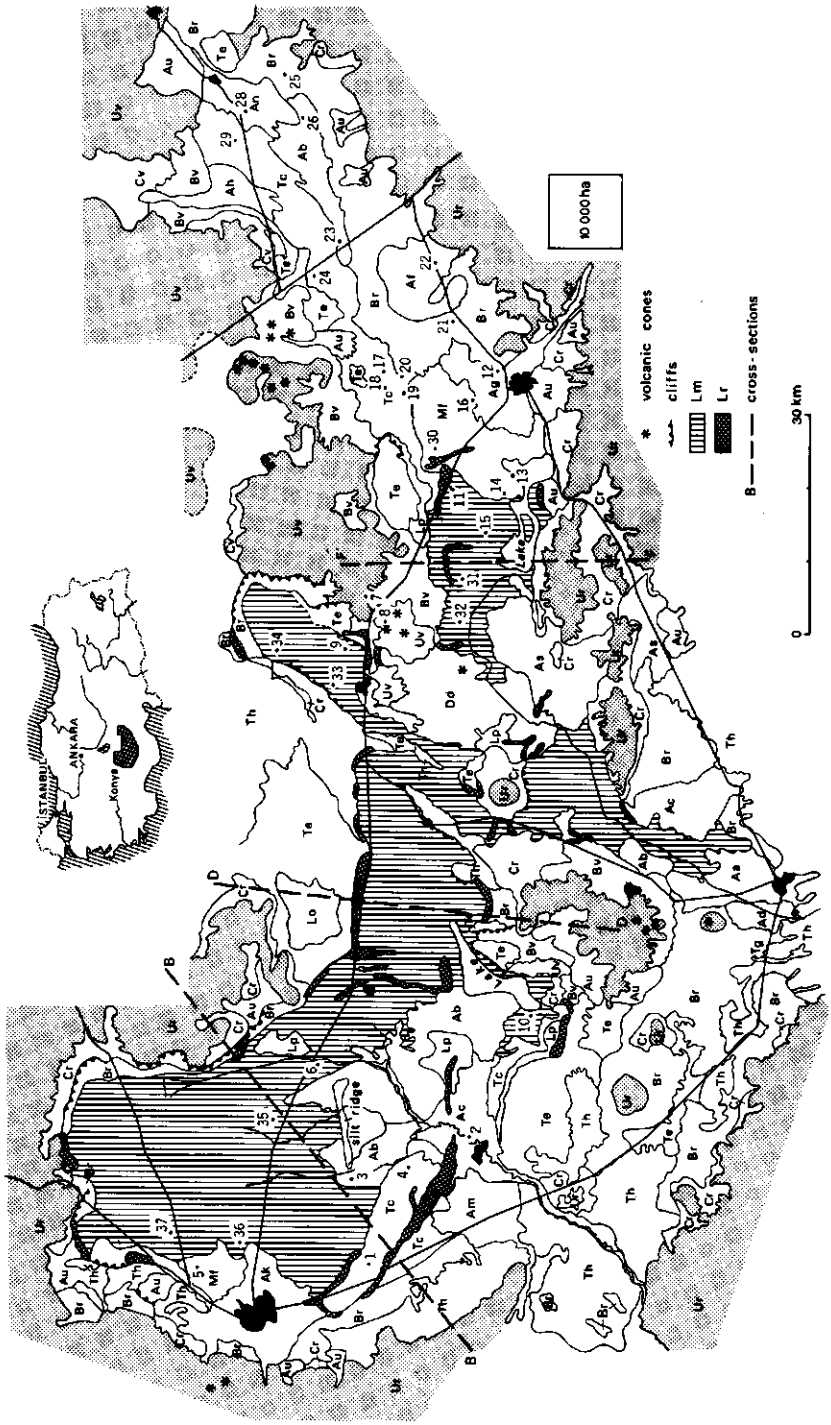

Fig. 3.2 Soil association map of the Great Konya Basin in Turkey (after de Meester, 1970) and the localities of the sampling sites. For cross-sections, see fig. 3.3.

Legend to fig. 3.2

Ur	Limestone Upland Soils	Af	Çakmak Fan Soils
Uv	Volcanic Upland Soils	Ag	Zanopa Fan Soils
Cr	Limestone Colluvial Soils	Ah	Bor Fan Soils
Cv	Volcanic Colluvial Soils	Ak	Meram and Sille Fan Soils
Te	Flat Terrace Soils	Am	May Fan Soils
Th	Undulating Terrace Soils	An	Bayat Fan Soils
Tc	Soft Lime Soils	As	Ayran Fan Soils
Br	Limestone Bajada Soils	Au	Soils of Medium Sized Fans
Bv	Volcanic Bajada Soils	Lm	Marl Soils
Aa	Çamurluk Fan Soils	Lr	Sandridge Soils
Ab	Former Backswamp Soils	Lp	Sandplain and Beach Soils
Ac	Çarşamba Fan Soils	Lo	Old Sandplain Soils
Ad	Deli Fan Soils	Mf	Marsh Soils
Ae	Selereki Fan Soils	Dd	Sand Dunes

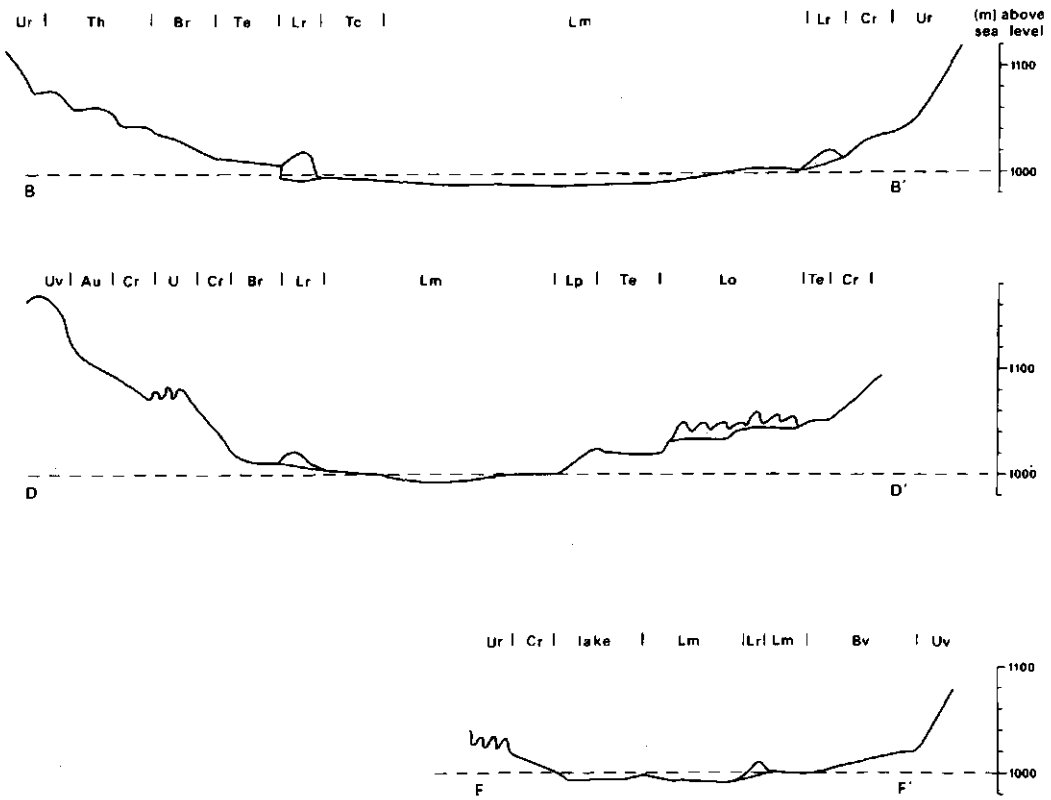

Fig. 3.3 Three schematic cross-sections through the Great Konya Basin. For position, see fig. 3.2 (from de Meester, 1970)

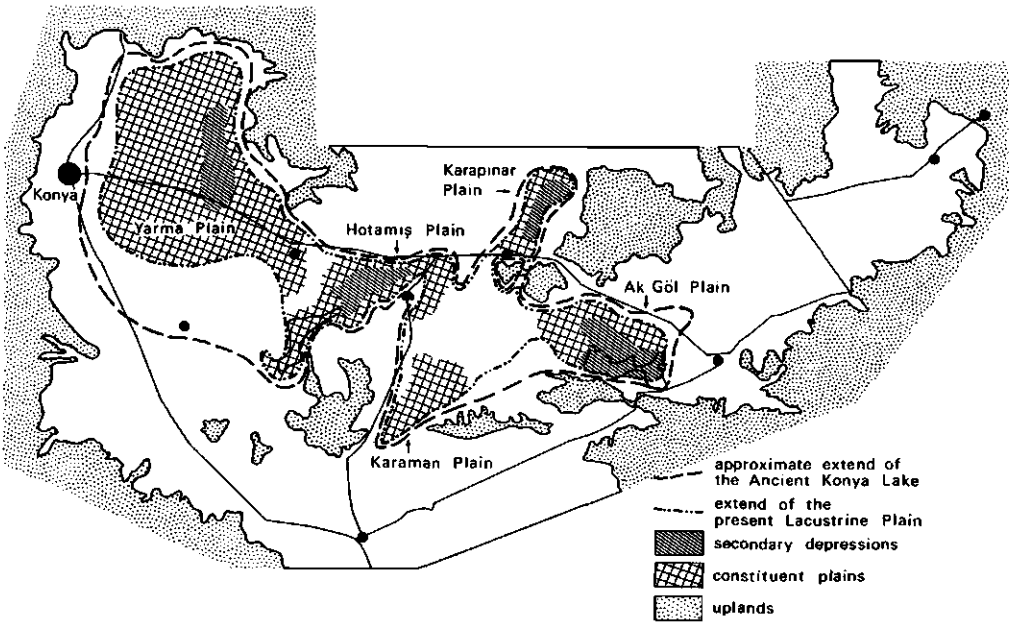

Fig. 3.4 Extent of the Lacustrine Plain in the Basin, of the constituent plains and of the depressions in them. (from de Meester, 1970)

The Aeolian Plain (D). This plain consists of sand dunes which have formed recently as a result of overgrazing.

The Marshes (M). They occur at the foot of the alluvial fans and near lakes.

3.4 CORRELATION OF OCCURRENCE OF SALTS WITH SOIL TYPE

Salt-affected soils can be found in the lower parts of the basin. The most extensive salt efflorescences occur on the lacustrine marl soils (Lm). Continuous salt crusts can be found in the depressions in the basin floor (see fig. 3.4), which is flooded for at least a few months per year. Here the salt originates by evaporation of surface water (flooded solonchaks). Some alluvial plain soils are very saline; the salinity of these soils increases towards the centre of the basin. On the lowest terrace soils, the soft lime soils (Tc), salt efflorescences can be found.

The Marsh soils, which cover the lowest parts of the basin, are generally very saline, but they are situated along perennial lakes and are moist during the whole year so no efflorescences can form.

3.5 SAMPLING AND ANALYTICAL PROCEDURE

As many different types of salt efflorescences as possible were sampled during the summer of 1978. The sampling sites are shown on fig. 3.2. When the salt consisted of a loose powder, small polyethylene tubes were filled with the salt. Coherent crusts were packed in toilet paper and transported in plastic boxes. Samples of ground water were also taken when possible, but in many cases it was impossible to penetrate the soil with a hand auger, and in some cases the ground water level was too deep to sample. Water samples from some inflow rivers were also taken.

Two different types of bottles were used for water samples: a 250 ml glass bottle which is impermeable to CO_2 was used for samples to be analysed for carbonates and a 250 ml polyethylene bottle for samples to be analysed for Na, K, Ca, Mg, Cl, SO_4 and silica. The glass bottles were brown to minimize as far as possible algal growth. All bottles were packed in a flanel cloth cover to avoid penetration of light and rise of temperature. A few drops of chloroform were added to the contents of polyethylene bottles. As little air-space as possible was left in the bottles after filling.

Temperature, pH, Eh and electroconductivity were measured at the sampling site. Immediately after arrival in Wageningen the carbonate system was analysed. Na, K, Ca, Mg, Cl, SO_4 and silica were analysed within four months after sampling. All analyses were performed in duplicate. The analyses of the water samples are reported in Table 3.1.

The salt minerals were identified by means of X-ray diffraction analysis with a Nonius Guinier camera FR 552 with a high-resolving Johansson $K\alpha_1$ monochromator, using Co $K\alpha_1$ radiation (λ = 0.17889 nm). Table 3.2 lists the salt minerals which have been found in the Basin. Table 3.3 represents the salt associations at the different localities.

3.6 CORRELATION BETWEEN THE FABRIC AND MINERALOGY OF THE SALT ASSOCIATIONS

Bloedite, thenardite and halite are the most abundant salt minerals in the Konya Basin and, therefore, they dominate the morphology of the salt assemblages.

When bloedite is the dominant species, the salt association is very fluffy and airy with large open holes and channels through the crusty particles. When it occurs in coherent crusts, the crust is very fragile and friable and on touching it desintegrates into small particles. When it occurs in the form of powder, the powder is very loose, again with large holes and pores. These

Table 3.1 Wateranalyses of waters from the Konya Basin, Turkey

Loc.	Kind of water	Ec ms/cm	pH_{field}	pH_{lab}	$Na^{1)}$	N	Ca	Mg	Cl^-	SO_4^{2-}	HCO_3^-	CO_3^{2-}	CO_2	H_4SiO_4	% deviation $^{2)}$
1.	Pond	4500	8.34	8.24	25.0	3.07	2.00	13.85	12.2	19.15	9.13	-	-	0.57	0.9
2.	River water	480	7.52	7.55	0.38	0.02	1.43	0.69	0.26	0.27	4.00	-	-	0.11	3.5
4.	Ground water	3700	7.25	7.37	15.8	1.98	2.18	8.3	9.36	9.5	13.27	-	-	0.90	6.9
5a.	Irriga. channel	2080	6.82	6.64	5.0	0.12	5.35	2.63	4.16	3.13	10.09	-	2.35	0.24	2.7
5b.	Ground water	2780	7.21	7.26	11.4	0.49	4.36	9.05	4.20	13.35	1.23	-	0.43	0.88	17
6.	Ground water	1690	7.05	7.05	1.74	0.31	3.18	4.89	3.20	2.27	10.47	-	1.06	0.47	0.1
8.	Krater lake	67000	8.45	8.25	7.88	16.4	16.05	110	769	126	9.15	-	-	0.07	2.6
9.	Ground water	167000	7.45	7.56	2174.	48.6	17.85	93	1686	241	7.16	-	0.37	0.10	12.4
10.	Ground water	2710	7.40	7.25	11.1	0.87	2.68	4.27	7.52	2.61	12.38	-	0.69	0.29	3.1
11.	Ground water	21000	7.38	7.35	136	7.16	8.95	83	164.8	79.0	5.49	-	-	0.43	0.4
12.	River water	250	8.38	8.28	0.07	-	1.0	0.38	0.08	0.05	2.65	-	-	0.08	0
13.	Ground water	23800	7.38	7.42	224	4.80	8.05	14.1	185	45	9.16	-	-	1.31	5.3
14.	Ground water	20700	7.45	7.45	174	3.96	7.85	30.5	139	52.5	5.27	-	-	0.95	2.2
15a.	Ground water	23000	8.08	8.01	230	2.81	0.35	1.46	165	22.1	29.56	-	-	0.88	1.3
15b.	Irriga. channel	1660	8.59	8.33	10.4	0.79	1.18	1.36	6.28	2.08	3.53	-	-	0.29	14.1
16.	Spring	49000	6.80	6.42	478	37.6	10.3	4.02	458	33.35	51.94	-	13.62	1.65	5.7
17.	Ground water	10000	7.49	7.54	68.5	1.13	12.15	15.95	33.0	43.95	6.03	-	-	0.99	0.7
22.	Ground water	4200	7.22	7.21	9.51	0.08	15.05	17.1	1.42	28.0	4.59	-	0.32	0.23	2.1
23.	Ground water	49000	7.40	7.28	435	2.76	17.5	131	459	124	4.80	-	-	0.17	1
24.	Ground water	10700	7.55	7.52	159	7.93	17.85	2.55	126	37.9	3.0	-	-	1.58	1.4
25.	Spring	9200	6.42	6.67	76.1	1.53	5.05	8.3	60.9	3.86	39.6	-	12.63	1.27	2.7
26.	Ground water	6500	6.85	7.05	56.0	1.10	2.32	3.58	34.6	3.86	29.6	-	3.53	0.80	4.3
27.	River	660	7.62	7.73	1.30	-	2.32	0.80	0.79	0.44	6.27	-	-	0.35	5
28.	Ground water	1520	7.05	7.18	5.65	0.69	2.93	2.01	5.84	1.50	8.27	-	0.34	1.0	5.3
29.	Ground water	2100	7.46	7.56	13.7	1.02	0.71	1.19	7.12	3.34	7.45	-	-	1.38	3.3
31.	Ground water	4400	8.58	8.51	42.4	0.87	0.15	0.38	22.6	2.35	16.5	0.44	-	1.03	0.9
32.	Ground water	3200	8.80	8.76	30.4	1.18	0.15	0.29	8.08	5.0	13.0	0.75	-	1.0	0.6
33.	Ground water	105000	7.42	7.69	1739	27.5	19.0	100	1517	220	3.77	-	-	0.11	2.2
35.	Ground water	18700	7.71	7.65	126	0.95	12.15	83	51.0	128.0	6.44	-	-	0.23	1.3
36.	Ground water	39000	7.00	7.32	380	7.80	16.05	102.5	388	98	7.11	-	-	0.49	5.4
37.	Ground water	67000	7.11	7.37	804	0	26.8	200.5	1065	112.5	3.14	-	-	0.20	2.6

1) all concentrations expressed as mol/m^3

2) deviations expressed as $\frac{|\Sigma^+ - \Sigma^-|}{\text{max. of } \Sigma^+ \text{ and } \Sigma^-} \times 100\%$

in which Σ^+ is the sum of the concentration of the positive ions in $eq./m^3$
and Σ^- " " " " " " " " negative " " " "

observations contrast with those of Driessen and Schoorl (1973) who state that bloedite forms glass-like crusts.

Thenardite occurs as small needles which push the soil particles in the upper layer of the soil apart. This layer becomes very puffed and when walking on the soil one sinks a few centrimetres in it.

Halite forms a coherent smooth salt layer which seals the soil and prevents further evaporation of the ground water. This layer is easy to remove from the soil.

The morphology of mixed salt associations depends upon the relative proportions of these three most abundant salt minerals: when halite predominates the association is more coherent, sealing and denser; when thenardite predominates the association is loose and powdery; when bloedite predominates, the association is more fluffy and airy.

Thenardite in association with halite adapts itself to halite, but thenardite without halite forms loose, powdery associations.
Bloedite makes the association more fluffy and airy.

3.7 METHODS OF WATERANALYSIS

The methods of wateranalysis which were used are described in detail in Begheyn (1980). In brief the following methods were used:

pH. Immediately after opening the brown glass bottle, the pH was measured with an Orion digital ionanalyzer model 801A.

Carbonate. The water was filtered through a 0.2 µm micropore filter. CO_3^{2-}- and HCO_3^--analyses were performed by potentiometric titration with H_2SO_4 0.1 N or 0.05 N and CO_2(aq) with NaOH 0.1 or 0.05 N. The steepest slopes of the titration curves were considered to be the end points.

Cl^-. Chlorine was analysed by potentiometric titration with $AgNO_3$ 0.02 N using an Ag_2S electrode.

SO_4^{2-}. Sulphate was determined turbidimetrically as $BaSO_4$ obtained with $BaCl_2.2H_2O$ in a medium of nitric acid, acetic acid, orthophosphoric acid, bariumsulphate suspension and a mixture of acacia gum solution and acetic acid.

Na^+ and K^+. The alkali ions were analysed by means of a Perkin Elmer Atomic Absorption Spectrofotometer after addition of an aluminium nitrate solution.

Ca^{2+} and Mg^{2+}. The earth alkali ions were analysed by means of a Perkin Elmer Atomic Absorption Spectrofotometer after addition of hydrochloric acid and a lanthanium chloride solution.

H_4SiO_4. Silica was analysed colorimetrically as blue β-silico-molybdenic acid after addition of an ammonium molybdate solution, sulfuric acid, tartaric acid and a reduction mixture of Na_2SO_3, metol and $K_2S_2O_5$- solution.

Table 3.2 Salt minerals found in the Konya Basin

Aphtithalite (aph)	$K_3Na(SO_4)_2$
Arcanite (arc)	K_2SO_4
Bloedite (bl)	$Na_2Mg(SO_4)_2.4H_2O$
Burkeite (brk)	$Na_6CO_3(SO_4)_2$
Calcite (cal)	$CaCO_3$
Dolomite (dol)	$CaMg(CO_3)_2$
Epsomite (eps)	$MgSO_4.7H_2O$
Eugsterite (eug)	$Na_4Ca(SO_4)_3.2H_2O$
Glauberite (gl)	$Na_2Ca(SO_4)_2$
Gypsum (gps)	$CaSO_4.2H_2O$
Halite (hal)	NaCl
Hexahydrite (hxh)	$MgSO_4.6H_2O$
Konyaite (kon)	$Na_2Mg(SO_4)_2.5H_2O$
Loeweite (lw)	$Na_{12}Mg_7(SO_4)_{13}.15H_2O$
Mirabilite (mb) [1]	$Na_2SO_4.10H_2O$
Nesquehonite (nqh)	$MgCO_3.3H_2O$
Schoenite (sch) (picromerite)	$K_2Mg(SO_4)_2.6H_2O$
Sodaniter (sdn)	$NaNO_3$
Starkeyite (st) (leonhardtite)	$MgSO_4.4H_2O$
Thenardite (tn)	Na_2SO_4
Trona (tr)	$NaHCO_3.Na_2CO_3.2H_2O$

1) Mirabilite could not be identified by means of X-ray diffraction analysis because transport of mirabilite proved to be impossible. Mirabilite is assumed to be present from observations of the crystals in situ.

Table 3.3 Salt associations in the Konya Basin

loc. no.	type of sampling site	salt association	fabric
1	along a temporary pond	bl,hxh,gps	very fluffy, very friable salt crust; breaks into small particles on touching
3	on the soil surface	bl,hxh,gps	like 1 but a little more coherent
4	on the soil surface	a: tn,gl	small salt particles mixed with loose soil particles
		b: tn,aph	like 4a
		c: bl,hal,gl	sealing, bumpy, coherent salt crust on hard soil
		d: bl,gps	soft, fluffy powder sticking to small, round aggregates
		e: bl,hal,hxh, sch	hard, coherent, very bumpy salt crust
5	on the soil surface	eps,bl,gps	like 1
6	on the soil surface	bl,hxh,gps	like 1, but a little more coherent
7	along a crater wall	hal,gps,sdn	small flinters
8	along a crater lake	hal,tn,nsqh, eug	hard pieces of salt
9	a dry, temporary lake	a: hal,gl,gps	sealing,flinterlike crust
		b: hal,tn,eug	like 9a
		c: tn	like 4a
10	on the soil surface	tn,aph	loose, powdery, fluffy salt
11	on the soil surface	bl,eug	loose, very soft powder
13	on the soil surface	a: hal,gps,eug	like 9a
		b: tn,eug	like 1
14	on the soil surface	hal,gps	like 4a
15	on the soil surface	a: hal,gps,brk	coherent, flinterly, sealing crust, easily removable from the surface
		b: hal,tn	like 15a, but a little thicker
16	spring deposit	a: hal,tn,eug	hard pieces
		b: gps,cal	oölitic material
17	on the soil surface	bl,eug	coherent, airy, hard salt crust

Table 3.3 continued

loc. no.	type of sampling site	salt association	fabric
19	on the soil surface	a: hal,gl,eug	sealing, coherent crust, difficult to remove from the soil
		b: bl,hal,gps	like 4d
21	on the soil surface	bl,hxh,gps	like 1
22	on the soil surface	bl,hxh,gps,kon	like 1
23	on the soil surface	a: bl,hal,gps	like 1, mixed with soil particles
		b: bl,hal,gl	like 19
24	on the soil surface	a: hal,gl	coherent, sealing, bumpy salt crust
		b: hal,gl,tn,gps, eug	like 24a but more bumpy and airy
25	around the spring of Tiana	hal,tn,nqh,gl, eug	coherent, sealing, thin salt crust
26	on the soil surface	hal,tr,brk	like 15a
28	on the soil surface		
	open patches	hal,tn,aph	like 4c
	between grass	tn,aph	like 4a
29	on the soil surface	a: hal,tn	soft, coherent salt between straws
		b: hal,eug	like 9a
		c: tn,aph	like 4a
31	on the soil surface	hal,tr,brk	bumpy, hard salt crust with air under the bubbles
32	on the soil surface	hal,tr,brk	like 31
33	dry, temporary lake	a: tn,hal,eug	like 9a
		b: tn,eug	coherent, bumpy crust with air under the bubbles
		c: tn	like 4a
35	on the soil surface	a: bl,hxh,gps,kon	loose, very fluffy powder
		b: bl,gps,lw	like 35a
36	on the soil surface	a: hal,bl	sugarlike, coherent crust
		b: hal,bl,stk,kon	like 35a
37	on the soil surface	hal,bl,gps,kon	like 4d

4. SALT-AFFECTED SOILS IN KENYA

4.1 PHYSIOGRAPHY AND CLIMATE

Samples of salt affected soils have been collected from three different regions in Kenya. These regions are (see fig. 4.1):
- The Amboseli basin along the Kenya-Tanzania border at the foot of Kilimanjaro
- A few localities along Lake Victoria
- East of Lake Turkana (the former Lake Rudolf) and the Chalbi Desert.

The climate differs in these three regions.

The Amboseli area has an arid climate with an annual rainfall of 255-510 mm. There are two rainy seasons, one in March-April, the other in November-December. The driest months are between June and October. The mean annual temperature is 22^{o} C.

The district east of Lake Turkana has a desert climate. Rainfall is normally less than 255 mm/yr apart from Mt. Kulal where rainfall is 255-510 mm/yr. In this region there is only one rainy season, between March and May, and the mean annual temperature is 27^{o} C.

Along Lake Victoria there is more rainfall than in the other two districts. At Homa Island the annual rainfall is 1015-1270 mm while at Sindo and Luanda it is 760-1015 mm. The rainfall is not restricted to a definite season; there are maxima in April and December. The mean annual temperature is 24^{o} C (Kenya Atlas).

4.2 GEOLOGY

All three areas are dominated by the volcanics associated with the East African (or Gregory) Rift Valley.
In Kenya, two types of volcanism occur (Williams, 1970):
- fissure and multi-centre eruptions (plateau volcanics)
- central volcanoes

The volcanics of the *fissure and multi-centre eruptions* consist mainly of basalts, phonolites and trachytes.
Basaltic eruptions occurred from the Miocene onwards. Miocene basalts can be

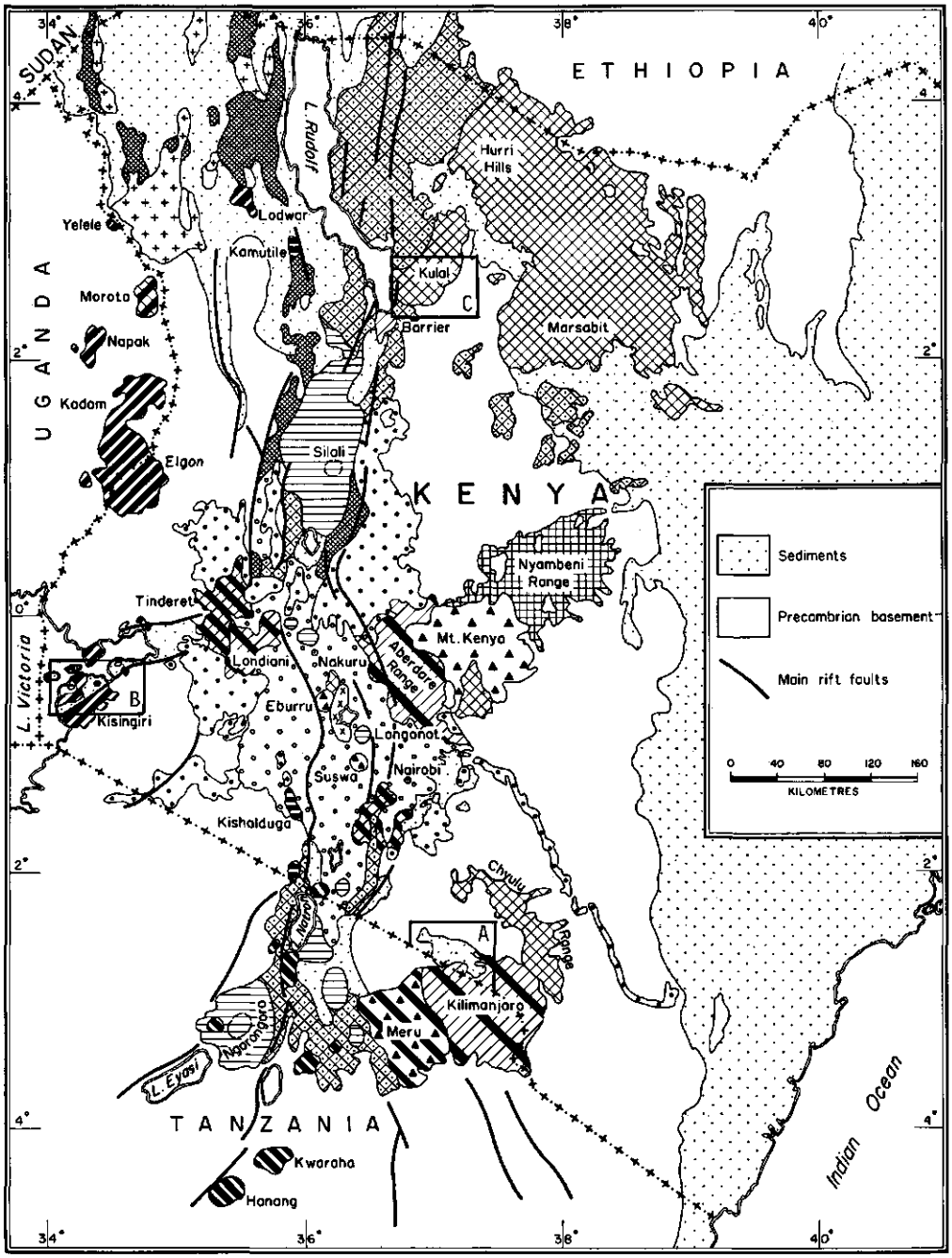

Fig. 4.1 Map showing the distribution of the main volcanic associations in Kenya (after Williams, 1970). The areas of sampling are indicated. a. Amboseli Basin. b. area along Lake Victoria. c. area east of Lake Turkana.

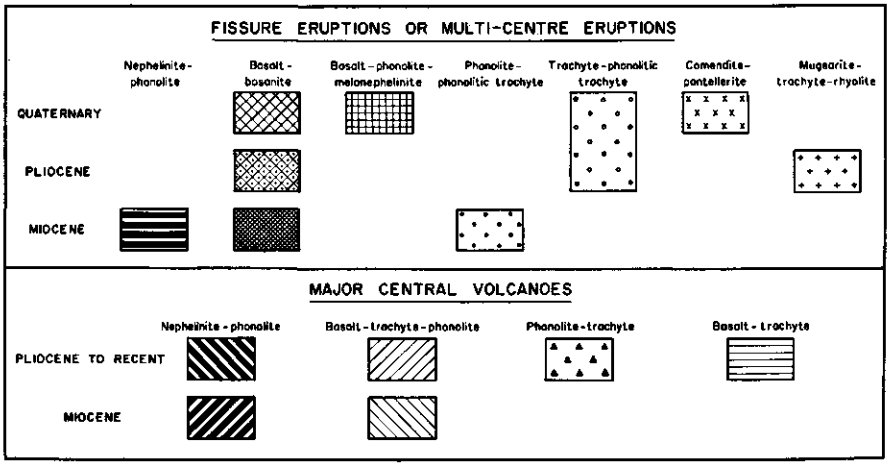

found in the central and northern parts of the rift. The Pliocene basalts form most of the floor and shoulders of the rift, which developed at that time. During the Quaternary, basaltic eruptions occurred to the east of the rift valley.
The phonolites are of upper Miocene age and cover large areas both east and west of the rift in the southern half of Kenya.
The trachytes range from upper Pliocene to Pleistocene age and they form large sections of the rift floor in southern Kenya.

The volcanics of the *central volcanoes* consist mainly of nephelinite-phonolites, phonolites, basalts and trachytes.

During the Miocene, large central volcanoes originated in western Kenya. The volcanic products belong to the nephelinite-phonolite series. During the Pliocene and Quaternary, major volcanic activity of this type occurred along the floor of the newly formed rift and also built some large volcanoes (e.g., Mt. Kenya and Kilimanjaro) which occur to the east of the rift.
The post-Miocene volcanoes consist also of basalts, trachytes and phonolites.

Fig. 4.1 shows the distribution of the main volcanic associations in Kenya and the location of the three areas visited. The geology of these areas will be dealt with in detail in the next three sections.

4.3 AMBOSELI BASIN

The reader is referred to Williams (1972) for a detailed description of the regional geology of the Amboseli Basin.

The basin is bordered to the north and west by metamorphic Precambrian rocks such as marbles, schists, gneisses and granulites. Towards the south and east the basin is bordered by the Kilimanjaro volcanic rocks, which consist mainly of olivine basalts but nephelites and phonolites also occur. The small eruption centres in the basin itself are surrounded by Pleistocene sediments which include lacustrine clays, marls and silts. The Pleistocene sediments which are known as the Amboseli Lake Beds have been subdivided stratigraphically into three formations by Williams (1972). The stratigraphy from bottom to top is as follows (Stoessell, 1978):

- *Sinya Beds*. These are exposed at Sinya to the south of Lake Amboseli. Three metres of hard, massive green sepiolite occur on top of five metres of massive, white dolomite. Pockets and veins of massive, white sepiolite and pastel kerolite occur throughout the dolomite and the green sepiolite.
- *Amboseli clays*. These consist of massive, green lacustrine clays with a thickness of up to 60 m under the lake which rest upon a basal conglomerate consisting of dolomite and sepiolite clast. The clays consist of calcite, dolomite, sepiolite, 1 nm clay and K-feldspar which is probably authigenic. In the southern half of Lake Amboseli large gaylussite crystals occur in the Amboseli clays, directly under the few centimetres alluvium which form the floor of the lake.
- *Old Tukai Beds*. These consist of silts, clays, clay-clast aggregates (metamorphic and volcanic detritus) and caliches, up to 25 m thick. The minerals in the clay-clast are authigenic.

In many places Quaternary deposits can be found, such as alluvial soils, sandy soils, dusty volcanic soils and windblown clayey silts and sands. A soil map of the basin is available, made by L. Touber, UNDP FAO Wildlife Management Project (in press).

The following soil types occur in the Amboseli Basin:

Plain soils

Soils developed on alluvium, predominantly derived from undifferentiated rocks of the basement system.

Soils developed on windblown deposits, predominantly derived from pyroclastic rock.

Soils developed on alluvium, predominantly derived from pyroclastic rock.

Soils developed on rocks of the basement system, undifferentiated.

Lavaflows

Soils developed on basic igneous rocks, rich in ferromagnesian minerals.

Bottomlands

Soils developed on alluvium, predominantly derived from undifferentiated volcanic rock.

Piedmont plains

Soils developed on colluvium and alluvium, predominantly derived from crystalline limestone.

External Solonchaks can be found on the plain soils. Salt efflorescences occur especially on the floor of Lake Amboseli, a temporary lake. For the

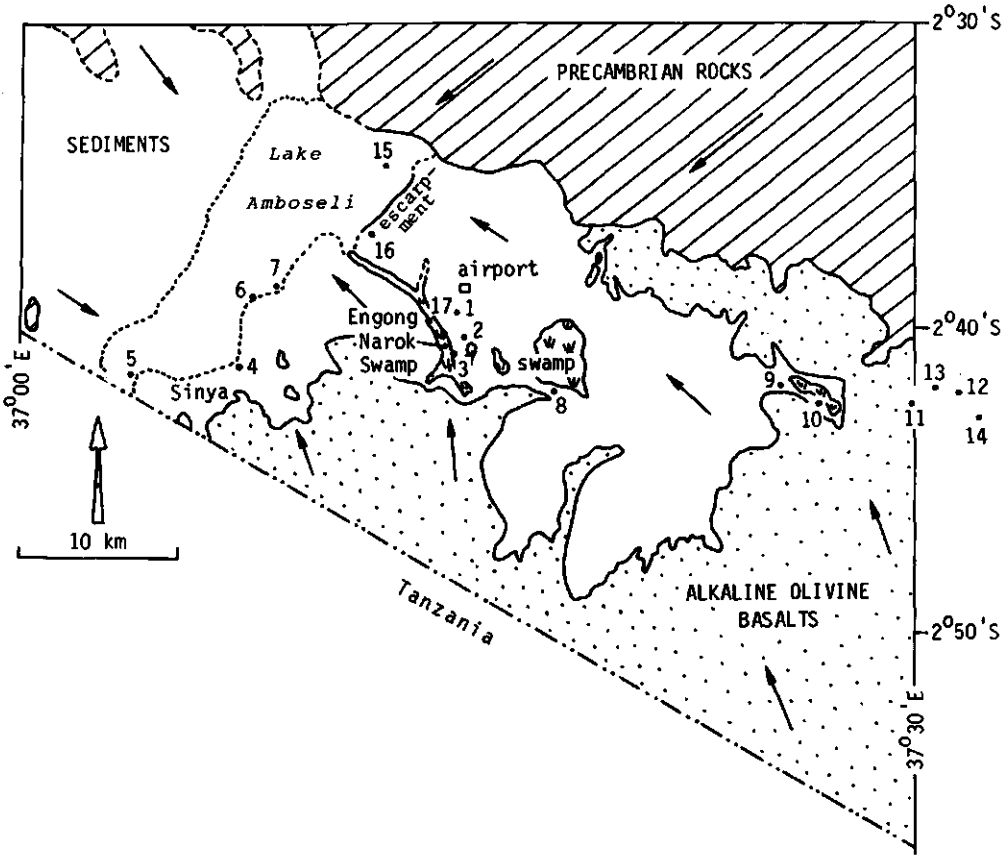

Fig. 4.2 Map showing the Amboseli Basin (after Stoessell, 1978) and the location of the sampling sites. The regional surface- and ground water-flow pattern is indicated by arrows.

location of the sampling sites, see fig. 4.2.

From the Kilimanjaro, molten snow and rainwater flow as surface streams and subsurface water in the direction of the basin. Most streams are dry at the foothills. Water also flows from the Precambrian rocks in the north to the basin but the regions where the saline soils occur are fed by water from the Kilimanjaro.

4.4 LAKE VICTORIA

Samples have been taken from different localities on Homa Peninsula and from the surroundings of the villages Sindo and Luanda in the coastal area of Lake Victoria (see fig. 4.3). The geology of this area is described in Saggerson (1952).

Homa Peninsula is dominated by Homa Mountain, which is a central volcano. Its activity began in the Miocene and lasted until late Pleistocene times. Homa Mountain is a typical carbonatitic complex with carbonatite, nephelinite and phonolite. On the lower slopes and on Homa Peninsula the volcanics are covered with Pleistocene and recent sediments. The sedimentary deposits thus partly formed when the volcano was still active. The Pleistocene deposits are lacustrine and consist of an alternation of tuffs, clays, sands, gravels and thin limestones. Samples have been taken from three different localities on Homa Peninsula: Lake Simbi, Miti Bili and Kanam. Lake Simbi, a volcanic maar, originated in historical times. The explosion that produced the vent probably broke through the old course of the River Awach, which now flows east of the lake. Lake Simbi is fed by groundwater, springs and rains. Salts have formed along the shore of the lake. At Miti Bili, a hot spring occurs only a few hundred metres from Lake Victoria. Surface and subsurface water has formed external solonchaks between the spring and the lake.
At Kanam salt efflorescences have formed along a dry riverbed.

The hinterland of Sindo and Luanda is formed by the Kisingiri Volcanic complex, one of the best examples of a Miocene nephelinite-phonolite central volcano in western Kenya. The plain along the shore of the lake consists of Pleistocene clays, sands and gravels. On this plain, salt efflorescences developed in the vicinity of the small villages Sindo and Luanda.

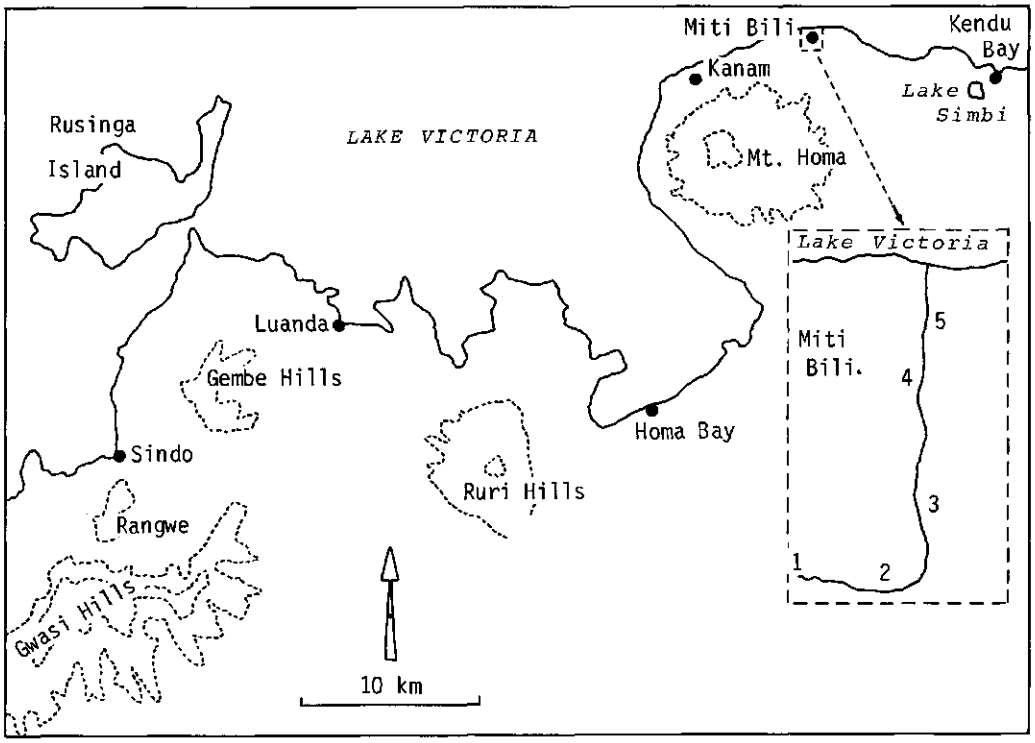

Fig. 4.3 Map showing the localities of the sampling sites along Lake Victoria.

4.5 EAST OF LAKE TURKANA AND THE CHALBI DESERT

Little is known about the geology of the area east of Lake Turkana (the former Lake Rudolf) and of the geology of the Chalbi Desert. A soil map 1:1.000.000 of this whole district is available (Sombroek, in press).

The Chalbi Desert consists of Cenozoic lacustrine sediments. This desert is barren of vegetation. Extensive External Solonchaks cover the Chalbi Desert. Normally, this salt plain is accessible by motor vehicle, but during the sampling trip (November 1977), the plain was flooded due to unusually heavy rainfall. Rainwater together with water draining from Ethiopia caused the desert to become a temporary lake and samples of the salts could only be taken at a few places where the rims of the desert could be reached (at Kalacha, Maikona and North Horr) (see fig. 4.4). The soils of the Chalbi Desert are classified as Orthic Solonchaks (very poorly drained, deep, firm, excessively saline clay

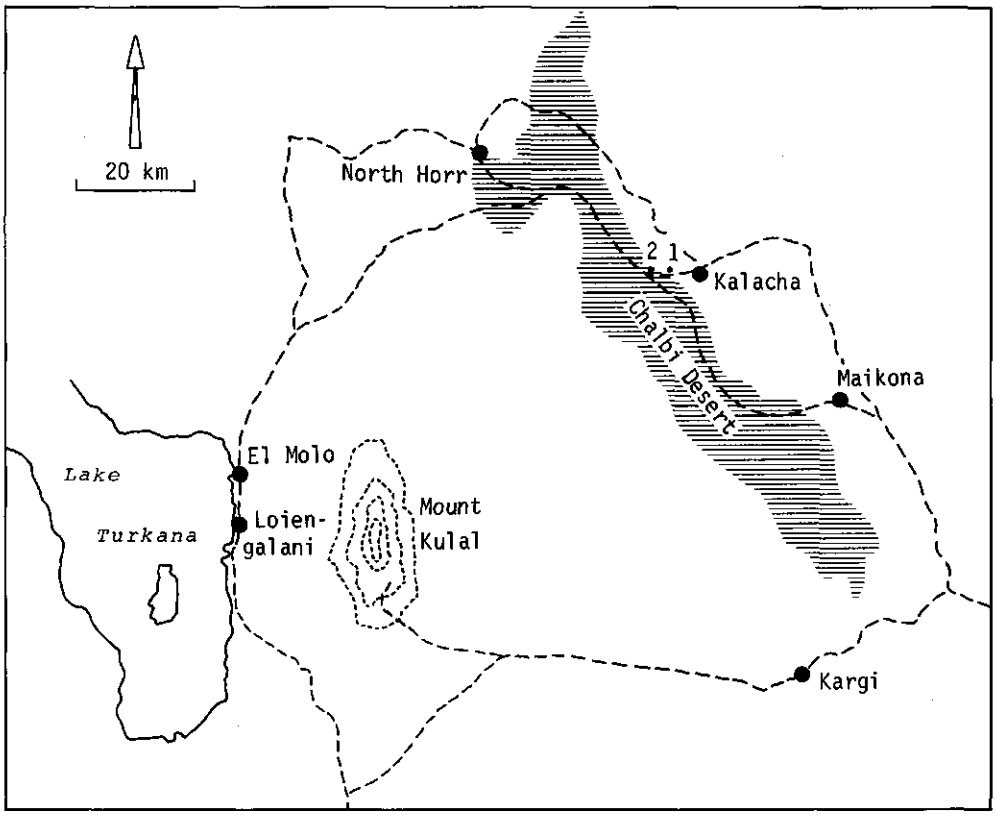

Fig. 4.4 Map showing the localities of the sampling sites in the region east of Lake Turkana and the Chalbi Desert. The dotted line indicates a track for vehicles.

with puffed salty crust) and Takyric Solonchaks (poorly drained, deep, very firm, excessively saline cracking clay).

Salt efflorescences occur at some sites along the shore of Lake Turkana. This district consists mainly of Quaternary olivine basalts of the fissure and multicentre type. The region where the salt efflorescences occur, near El Molo and Loiengalani (see fig. 4.4), is dominated by Mt. Kulal, a Pliocene basaltic central volcano. The salt occurrences are related to the drainage of the water flowing from Mt. Kulal towards Lake Turkana. The soils along the shore of Lake Turkana have been classified as Solonchaks gravelly phase (imperfectly drained, deep , moderately calcareous, strongly saline, gravelly clay loam, with gravelly desert pavement).

4.6 SAMPLING AND ANALYTICAL PROCEDURE

The sampling and the analytical procedure were the same as described in section 3.5.

Unfortunately the sampling program was partially disturbed by unusually heavy rainfall. The Amboseli Basin and the region along Lake Victoria were visited before the rains started. All of the water samples from Amboseli and some water samples from localities near Lake Victoria were taken before the rains began. Both districts were visited again after the rains. Lake Amboseli was no longer accessible by motor vehicle and most of the salt had disappeared. Along Lake Victoria the salt had also disappeared and therefore only some additional water samples were taken after the rains. The first sampling trip to Lake Turkana was unsuccessful because the exceptionally heavy rainfall caused the tracks to become impassable. This region was only visited after the rains, which had made the desert green and full of flowers.

Table 4.1 shows the water analyses. Table 4.2 shows the salt minerals which have been found. In table 4.3 the salt associations at the different localities are presented.

4.7 CORRELATION BETWEEN THE FABRIC AND MINERALOGY OF THE SALT ASSOCIATIONS

The most abundant salts in the areas visited in Kenya are halite, thenardite, trona and thermonatrite. These minerals dominate the morphology of the salt efflorescences on the soil surface (see table 4.3).

Thenardite and halite show the same morphological features as in Konya. The thenardite needles push the soil particles apart and cause the upper layer of the soil to become puffed. Halite has a sealing effect. It makes the crust more dense and coherent.

All associations with thermonatrite are very fluffy. When it occurs in crusts, these crusts are very friable and break easily into fluffy pieces. Enough pores and channels are present to avoid sealing of the underlying soil.

The crusts in which trona occurs are usually more rigid and coherent than those in which thermonatrite occurs. The surfaces of the trona containing crusts are very irregular and usually they are very airy with many voids and channels as is the case with thermonatrite.

Table 4.1 Wateranalyses of waters from Kenya

Loc.	Kind of water	Ec ms/cm	pH_{field}	pH_{lab}	Na^{+} 1)	K^{+}	Ca^{2+}	Mg^{2+}	Cl^{-}	SO_4^{2-}	HCO_3^{-}	CO_3^{2-}	CO_2	H_4SiO_4	% deviation 2)
Amboseli waters															
Am 3	groundwater	9000	7.99	8.01	73.0	7.52	1.88	1.07	4.40	5.35	69.5	-	-	1.0	2.1
Am 4	groundwater	1420	8.65	8.71	16.3	0.92	0.13	0.13	3.20	0.25	11.9	0.78	-	1.08	3.4
Am 5	pond	21800	9.68	9.67	202	1.89	0.23	0.135	63.0	2.17	59.4	40.65	-	0.14	1.5
Am 6	groundwater	1580	7.75	7.69	12.8	1.73	0.72	0.59	0.60	0.55	17.0	-	0.48	1.94	9.4
Am 8	groundwater	6800	7.55	7.68	48.7	6.55	0.72	1.56	11.8	1.42	52.2	-	-	1.18	11.7
Am 11	riverwater	250	7.88	7.63	1.20	0.22	0.38	0.29	0.25	0.03	2.70	-	-	0.79	9.9
Am 13	groundwater	19000	7.90	7.99	202	6.65	0.24	0.53	1.5	0.55	203	3.05	-	1.03	0.5
Am 14	riverwater	520	7.43	7.52	3.35	0.36	0.72	0.50	0.30	0.03	5.75	-	-	0.77	0.3
Turkana waters															
Maikona	groundwater	124000	7.62	7.32	773.	39.5	28.55	49	820.	58	1.64	-	-	0.26	3.1
Kalacha I	groundwater	2020	8.28	8.24	15.9	1.05	0.90	1.48	7.0	2.71	9.71	-	-	1.08	5.1
Kalacha II	groundwater	22000	7.85	8.46	153	6.55	1.07	0.93	84.0	33.15	4.46	0.32	-	0.43	5.5
North Horr	groundwater	508000	9.72	9.73	4174	63.4	-	-	2290	471	95.5	459.5	-	0.77	0.2
Furaful	riverwater	1680	9.07	8.98	17.0	0.24	0.17	0.06	6.0	2.96	4.26	0.52	-	0.41	2.8
Loyengalani	spring	710	8.38	8.19	4.70	0.16	0.60	0.97	1.60	0.29	5.63	0.28	-	0.88	4.6
Lake Victoria waters															
Simbi 1	spring	33900	8.02	8.12	10.4	0.17	0.71	0.04	0.40	0.07	9.94	-	-	1.30	13.2
Simbi 2	groundwater	28000	7.82	7.92	36.1	0.21	4.76	0.20	1.80	0.49	28.6	-	-	1.84	32
MitiBili 1 b.r.*	spring	29000	7.30	7.59	278	2.98	-	0.40	33.5	8.25	224	-	-	1.79	2.8
MitiBili 1 a.r.	spring	26700	7.35	7.57	267	2.93	0.90	0.73	32.0	8.50	219	-	-	1.81	1.8
MitiBili 2 a.r.	groundwater	42700	9.17	9.14	449	4.26	0.07	0.06	55.0	12.8	235	51.5	-	0.19	7.7
MitiBili 3 a.r.	groundwater	57000	9.34	9.25	551	4.77	0.22	0.04	84.5	15.7	265	94	-	0.24	2.3
MitiBili 4 b.r.	groundwater	45700	9.27	9.33	522	4.94	-	0.10	59.5	14.8	235	72	-	0.28	11.2
MitiBili 4 a.r.	groundwater	40000	9.59	9.43	384	3.22	0.18	0.02	52.5	9.4	155	74.5	-	0.08	3.4
MitiBili 5 a.r.	surface water	2780	9.74	9.55	31.7	0.26	0.12	0.02	4.60	0.85	15.0	5.7	-	0.17	10.7
Lake Victoria at	Miti Bili	180	8.44	7.40	1.04	0.11	0.31	0.10	0.20	-	1.87	-	-	0.15	5.6
Kanam 1 b.r.	groundwater	31300	8.47	8.63	330	3.32	-	0.10	39	14.6	207	15.2	-	0.51	8.7
Kanam 1 a.r.	groundwater	26300	8.55	8.38	278	2.90	0.07	0.09	34	10.05	200	-	-	0.32	9.3
Kanam 2 a.r.	groundwater	43300	9.58	9.32	399	4.60	0.15	0.05	63.0	18.55	190	73	-	0.14	7.9
Luanda	groundwater	47300	7.21	7.62	313	2.90	14.3	31.85	84.0	160.5	23.1	-	-	0.50	4.1
Sindo	groundwater	70000	7.14	7.40	507	4.77	11.9	25.25	357	207	29.1	-	-	1.01	1.2

* b.r. = before rains
* a.r. = after rains

1) all concentrations expressed as mol/m^3

2) deviations expressed as $\frac{|\Sigma^{+} - \Sigma^{-}|}{\text{max.of } \Sigma^{+} \text{ and } \Sigma^{-}} \times 100\%$

in which Σ^{+} is the sum of the concentration of the positive ions in $eq./m^3$
and Σ^{-} " " " " " " " " " negative " " " "

Table 4.2 Salt minerals observed in the Kenya sample sites

Amboseli	
aphtithalite (aph)	$K_3Na(SO_4)_2$
aragonite (ar)	$CaCO_3$
burkeite (brk)	$Na_6CO_3(SO_4)_2$
calcite (cal)	$CaCO_3$
dolomite (dol)	$CaMg(CO_3)_2$
gaylussite (gay)	$Na_2CO_3.CaCO_3.5H_2O$
pirssonite (prs)	$Na_2CO_3.CaCO_3.2H_2O$
thermonatrite (tm)	$Na_2CO_3.H_2O$
thenardite (tn)	Na_2SO_4
trona (tr)	$NaHCO_3.Na_2CO_3.2H_2O$
Turkana	
burkeite (brk)	$Na_6CO_3(SO_4)_2$
eugsterite (eug)	$Na_4Ca(SO_4)_3.2H_2O$
gypsum (gps)	$CaSO_4.2H_2O$
halite (hal)	NaCl
thenardite (tn)	Na_2SO_4
trona (tr)	$NaHCO_3.Na_2CO_3.2H_2O$
Lake Victoria	
burkeite (brk)	$Na_6CO_3(SO_4)_2$
calcite (cal)	$CaCO_3$
eugsterite (eug)	$Na_4Ca(SO_4)_3.2H_2O$
gaylussite (gay)	$Na_2CO_3.CaCO_3.5H_2O$
gypsum (gps)	$CaSO_4.2H_2O$
halite (hal)	NaCl
nahcolite (nah)	$NaHCO_3$
thermonatrite (tm)	$Na_2CO_3.H_2O$
thenardite (tn)	Na_2SO_4
trona (tr)	$NaHCO_3.Na_2CO_3.2H_2O$

Table 4.3 Salt associations observed in Kenya

loc. no.	type of sampling site	salt association	fabric
Amboseli			
1	against wall of profile pit, 20 cm	a: tn,tr,aph	thin, slightly bumpy, rather flat and friable coherent salt crust
	ditto, 70 cm	b: tr,cal,gay	yellowish powder
2	on the soil surface	tr,cal,gay	like 1a
4	on the soil surface	a: tr	soft, fluffy, coherent salt crust
	on the soil surface	b: tm,tr,cal	like 4a
	on the soil surface	c: tr,cal,prs, tm	flat, thin, coherent salt crust
	on the soil surface	d: tr,tm,gay	fluffy, small, loose salt particles mixed with other soil particles
5	along pond	a: tr,cal,gay, tm	like 4a
	along pond	b: cal,ar	salt peels
6	on the soil surface	tr,cal,gay, tm,aph	very fluffy, coherent salt, breaks into pieces on touching
7	on the soil surface	tr,brk	coherent, puffed crust, irregular surface
8	on the soil surface	a: tr,tm,gay	very loose, fluffy, irregular shaped salt particles
	on the soil surface	b: tr,aph	like 8a, but more coherent and little more yellowish
	on the soil surface	c: tr,aph,gay, prs	coherent, thin, irregular, dense salt crust
9	on the soil surface	tr,prs,cal	slightly fluffy, coherent, soft crust
12	on the soil surface	a: tr,brk	very irregular, airy, coherent salt crust
	on the soil surface	b: tr,tm,brk	like 12a but more friable
		c: tr	like 4a
13	on the soil surface near swamp	tr,aph,gay, cal	fluffy, friable, coherent salt crust
15	on the soil surface	tn	white salt fluffs between clay particles
16	on the soil surface	a: tn	thin, dense, bulged salt crust
	on the soil surface	b: tn	like 15
17	on the soil surface	tn,aph	like 12a

Table 4.3 continued

loc. no.	type of sampling site	salt association	fabric
Turkana			
Maikona	on the soil surface	a: hal,tn	thin salt layer deposited between basaltic gravel on the soil, not removable as a crust from the soil
		b: hal,gps	powdery salt on quartz pieces
Kalacha 1	on the soil surface	hal,tn.eug	glassy salt layer on the soil surface
Kalacha 2	on the soil surface	hal, tn	like Kalacha 1
North Horr	on the soil surface	hal,tr,brk	thin, flinterly, dense, smooth salt crust
Furaful	on the soil surface	hal,tn	thin, coherent, easy removable, rough salt crust
El Molo	on the soil surface	tn	very irregular, thin, coherent, puffed salt crust
Oasis	on the soil surface	a: tn,hal	flinterly, smooth, white salt crust
	on the soil surface	b: tn,hal,brk	like a, but a little more glassy and yellowish
Lake Victoria			
Simbi	on the soil surface near lake	a: tr,tm	very fluffy salt particles mixed with clay
	ditto	b: tm,tr,gay	like a
Miti Bili 1	around spring	tr,cal,gay, nah	thin, bumpy, hard salt layer on surface
Miti Bili 2	on the soil surface	a: tr	dark coloured, hard salt layer
	on the soil surface	b: tr,tm	airy, white, irregular salt crust
Miti Bili 3	on the soil surface	tr,gay	thin, white, smooth salt film
Miti Bili 4	on the soil surface	a: tr,tm,hal, brk	very fluffy salt crust
		b: tr,hal	like Miti Bili 2b
		c: tr,nah,gay	thin, flinterly film
		d: tr,gay	bumpy, irregular salt crust
		e: tr,hal,brk	airy, irregular salt crust
Kanam	on the soil surface	a: tr,nah	thin, flintery crust with a rough surface
		b: tr,tm,gay	powdery salt on coarse gravel
		c: tr,hal,gay	puffed, rough crust
		d: tr,hal,tm, gay	like c
		e: tr,gay	like Miti Bili 4d

Table 4.3 Continued

loc. no.	type of sampling site	salt association	fabric
Sindo	on the soil surface	a: hal,tn	salt film on clay
		b: gps	white spots
		c: hal,eug	like a
Luanda	on the soil surface	eug,gps	white spots in dark soil

5. BRINE EVOLUTION IN CLOSED BASINS

5.1 INTRODUCTION

The occurrence of salt-affected soils is dependent both on geological and climatic factors. Salt-affected soils form easily in semi-arid regions where evaporation is high and usually exceeds rainfall.
The origin of salt-affected soils may be anthropogenic or natural. Anthropogenic salt-affected soils originate when during irrigation no concomitant drainage is applied to remove the dissolved salts, as was discussed in chapter 2. Natural salt-affected soils preferentially occur in hydrographically closed basins.

Geologically speaking, two different types of closed basins can be distinguished (Eugster and Surdam 1973, Surdam and Sheppard 1978) which show a completely different hydrology. Both types have a tectonic origin:

a. Playa-lake complex type (see fig. 5.1[a])
   A Playa-lake complex is a broad flat basin surrounded by mountains. Rivers descending into the basin from the mountains have usually disappeared before reaching the center of the basin, which may consist of a perennial or annual lake. The groundwater flow is shallow. Most clastic debris is deposited in alluvial fans at the foot of the mountains.
b. Rift-system type (see fig. 5.1[b])
   In a rift-system closed basin an annual or perennial lake occupies the floor of a narrow flat valley which is bordered by steep mountains. The groundwater flow is deep and usually discharge takes place at the edge of the lake by springs. As springs are devoid of clastic material no alluvial fans originate.

The Konya Basin in Turkey is a typical example of a playa-lake complex type (compare fig. 5.1[a] and fig. 3.3). Lake Magadi which is located in the East African rift valley in Kenya is a typical example of a rift-system type.

The genesis of salt affected soils in closed basins is as follows:
Dissolved material is brought in by rivers, groundwaters and springs from the surroundings into the basin. During evaporation, the remaining solution becomes more and more concentrated until it becomes saturated with respect to some minerals, which then precipitate. It depends on the position of the water where

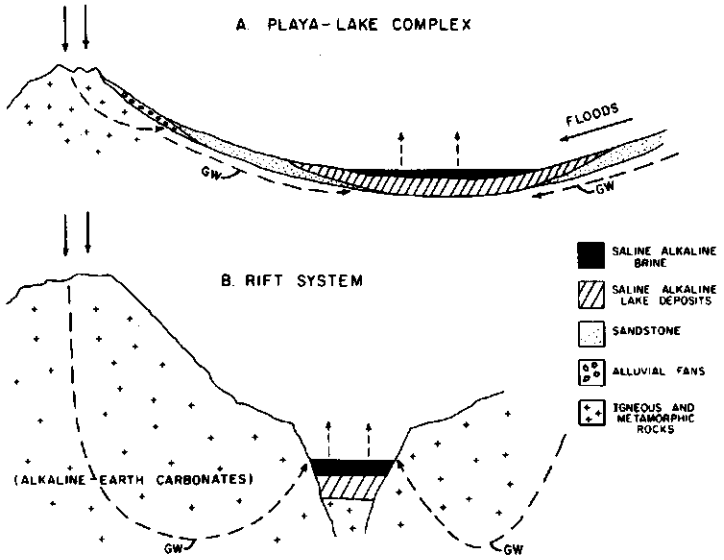

Fig. 5.1 Hydrology and brine evolution in a playa-lake complex (A) and a rift system (B). Solid arrows, rainwater; GW, ground water circulation path. (from Surdam & Sheppard, 1978)

the salt will accumulate if the water evaporates as surface-water, for example the water of a temporary or permanent lake in the center of the basin, white salt rims form around the lake. Most of the time, however, the water evaporates as groundwater within the soil. Minerals will precipitate at different levels in the soil profile depending on their solubility. The less soluble minerals will precipitate in a horizon somewhere in the soil profile (internal Solonchak) and the more soluble minerals will accumulate at the soil surface (external Solonchak).

5.2 CHEMICAL EVOLUTION

The chemical evolution of waters in closed basins can be separated into three main phases:

- acquisition of solutes
  Dilute waters acquire solutes by weathering reactions with soils and bedrock (Garrels and McKenzie 1967).
- evaporation
  The dilute waters evaporate, which causes concentration of the dissolved material leading to precipitation of minerals (Eugster and Hardie 1978, Hardie and Eugster 1970).

- re-solution
  Partial re-solution of salts deposited on the soil surface takes place. This influences the composition of the groundwater (Drever and Smith 1977; Jones, Eugster and Rettig, 1977).

5.3 ACQUISITION OF SOLUTES

Chemical weathering of primary silicates by CO_2-charged waters causes the solution to become enriched with cations, silica and bicarbonate. The weathering reaction can be represented by (Garrels and McKenzie, 1967):

primary silicate + H_2O + CO_2 → clay minerals + cations + HCO_3^- + $H_4SiO_4^o$ (aq) (1)

During weathering of igneous and metamorphic rocks, HCO_3^- will be the predominant anion in the solution. Weathering of preexisting evaporites can produce solutions in which Cl^- and SO_4^{2-} are the predominant anions. They both may also be essential constituents of rainwater. In addition, chlorine often originates from fluid inclusions in minerals, and sulphate may enter solution by oxidation of sulfides, for example by weathering of pyrite.

5.4 EVAPORATION

Dilute waters of different composition behave in different ways during evaporation. The direction in which the solution will evolve is completely determined by the ratio of the ions present in the dilute waters after the stage of acquisition. This principle can be demonstrated with a simple example: the precipitation of NaCl (Al-Droubi, 1976). A fictive solution containing only Na^+ and Cl^- ions will be considered. Under natural circumstances such a fictive solution will never occur, because carbonate-ions are always present in waters in equilibrium with an atmosphere containing CO_2. With carbonate-ions we have the complication that they are involved in the following equilibria (Stumm & Morgan, 1970):
(the values of the K's are at 25° C, $H_2CO_3^* = H_2CO_3 + CO_2(aq)$)

$$CO_{2(g)} + H_2O \rightleftarrows H_2CO_3 \qquad K = \frac{(H_2CO_3^*)}{P_{CO_2}} = 10^{-1.47} \qquad (2)$$

$$H_2CO_3 \rightleftarrows H^+ + HCO_3^- \qquad K_1 = \frac{(H^+)(HCO_3^-)}{(H_2CO_3^*)} = 10^{-6.35} \qquad (3)$$

$$HCO_3^- \rightleftharpoons H^+ + CO_3^{2-} \qquad K_2 = \frac{(H^+)(CO_3^{2-})}{(HCO_3^-)} = 10^{-10.33} \qquad (4)$$

$$H_2O \rightleftharpoons H^+ + OH^- \qquad K_w = \frac{(H^+)(OH^-)}{H_2O} = 10^{-14} \qquad (5)$$

In a fictive solution containing only Na^+ and Cl^- ions, these ions must be present in equal amounts to maintain electroneutrality. During evaporation the concentrations of Na^+ and Cl^- will increase by the same factor until the solution becomes saturated with respect to NaCl. The salt will precipitate, Na^+ and Cl^- will be taken from the solution in equal amounts and during further evaporation the composition of the solution in equilibrium with halite remains constant (point 1 in fig. 5.2). If in addition to Na^+, K^+ is also present as a cation, the electroneutrality restriction implies $[Na^+] + [K^+] = [Cl^-]$ and $[Cl^-]/[Na^+]>1$ (square brackets denoting molar concentrations and round brackets denoting activities). During evaporation $[Cl^-]/[Na^+]$ remains constant, the concentrations following, for example, line 1^a in fig. 5.2 until the solution becomes saturated with respect to NaCl. At this stage an equal amount of Na^+ and Cl^- will be taken from the solution but during further evaporation the concentration of chlorine will increase and as $(Na^+).(Cl^-)$ = constant, the concentration of Na^+ will

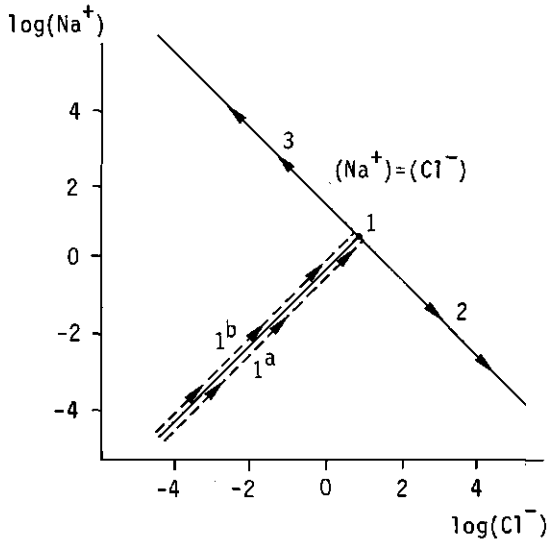

Fig. 5.2 Evolution during evaporation of a solution containing Na^+- and Cl^--ions in case in the initial solution: 1. $[Na^+] = [Cl^-]$; 1^a. $[Cl^-] > [Na^+]$ and 1^b. $[Na^+] > [Cl^-]$.

decrease. The concentrations follow the line describing the solubility product of NaCl (direction 2 in fig. 5.2). On the other hand, when for example SO_4^{2-} is present in addition to Na^+ and Cl^-, $[Cl^-]/[Na^+]<1$ and the solution will evolve in the opposite direction (direction 3 in fig. 5.2).

During the precipitation of carbonates, analogous restrictions to those governing the precipitation of NaCl must be valid.

If, during evaporation, calcite precipitates (Hardie and Eugster, 1970):

1. Ca^{2+} and CO_3^{2-} must be lost from the solution in equal molar proportions;
2. The activity product of calcite ($(Ca^{2+})(CO_3^{2-})$) must remain constant at constant P and T.

In a solution in equilibrium with atmospheric CO_2 containing only Ca^{2+}, H^+, CO_3^{2-}, HCO_3^-, and OH^- the following electroneutrality equation is valid:

$$2[Ca^{2+}] = 2[CO_3^{2-}] + [HCO_3^-] + [OH^-] - [H^+] \tag{6}$$

$[H^+]$, $[HCO_3^-]$ and $[OH^-]$ can be expressed in terms of $[CO_3^{2-}]$ as follows:

$$\gamma_{H^+}\ [H^+] = \frac{K_1 K_2 p_{CO_2} K}{\gamma_{CO_3^{2-}}\ [CO_3^{2-}]} \tag{7}$$

$$\gamma_{HCO_3^-}\ [HCO_3^-] = \frac{K_1}{K_2} \cdot p_{CO_2} \cdot K \cdot \gamma_{CO_3^{2-}}\ [CO_3^{2-}] \tag{8}$$

$$\gamma_{OH^-}\ [OH^-] = \frac{K_W}{\gamma_{H^+}[H^+]} \tag{9}$$

In these equations γ_i means the activity coefficient of ion i. The following relation exists between activity and concentration:

$$\gamma_i \cdot \text{concentration}_i = \text{activity}_i \quad \text{or} \quad \gamma_i[i] = (i) \tag{10}$$

Substituting into equations 7 to 9 the values for the K's at 25°C and $p_{CO_2}=10^{-3.5}$, neglecting $[H^+]$ and substituting the obtained results into equation 6, the following equation results:

$$[Ca^{2+}] = [CO_3^{2-}] + \tfrac{1}{2}\left(10^{-3.175}\cdot\frac{\gamma_{CO_3^{2-}}^{\frac{1}{2}}}{\gamma_{OH^-}}\ [CO_3^{2-}]^{\frac{1}{2}} + 10^{-0.495}\cdot\frac{\gamma_{CO_3^{2-}}^{\frac{1}{2}}}{\gamma_{HCO_3^-}}\ [CO_3^{2-}]^{\frac{1}{2}}\right) \tag{11}$$

or, in activities:

$$\frac{(Ca^{2+})}{\gamma_{Ca^{2+}}} = \frac{(CO_3^{2-})}{\gamma_{CO_3^{2-}}} + \tfrac{1}{2}\left(\frac{10^{-3.175}\,(CO_3^{2-})^{\frac{1}{2}}}{\gamma_{OH^-}} + \frac{10^{-0.495}(CO_3^{2-})^{\frac{1}{2}}}{\gamma_{HCO_3^-}}\right) \qquad (12)$$

In the dilute stage, activity coefficients may be neglected which yields :

$$[Ca^{2+}] = [CO_3^{2-}] + 10^{-0.795}\,[CO_3^{2-}]^{\frac{1}{2}} \qquad (13)$$

This equation represents the relation between the Ca^{2+} - and the CO_3^{2-} -concentrations in the system $CaO-CO_2-H_2O$ during evaporation under atmospheric conditions at 25^{o} C (line 1 on fig. 5.3). When the system becomes saturated with respect to calcite, calcite precipitates and the composition of the solution remains constant at a composition indicated by point 1' in fig. 5.3. If Na, K, Mg, Cl, and SO_4, which are normal constituents of natural waters, are present in

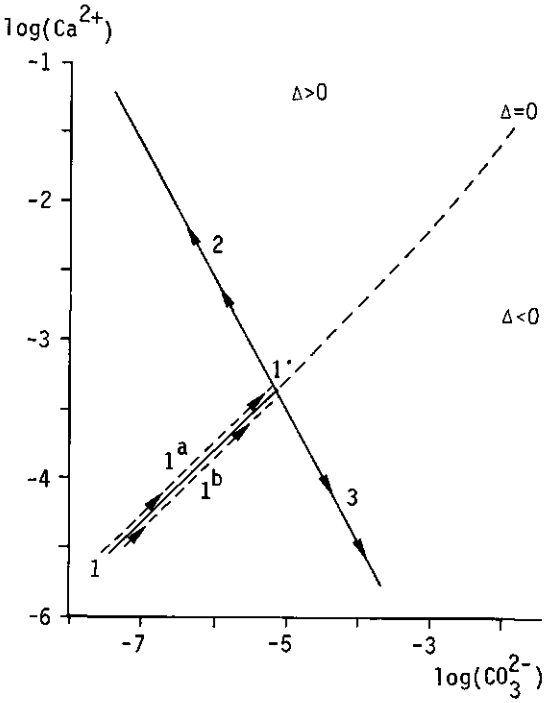

Fig. 5.3 Evolution of the system $CaO-CO_2-H_2O$ during evaporation in case 1. $\Delta = 0$, 1^a. $\Delta > 0$ and 1^b. $\Delta < 0$.

addition to the ions mentioned in equation 6, the electroneutrality equation becomes:

$$[Ca^{2+}] = \underbrace{[CO_3^{2-}]+\tfrac{1}{2}([HCO_3^-]+[OH^-]-[H^+])}_{[CO_3^{2-}]+\ 10^{-0.795}[CO_3^{2-}]^{\frac{1}{2}}}+\underbrace{\tfrac{1}{2}([Cl^-]+2[SO_4^{2-}])-\tfrac{1}{2}([Na^+]+[K^+]+2[Mg^{2+}])}_{\Delta} \quad (14)$$

at small I (= ionic strength)

If Δ is zero the relation between the Ca^{2+}- and CO_3^{2-}-concentrations during evaporation can again be described by line 1. When the concentrations of the other ions become too large, the activity coefficients may become important which influences the position of curve 1 in fig. 5.3, as can be seen from equation (11).

If Δ is positive, $[Ca^{2+}]$ is in excess over carbonate and during evaporation the Ca^{2+}- and CO_3^{2-}-concentrations are described by a curve on the Ca-rich side of curve 1 (for example curve 1^a).

Fig. 5.3 suggests that curves 1, 1^a and 1^b are parallel, but as the absolute value of Δ increases during evaporation, these curves are not parallel but their vertical separation increases.

When the solution becomes saturated with respect to calcite, Ca^{2+} and CO_3^{2-} will be removed from the solution in equal molar amounts and the composition of the solution will change according to the line representing the solubility product of calcite in direction 2 (fig. 5.3).

When Δ is negative, the composition of the solution will change in the opposite direction (3).

The precipitation of *calcite* is *the first decisive step* in the evolution of a brine (Hardie and Eugster, 1970; Eugster and Hardie, 1978). The solution becomes either carbonate-rich or carbonate-poor, depending on the ratio of calcium to carbonate in the initial solution, which is correlated to the sign of Δ of (14).

The next cation which usually will be removed from the solution is Mg^{2+}. Nesbitt (1974) found that in waters with intermediate $(Ca^{2+} + Mg^{2+})/(HCO_3^-)$ ratios more and more Mg will be incorporated in the calcite as Mg is enriched in the solution relative to Ca as a result of calcite precipitation until finally protodolomite and magnesite may be formed. Gac et al (1977) have shown experimentally that in the Lake Chad environment Mg and Si coprecipitate which finally leads to the formation of Mg-rich montmorillonite. Hardie (1968) found

coprecipitation of Mg and Si in the form of sepiolite at Saline Valley, California.

Let us consider what happens theoretically to a solution if, during evaporation, calcite and sepiolite coprecipitate. Mg precipitates as sepiolite according to (Garrels and McKenzie, 1967):

$$2Mg^{2+} + 3SiO_2(aq) + (n+2)H_2O \rightleftharpoons Mg_2Si_3O_8.nH_2O + 4H^+ \qquad (15)$$

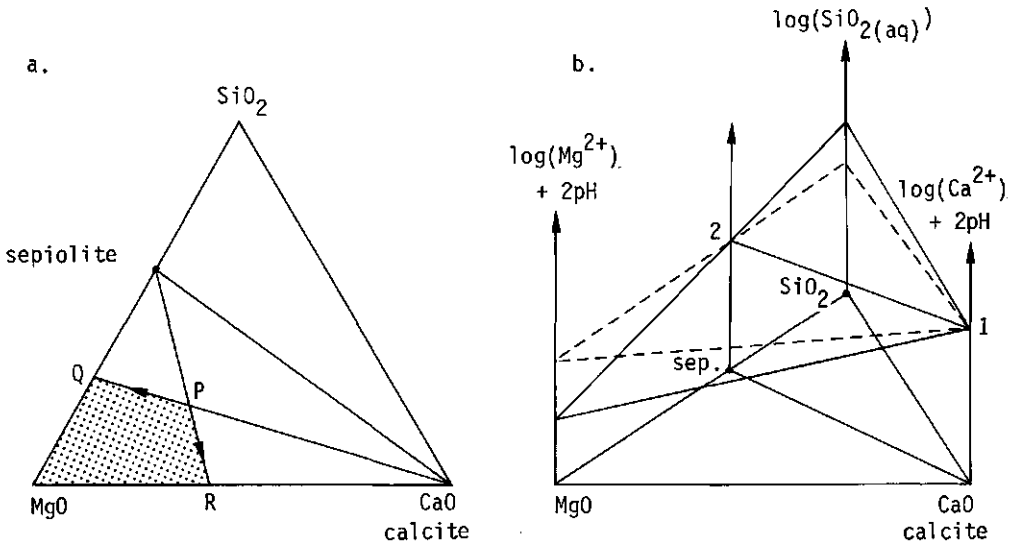

Fig. 5.4a MgO-SiO_2-CaO-diagram. During coprecipitation of sepiolite and calcite from a solution with composition P, the composition of the resulting solution moves somewhere in the shaded area.

Fig. 5.4b Activities of components pivot around join 1-2 during coprecipitation of calcite and sepiolite.

The composition of the solution can be represented in a MgO-SiO_2-CaO-diagram (fig. 5.4[a]). The activities of the components can be plotted along axes perpendicular to the plane of composition (fig. 5.4[b]). From the relation $Ca^{2+} + H_2O \rightleftharpoons CaO + 2H^+$ it follows that log(CaO) is analogous to $\log(Ca^{2+}) + 2pH$ and from $Mg^{2+} + H_2O \rightleftharpoons MgO + 2H^+$ it follows that log(MgO) is analogous to

$\log(Mg^{2+}) + 2pH$.

During calcite precipitation at constant p_{CO_2}:

$$\log(Ca^{2+}) + 2pH = \text{constant} \quad \text{(point 1 in fig. 5.4}^{b}\text{)} \tag{16}$$

which follows from the reaction equation $Ca^{2+} + CO_2 + H_2O \rightleftarrows CaCO_3 + 2H^+$.

During sepiolite precipitation:

$$3\log(SiO_{2(aq)}) + 2(\log(Mg^{2+}) + 2pH) = \text{constant} \tag{17}$$

because the solubility product of sepiolite (18) is constant.

$$K = \frac{(H^+)^4}{(Mg^{2+})^2(SiO_{2(aq)})^3} = \text{constant} \tag{18}$$

Therefore, point 2 in fig. 5.4^{b} is fixed.

If calcite and sepiolite coprecipitate from a solution with composition P, the composition of the remaining solution plots somewhere in the segment formed by the joins of calcite and the original solution and of sepiolite and that solution (shaded area in fig. 5.4^{a}). The activities of the components in solution are represented by the dissection from the axes by a plane which pivots around the line between point 1 and 2 in fig. 5.4^{b}. During sepiolite precipitation, Mg and Si are removed from the solution in a molar ratio of 2/3. If at the moment sepiolite starts to precipitate Mg/Si > 2/3, which means that the composition of the solution plots in the CaO-MgO -sepiolite triangle of fig. 5.4^{a}, this ratio increases with further precipitation. Conversely, when the composition plots in the CaO-SiO_2-sepiolite triangle, the Mg/Si ratio decreases during precipitation of sepiolite.

In the following discussion what may happen to a solution if sepiolite starts to coprecipitate with calcite will be dealt with systematically. It is assumed that at the moment sepiolite and calcite start to coprecipitate:

[Mg] / [Si] > 2/3. During further evaporation and coprecipitation this ratio increases.

- If $(SiO_{2(aq)})$ is constant, it follows that

$$\left.\begin{aligned} &\log(Mg^{2+}) + 2pH = \text{constant} \\ &\delta\log(Mg^{2+}) = -2\delta pH \\ &\delta\log(Ca^{2+}) = -2\delta pH \end{aligned}\right\} \longrightarrow \quad \delta\log(Ca^{2+}) = \delta\log(Mg^{2+}).$$

As ($SiO_{2(aq)}$) is constant, and Mg/Si must increase, it follows that Mg must increase and therefore Ca increases also and pH decreases.

- If ($SiO_{2(aq)}$) increases, it follows that

  $\log(Mg^{2+})$ + 2pH decreases. This is possible only if

a. 2pH decreases more than $\log(Mg^{2+})$ increases → $\delta\log(Ca^{2+}) > \delta\log(Mg^{2+})$ both ↑
b. 2pH increases less than $\log(Mg^{2+})$ decreases → $|\delta\log(Mg^{2+})| > \delta\log(Ca^{2+})$ Mg ↓ Ca
c. 2pH decreases and $\log(Mg^{2+})$ decreases → $\log(Mg^{2+})$ ↓ $\log(Ca^{2+})$ ↑
d. 2pH decreases and $\log(Mg^{2+})$ remains constant → $\log(Mg^{2+})$ constant $\log(Ca^{2+})$ ↑
e. 2pH remains constant and $\log(Mg^{2+})$ increases → $\log(Mg^{2+})$ ↑ $\log(Ca^{2+})$ const.

Because Mg/Si must increase and ($SiO_{2(aq)}$) increases, Mg must increase too, so only case a. fulfills the requirements.

- If ($SiO_{2(aq)}$) decreases, it follows that

  $\log(Mg^{2+})$ + 2pH increases. This is possible if

a. 2pH decreases less than $\log(Mg^{2+})$ increases → $\delta\log(Mg^{2+}) > \delta\log(Ca^{2+})$ both ↑
b. 2pH increases more than $\log(Mg^{2+})$ decreases → $|\delta\log(Ca^{2+})| > |\delta\log(Mg^{2+})|$ both ↓
c. 2pH increases and $\log(Mg^{2+})$ increases → $\log(Ca^{2+})$ ↓ $\log(Mg^{2+})$ ↑
d. 2pH remains constant and $\log(Mg^{2+})$ increases → $\log(Ca^{2+})$ = const. $\log(Mg^{2+})$ ↑
e. 2pH increases and $\log(Mg^{2+})$ remains constant → $\log(Ca^{2+})$ ↓ $\log(Mg^{2+})$ = const.

Because Mg/Si must increase and ($SiO_{2(aq)}$) decreases, cases a-e are all valid. However, case b. is only valid if $|\log(Mg^{2+})| < 2/3\log(SiO_{2(aq)})$.

The same type of reasoning as has been applied for [Mg]/[Si]>2/3, can be applied for the cases [Mg]/[Si] = 2/3 and for [Mg]/[Si]<2/3.

The results are summarized in table 5.1. As only directions in which the solution evolves are indicated and absolute concentrations are not given, activity coefficients can be disregarded.

The following symbols are used in the table:

Ca = $\log(Ca^{2+})$

Mg = $\log(Mg^{2+})$

Si = $\log(SiO_{2(aq)})$

↑ = concentration increases

↓ = concentration decreases

— = concentration remains constant

The composition of the water at the moment sepiolite starts to coprecipitate with calcite plots:

▲ in the MgO-CaO-sepiolite triangle

▲ in the CaO-SiO_2-sepiolite triangle

△ on the line joining calcite and sepiolite

Table 5.1

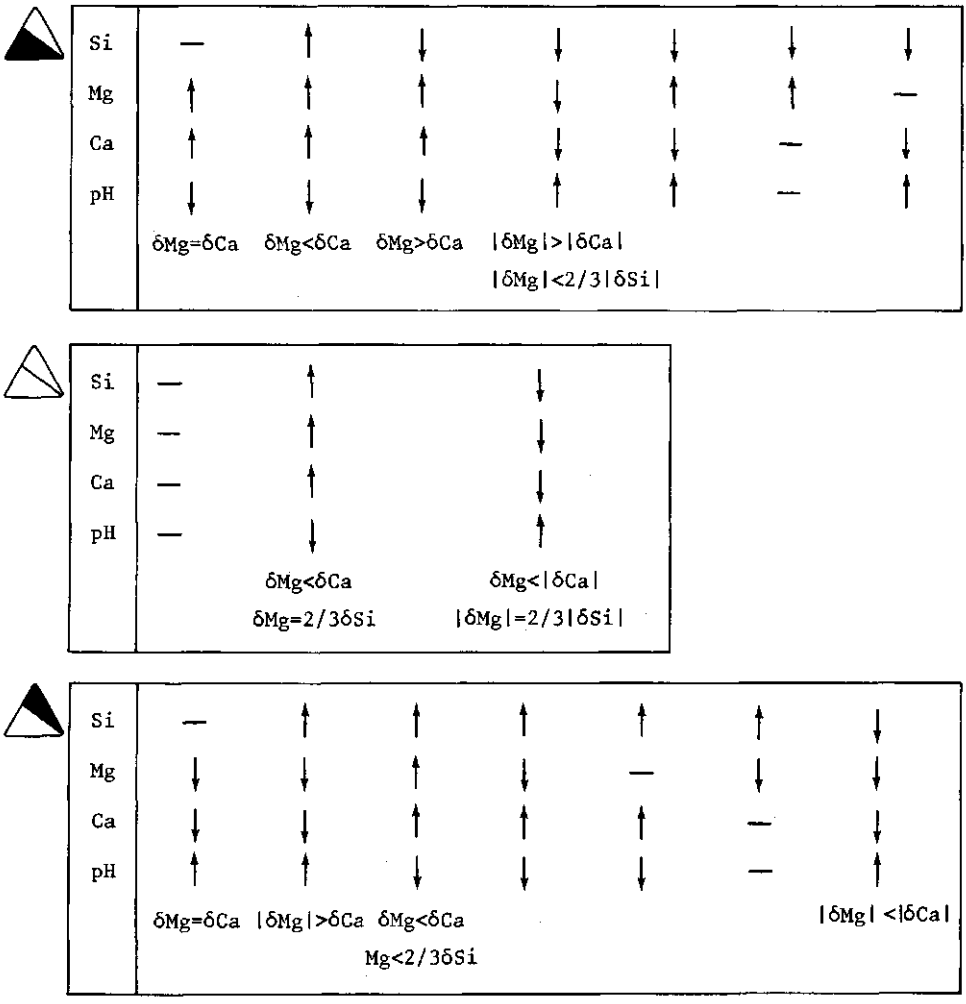

The problem can also be approached from the side of the electroneutrality-equation, rewritten from (14):

$$2[Ca^{2+}]+2[Mg^{2+}] = \underbrace{[HCO_3^-]+2[CO_3^{2-}]+[OH^-]-[H^+]}_{\text{alkalinity}}+\underbrace{[Cl^-]+2[SO_4^{2-}]-[Na^+]-[K^+]}_{\Delta'} \qquad (19)$$

From the carbonate equilibria (equation 2 to 5) an intimate relation between pH, p_{CO_2} and alkalinity can be derived (van Beek and van Breemen, 1973). At constant p_{CO_2} an increase of alkalinity implies an increase of pH and vice versa. When, during evaporation, calcite and sepiolite coprecipitate, Δ' remains constantly zero or the absolute value of Δ' increases. For the case Δ' remains zero we can derive the following relations:

a. alkalinity remains constant
   → pH constant and because $\log(Ca^{2+}) + 2pH$ = constant → (Ca^{2+}) is constant. From (19) it follows that the Mg-concentration must also remain constant. This combination is only possible when the composition of the solution at the moment sepiolite starts to coprecipitate with calcite (further called "comp.$_{sep.}$") plots on the join between sepiolite and calcite in the CaO-SiO_2-MgO diagram (see table 5.1).
b. alkalinity increases
   → pH increases → (Ca^{2+}) decreases. If alkalinity increases, the sum of the Ca and Mg concentrations must also increase which follows from equation (19) and therefore the Mg-concentration must increase more than the Ca-concentration decreases. From table 5.1 it follows that "comp.$_{sep.}$" plots in the MgO-CaO-sepiolite triangle.
c. alkalinity decreases
   → pH decreases → (Ca^{2+}) increases and therefore the Mg-concentration must decrease faster than Ca increases. "Comp. $_{sep.}$" plots in the CaO-SiO_2-sepiolite triangle.

The same type of reasoning can be followed for Δ' is negative and becomes more and more negative during evaporation and for Δ' is positive and becomes more and more positive during evaporation. The results are summarized in table 5.2.

If table 5.1 and 5.2. are combined, the relations between $2[Ca^{2+}] + 2[Mg^{2+}]$, the alkalinity, the Mg/Si-ratio and the sign of Δ' (see formula (19)) during coprecipitation of calcite and sepiolite can be derived. These relations are represented in fig. 5.5. The figure shows that if Mg precipitates as a silicate instead of a carbonate, increase of $[Ca^{2+}] + [Mg^{2+}]$ concentration does not necessarily imply a decrease in alkalinity and vice versa. This is in contrast to the conclusion of Surdam and Sheppard (1978). The precipitation of *sepiolite* may be the *second decisive step* in the evolution of brines.

If the alkalinity decreases after the precipitation of calcite and sepiolite a Na-Ca-Cl-SO_4 or a Na-Mg-Ca-Cl-SO_4-brine results. In such brines the

Table 5.2

$\Delta' = 0$

	1^a	1^b	1^c
alk.	—	↑	↓
pH	—	↑	↓
$Ca^{2+}+Mg^{2+}$	—	↑	↓
Ca^{2+}	—	↓	↑
Mg^{2+}	—	↑	↓
"comp.$_{sep.}$"	△	◭	△

$\Delta' > 0$

	2^a	2^b	2^{c1}	2^{c2}	2^{c3}
alk.	—	↑	↓	↓	↓
pH	—	↑	↓	↓	↓
$Ca^{2+}+Mg^{2+}$	↑	↑	—	↓	↑
Ca^{2+}	—	↓	↑		↑
Mg^{2+}	↑	↑	↓	↓	⇅
"comp.$_{sep.}$"	◭	◭	△	△	◭

$\Delta' < 0$

	3^a	3^{b1}	3^{b2}	3^{b3}	3^c
alk.	—	↑	↑	↑	↓
pH	—	↑	↑	↑	↓
$Ca^{2+}+Mg^{2+}$	↓	—	↑	↓	↓
Ca^{2+}	—	↓	↓	↓	↑
Mg^{2+}	↓	↑	↑	⇅	↓
"comp.$_{sep.}$"	△	◭	◭	◭	△

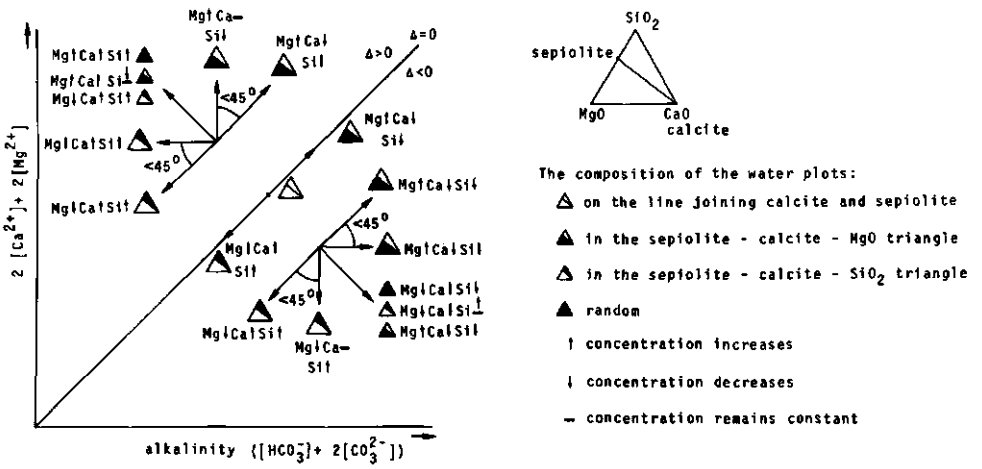

Fig. 5.5 The direction in which $2([Ca^{2+}]+[Mg^{2+}])$ and the alkalinity evolve, when during evaporation calcite and sepiolite coprecipitate, in relation with the initial Mg/Si ratio of the solution and the sign of Δ' (see (19)) at the moment the two minerals start to coprecipitate.

precipitation of *gypsum* is the *third decisive step*. The Ca^{2+}- and SO_4^{2-}-concentrations will change in opposite directions when during evaporation gypsum precipitates.

When the alkalinity increases after calcite and sepiolite coprecipitation, it depends on the initial Mg/Si ratio of the solution whether the $Na\text{-}CO_3\text{-}SO_4\text{-}Cl$-brine will contain Mg or not.

In this way six essentially different brines can originate after precipitation of calcite, precipitation of sepiolite and precipitation of gypsum as can be seen in fig. 5.6 (modified and simplified after Eugster and Hardie, 1978). From these brines six essentially different salt assemblages and different types of solonchaks originate through evaporation.

Sodium, unfortunately the most harmful ion for vegetation and for the physical properties of the soil, and chlorine are always present in the salt assemblages of external solonchaks, as can be seen from the flow-diagram of fig. 5.6. It depends on the initial composition of the inflow-waters whether the salts will contain Mg, Ca, SO_4 and carbonate in considerable amounts. A small difference of the Mg/Si ratio in the dilute stage may be enough to determine whether the groundwater will show Mg-enrichment or not, which in turn gives rise to completely different types of solonchaks.

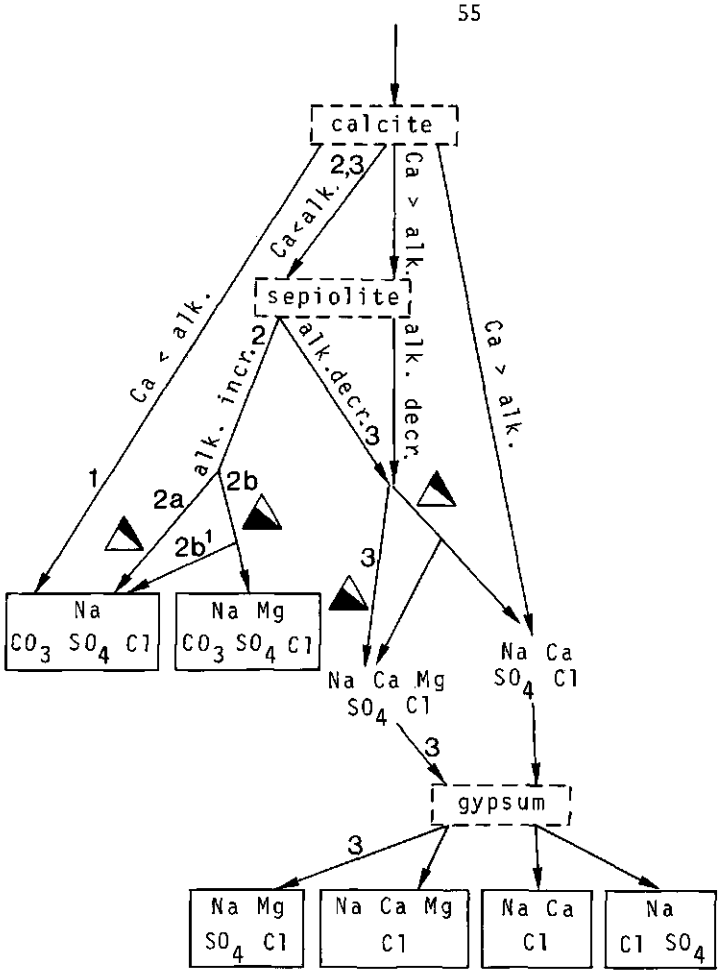

Fig. 5.6 A flow sheet of the evolution of waters during evaporation calcite-, sepiolite- and gypsum-precipitation. For explanation of the triangles, see fig. 5.5. (modified and simplified after Eugster & Hardie, 1978)

5.5 APPLICATION TO IRRIGATION OF SALT AFFECTED SOILS

The flow diagram of fig. 5.6 can be used in the opposite direction when irrigation is applied on salt-affected soils.

For example, if irrigation is planned for a salt-affected soil with salts of the Na-Cl-SO_4-type on it soil surface. The first irrigation water is used for leaching of these salts. If the crop which will be grown is sulphate-sensitive but chlorine tolerant, such as Parthenium argentatum Gray or Linum L., sufficient Ca must be added to the first irrigation water, causing the molar ratio of Ca/SO_4 to become larger than 1. This Ca can be added for example as calcium chloride. Subsequent evaporation and precipitation of gypsum will lower the sulphate concentration and the constituents of the soil solution will be Na, Ca and Cl.

6. APPLICATION OF THE MODEL OF BRINE EVOLUTION TO KONYA AND KENYA

6.1 SALTS

If we consider the salts which have been found on the soil surface (see table 3.2 and 4.2) there appears to be a striking difference in the type of salt minerals found in Kenya and those found in the Konya Basin.

The salts which occur at the soil surface are the most soluble ones. The less soluble salt minerals, which determine the composition of the residual brine, have precipitated at an earlier stage somewhere within the soil profile.

Konya

In the Konya Basin the salts are generally of the Na-Mg-SO_4-Cl-type. Halite and sulphates of sodium and magnesium are predominant but potassium and calcium bearing sulphates also occur. No chlorides of magnesium and calcium occur. From the flow diagram of Fig. 5.6 it is clear that precipitation of calcite, sepiolite and gypsum must have preceded the precipitation of the more soluble minerals at the soil surface in order to generate a brine of the Na-Mg-SO_4-Cl-type.

In the Akgöl plain (see fig. 3.4) different types of salts occur. Sodium bearing carbonates such as trona, thermonatrite, and burkeite have been found in addition to halite and thenardite.
Only the precipitation of calcite is required for the generation of the brine of the Na-CO_3-SO_4-Cl-type from which the salts found in the Akgöl plain have originated.

Along the craterwall of Krater Göl in the centre of the basin, sodaniter, a sodium nitrate, occurs in association with halite and gypsum.

The basin is covered with marl soils; therefore, it is difficult to see whether the calcite is a recent precipitate or is of detrital origin. Gypsum is also present in considerable amounts, both in the soil itself and at the soil surface where it is associated with the more soluble minerals.
Sepiolite was not found in the Konya Basin, but at the time of sampling there was no reason to search for it carefully.

Kenya

The salt associations observed in Kenya are different from those observed in

the Konya Basin. The most striking difference is the absence of Mg-salts from the salt assemblages on the soil surface in any of the Kenyan localities visited.

In Amboseli sodium carbonates such as trona and thermonatrite are predominant. Calcium is present in calcite and in the double-salts gaylussite and pirssonite. In addition, some sulphates occur, but no chlorides have been found. The type of minerals in the Amboseli Basin can best be described by the $Na\text{-}CO_3\text{-}SO_4\text{-}Cl$-type of fig. 5.6. Despite the fact that chlorides have not been found, the mineral association can be described by this type because chlorine does not take part in a decisive precipitation reaction and, therefore, when it is present in the initial dilute water, occurs in all six types of brines of fig. 5.6. This type of association originates if calcite and/or sepiolite precipitation are assumed. In Amboseli both calcite and sepiolite are present in considerable amounts (Stoessell, 1978).

The salt associations at Miti Bili, Kanam and Lake Simbi along Lake Victoria show the same type of minerals as those described from the Amboseli Basin. However, halite is present in addition to abundant trona and thermonatrite and, furthermore, sepiolite has not been found. At Sindo and Luanda only sulphate and chloride were observed. These associations can be characterised by the $Na\text{-}Cl\text{-}SO_4$-type. Calcite and gypsum precipitation are theoretically required to generate this type of brine and abundant calcite and gypsum are indeed present.

In the North of Kenya, east of Lake Turkana and in the Chalbi Desert, the salt minerals are mainly of the $Na\text{-}Cl\text{-}SO_4$-type with halite and thenardite as the main representatives.
This type requires the precipitation of calcite and gypsum and these minerals have been found. Sodium carbonates occur locally at North Horr in the north of the Chalbi Desert. The main salt representatives are trona and thenardite and the brine at this locality is of the $Na\text{-}CO_3\text{-}SO_4\text{-}Cl$-type. Such a brine can only originate if the composition of the dilute inflow water is such that calcite precipitation causes the final brine to become alkaline.

6.2 WATERCOMPOSITION IN THE SYSTEM $(Na+K)\text{-}Ca\text{-}Mg\text{-}Cl\text{-}SO_4\text{-}(HCO_3+CO_3)$

As with the salt associations, there are pronounced differences in the composition of groundwater at the different localities where the salt efflorescences have been sampled.

The water analyses (see table 3.1 and 4.1) can be plotted in the system $(Na+K)\text{-}Ca\text{-}Mg\text{-}Cl\text{-}SO_4\text{-}(HCO_3+CO_3)$. The molar ratios of the anions are plotted in a $Cl\text{-}SO_4\text{-}(HCO_3+CO_3)$-composition triangle and the molar ratios of the cations are

plotted in a (Na+K)-Ca-Mg-triangle (fig. 6.1). Such diagrams give information about the ratio of the ions present in the solution; they do not give information about total concentrations. It goes without saying that the sum of the anion-concentrations of a specific water is the same as the sum of the cation-concentrations. The composition of the waters will be dealt with on the basis of these diagrams.

Konya (Fig. 6.1a)

The three solid symbols in the diagram represent the inflow rivers - the Çarsamba from the southwest (locality T2), the Zanopa from the southeast (locality T12) and the Bor from the northeast (locality T27, fig. 3.2). The ratio carbonate/$Cl+SO_4$ for these inflow waters is much larger than for the more concentrated groundwaters. As a result of evaporation and precipitation of minerals, the composition of the solution changes in such a way that the ratio of the anions moves away from the carbonate corner and the ratio of the cations moves towards the sodium corner.

The waters from Akgöl are indicated with a different symbol because the mineralogical composition of the salt assemblages in the Akgöl plain differs from that at other sites. The Akgöl waters are rather poor in sulphate and magnesium.

Kenya (Fig. 6.1b)

From fig. 6.1b it is obvious that the composition of the waters from Kenya is different from that of the Konya waters (fig. 6.1a). The dilute inflow waters are poorer in Ca and Mg than the Konya-inflow waters. The composition of the more concentrated waters shows pronounced development towards the sodium-rich side of the diagram. With regard to the anionic composition, the ratio carbonate/$Cl+SO_4$ in both the dilute waters and the concentrated waters is very high, especially in the waters from Amboseli and those from Lake Victoria. It is evident that the waters from Sindo and Luanda are exceptional, just as the mineralogy of the salt associations at these localities are exceptional. Some Turkana waters also show a relatively high sulphate and chlorine content.

6.3 WATERCOMPOSITIONS IN THE SYSTEM $MgO-SiO_2-CaO$

A plot of the water compositions in the system $MgO-SiO_2-CaO$ can reveal whether sepiolite was a precipitate (see fig. 5.4a); if calcite and sepiolite coprecipitate during evaporation, the composition of the consequent concentrated waters

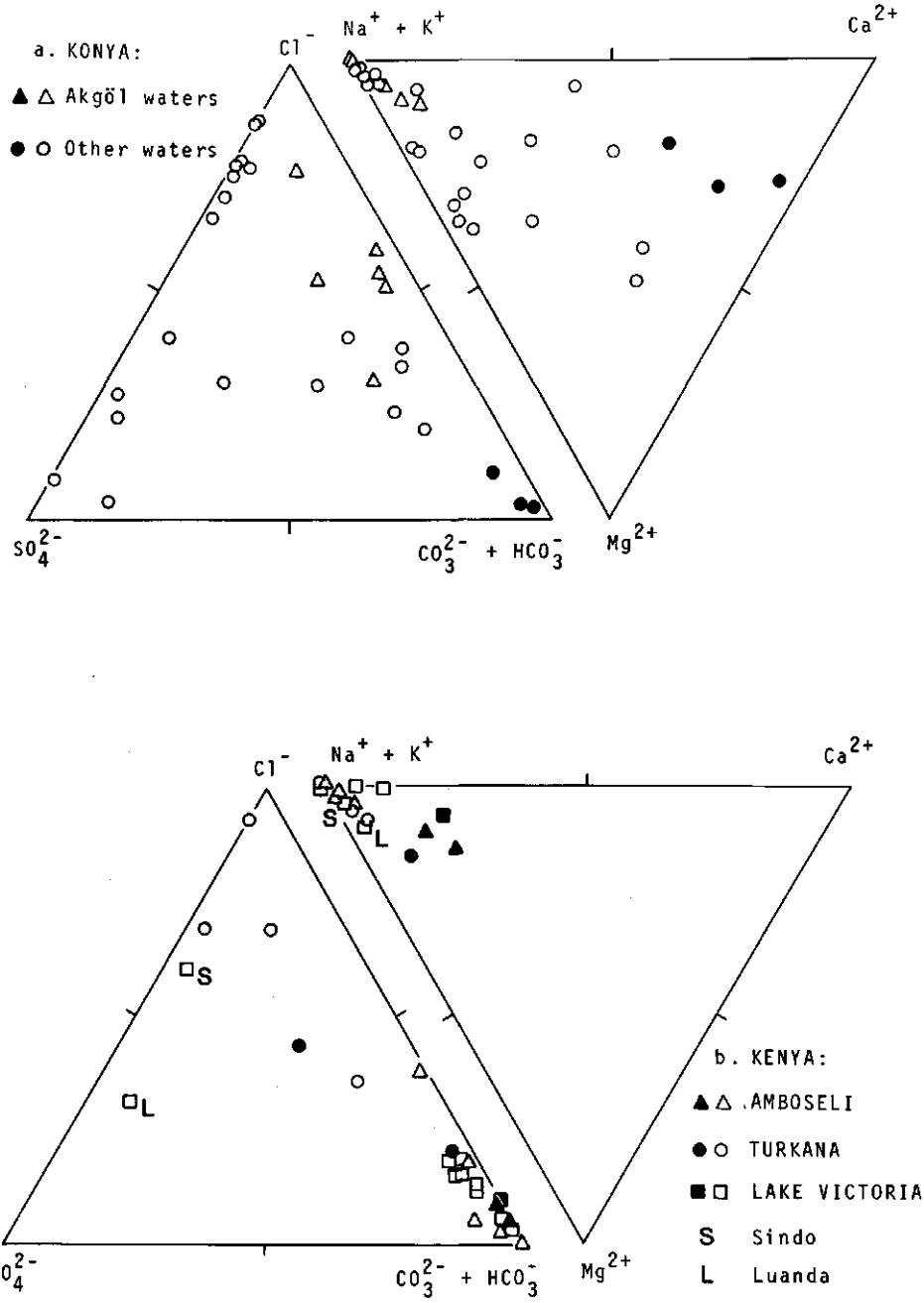

Fig. 6.1 Composition of water samples plotted in the system $Ca-(Na+K)-Mg-Cl-SO_4-(HCO_3+CO_3)$ from the Konya Basin in Turkey (a) and from different regions in Kenya (b) expressed in mole per cent. Solid symbols: surface inflow waters; open symbols: ground waters.

plot in the segment formed by the joins of calcite and the dilute inflow waters and of sepiolite and these waters (segment P, Q, MgO, R in fig. 5.4a).

Konya

Fig. 6.2a shows a plot of the waters from Konya in the $MgO-SiO_2-CaO$-system. Most waters plot in the MgO-calcite-sepiolite triangle and the more concentrated waters plot in the segment Q-MgO-R-dilute waters.
Although no sepiolite has been found in the Konya Basin, the pattern as shown in fig. 6.2a is an indication that sepiolite or another correlated Mg-silicate has precipitated.

Some waters from the Akgöl plain and three other waters form an exception to this pattern. However, this is not surprising because it has already been noted that the salt associations are also different and that for the generation of the Akgöl waters no sepiolite precipitation is required theoretically. Finally, the composition of the dilute inflow waters in the Akgöl plain is not known.

Kenya

Fig. 6.2b shows the composition of the waters from Kenya in terms of the system $MgO-SiO_2-CaO$. Again a striking difference with the Konya waters is apparent from this diagram.

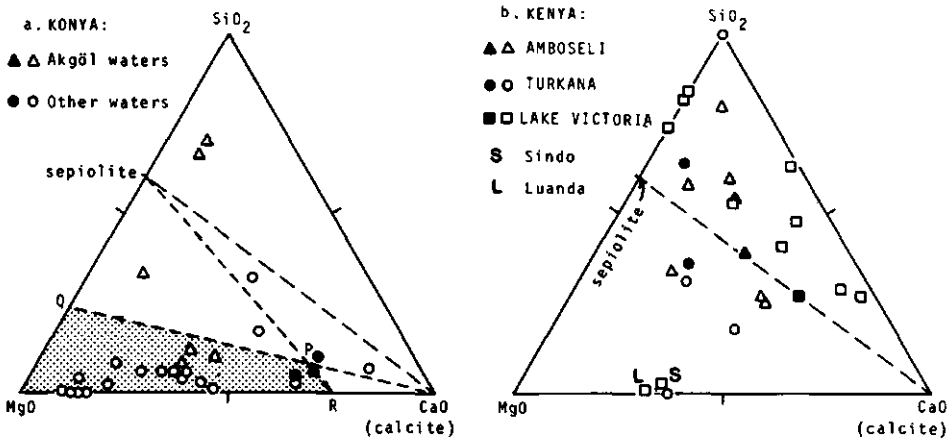

Fig. 6.2 Composition of water samples plotted in the system $CaO-MgO-SiO_2$ from the Konya Basin in Turkey (a) and from different regions in Kenya (b) expressed in mole per cent. Solid symbols: surface inflow waters; open symbols: ground waters.

The dilute water from the region along Lake Victoria plots on the join between calcite and sepiolite and the more concentrated waters plot above this join. This pattern is consistent with the coprecipitation of sepiolite and calcite. The exceptional position of the waters from Sindo and Luanda is clear. The generation of the type of brine at these localities does not require precipitation of sepiolite.

The waters both from the Amboseli Basin and from the region east of Lake Turkana and the Chalbi Desert show a rather scattered pattern around the join between calcite and sepiolite. No conclusions can be drawn from these patterns.

6.4 CONCENTRATION OF INDIVIDUAL IONS VERSUS CHLORINE CONCENTRATION

The evolution of the concentration of the individual ions can be evaluated by plotting the concentrations of these ions against chlorine concentration of the same sample. The chlorine concentration can be considered a measure of the concentration factor of the brines because the chlorides of the main compounds occurring in natural groundwaters and surface waters are very soluble (Eugster and Jones, 1977, 1979; Jacks, 1973).
Chlorides precipitate only at the final stage of evaporation and hence if an ion is not lost from a solution by precipitation or an other removal mechanism, its concentration factor is the same as that of chlorine. Therefore, if the log of the concentration of this specific ion is plotted versus the log of the chlorine concentration, the points form a straight line with slope 1. If an ion is removed from the solution and the log of its concentration is plotted versus its chlorine concentration, we will find a point which falls below this line of slope 1 and vice versa when an ion is enriched we will find a point which falls above this line.

Konya

In fig. 6.3 the log of the concentrations of Na, K, Ca, Mg, sulphate and the alkalinity are plotted versus the log of the chlorine concentration in the samples from the Konya Basin. It must be emphasized that the most soluble salts which can be found on the soil surface have not yet precipitated from these solutions. Again in these plots the Akgöl waters have been distinguished from the other waters.

The plot of Na versus Cl shows that during evaporation sodium is, like chlorine, a very conservative element. The sodium concentrations of the Akgöl waters and the other waters plot on a straight line with slope 1.

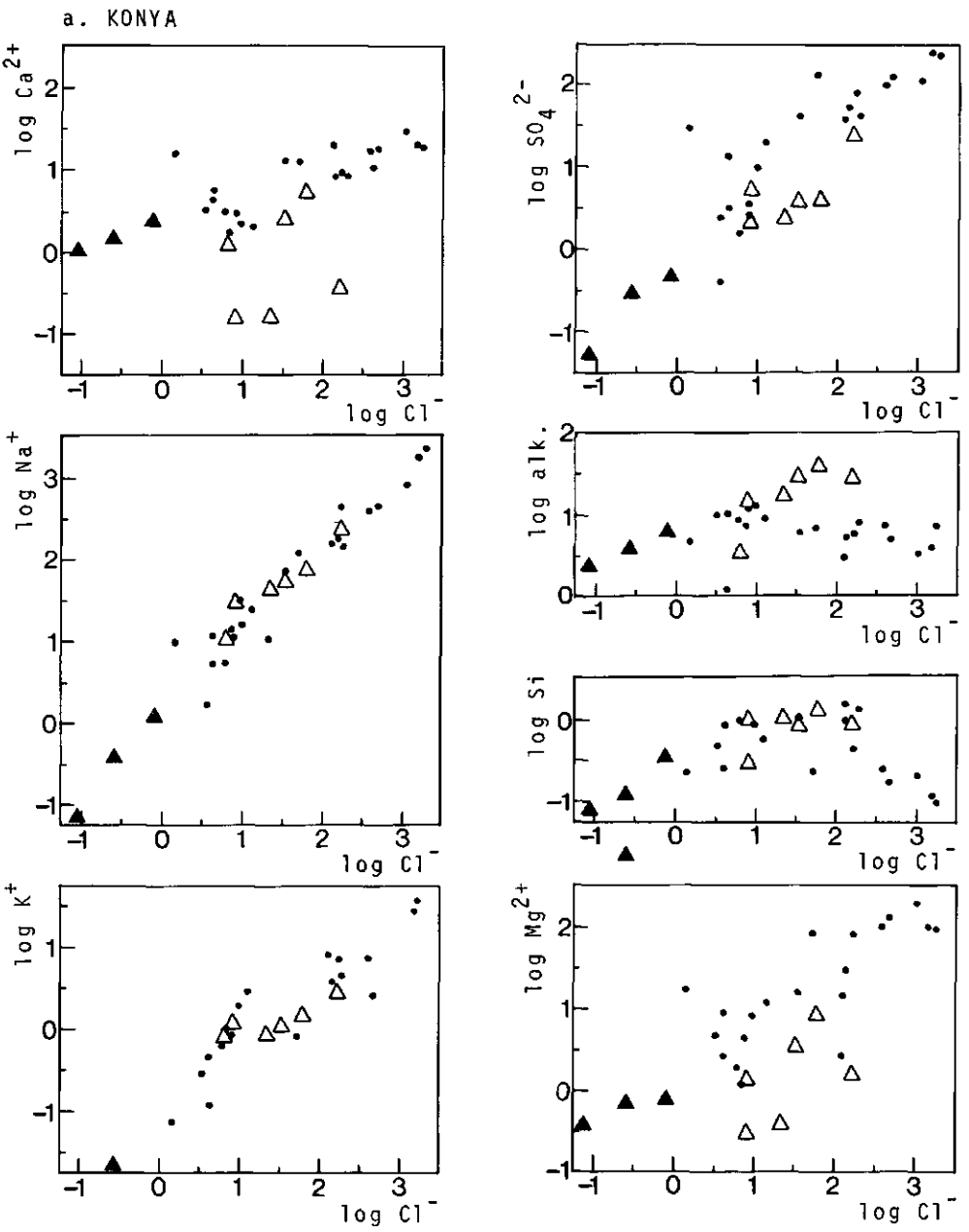

Fig. 6.3 Plots of the logarithm of ionic concentrations versus the logarithm of chlorine concentrations of water samples from the Konya Basin in Turkey. All concentrations expressed in mol m^{-3}, apart from alkalinity (eq m^{-3}). Solid triangles: surface inflow waters; open triangles: waters from the region near Akgöl; solid dots: other waters.

Potassium shows for the most part the same linear relationship as sodium apart from a small group of samples with a $\log Cl^-$ of about 1 which shows a larger increase in potassium concentration than can be explained by simple evaporation alone. The Akgöl waters are depleted in potassium; they show only a slight increase in potassium-concentration.

The absolute Ca-concentration gradually increases during evaporation with a slope less than 1. Therefore, Ca is already being removed from the solution at the dilute stage. The removal of Ca can easily be explained by the precipitation of calcite, which is consistent with the gradual decrease of the alkalinity. The Akgöl waters show just the opposite behaviour. The alkalinity, which is higher at the same chlorine concentration than the alkalinity of the other waters, increases. The Ca-pattern of the Akgöl waters shows no consistent behaviour but the Ca-concentration is in any case lower than the Ca-concentrations of the other waters.

The pattern of sulphate is rather scattered but in general sulphate is conserved till $\log Cl^-$ is about 2. From that stage on a small amount of sulphate is removed from the solution, but the concentration of sulphate in the solution still increases.
At this stage of evaporation sulphate is possibly removed by the precipitation of gypsum, which has been found in internal solonchaks (Driessen, 1970).

Silica is lost from the solution from the dilute stage. The silica concentration first slowly increases and thereafter decreases. The decrease of the silica concentration may be an indication that silica precipitates in combination with other components and not as, for example, silicagel or opaline silica. Precipitation of such species would cause the silica concentration to remain constant at constant pH. As the pH in the Konya Basin shows little variation (only at Akgöl is the pH somewhat higher than in the rest of the basin), pH variation is not the reason for the inflection of the silica concentration. The silica concentration of the Akgöl waters remains at a rather constant level so in the Akgöl plain silica may have precipitated as a low temperature polymorph of SiO_2.

The magnesium concentration initially increases and shows a positive correlation with chlorine, although there is a large spread in the data. From $\log Cl^-$ of about 2 the increase of the magnesium concentration levels off and finally magnesium concentration decreases. The decrease in magnesium concentration may be correlated with the decrease in the silica concentration, both being caused by sepiolite precipitation. The magnesium concentrations in the Akgöl waters are clearly lower than those in the other waters at the same con-

centration of chlorine. The pattern of Mg is irregular but corresponds with the irregular Ca-pattern of the Akgöl waters. This may be an indication that at Akgöl magnesium is not removed by sepiolite precipitation but by a co-precipitate of Mg and Ca such as magnesium calcite or dolomite.

Kenya

Conclusions drawn from plots of the concentration of the different ions versus chlorine are valid only for the Amboseli Basin because the homogeneity of the inflow waters has not been established for the other regions which were sampled in Kenya. Analyses from the samples of this study have been supplemented by the analyses given by Stoessell and Hay (1978). Stoessell and Hay's water-samples were collected in August, 1975, from streams, wells, swamps and pits. The waters from Amboseli show less clear patterns than the waters from Konya, but general trends can be deduced (fig. 6.4).

Sodium again appears to be a very conservative element. No removal takes place until the very concentrated stage.

Potassium is also conservative in the dilute stage but from a $\log Cl^-$ of about 0.5 a sudden removal of potassium takes place and the potassium concentration even decreases during further evaporation. Potassium removal can be explained by the precipitation of aphtithalite ($K_3Na(SO_4)_2$) which is found at different localities not only on the soil surface but even at a depth of about one metre in the soil profile itself. Sulphate is, like potassium, conservative in the dilute stage but again at $\log Cl^-$ of about 0.5 and higher sulphate is lost from the solution, although its concentration still increases. Whereas, during aphtithalite precipitation, both the sulphate and the sodium concentrations increase, the potassium concentration must necessarily decrease during further evaporation. This is compatible with the sodium, potassium and sulphate patterns.

Both the alkalinity and Ca in the solution increase up till a $\log Cl^-$ of about -0.5 is reached. From that point onwards both are removed from the solution. Alkalinity still increases but the Ca-plot shows an inflection point and the Ca concentration decreases. The contrasting behaviour of Ca and alkalinity during evaporation can be ascribed to the precipitation of calcite.

Si and Mg show the same behaviour. They both remain completely in solution till $\log Cl^-$ is about -1, then both are removed from the solution and their concentrations remain at a rather constant level and, finally, their concentrations decrease. Decrease of both magnesium and silica can be ascribed to the co-precipitation of sepiolite and calcite only when the Ca-concentration decreases and the alkalinity increases (see fig. 5.5). This is the case at Amboseli so

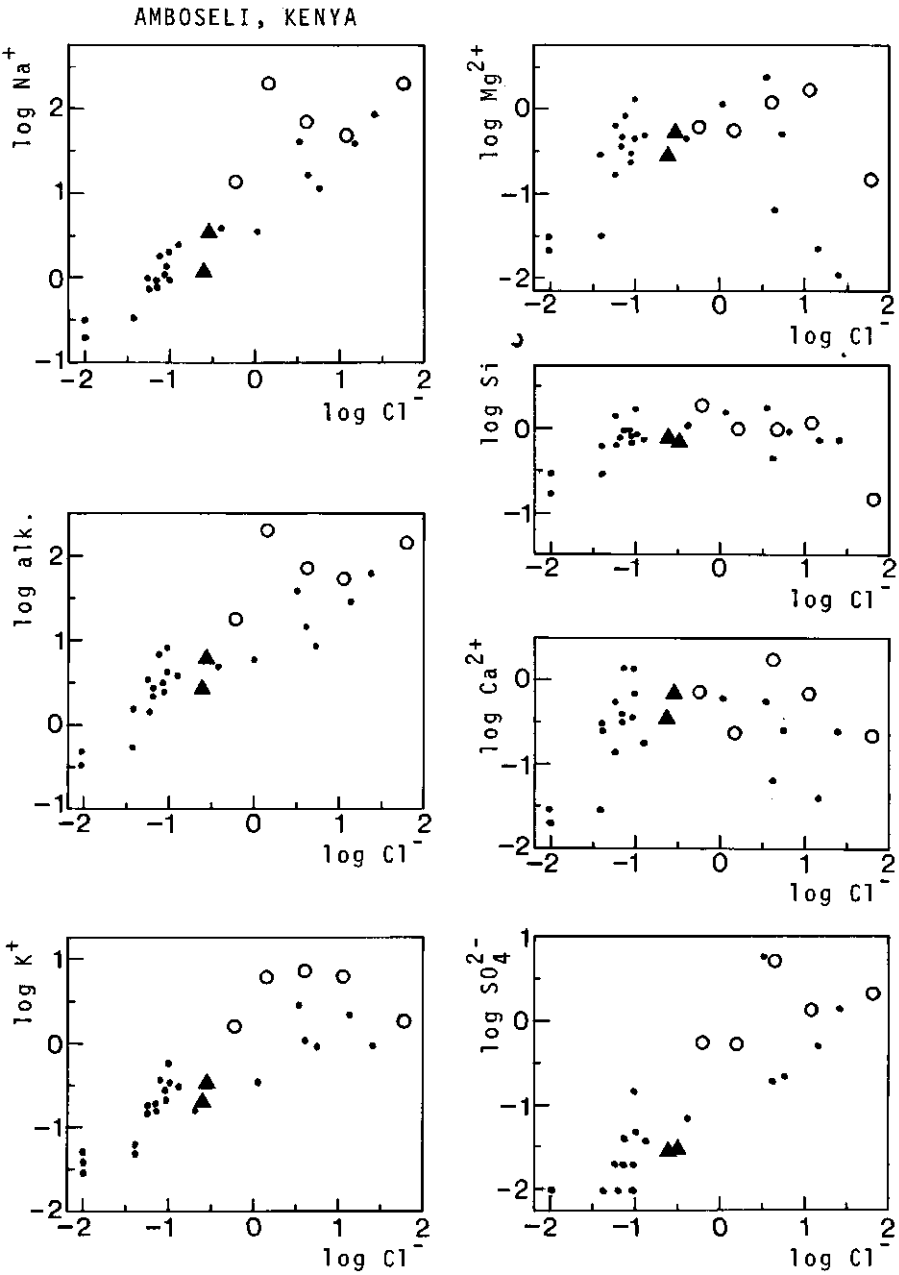

Fig. 6.4 Plots of the logarithm of ionic concentrations versus the logarithm of chlorine concentrations of water samples from the Amboseli Basin in Kenya. All concentrations expressed in mol m^{-3}, apart from alkalinity (eq m^{-3}). Solid dots: data from Stoessell & Hay (1978); solid triangles: surface inflow waters; open circles: ground waters.

the behaviour of Mg and Si can be explained by sepiolite precipitation.

6.5 CONCLUSIONS

The salts observed in the Konya Basin were compared with those observed in Kenya. Various diagrams were used to investigate the evolution of the main species in solution during evaporation and to test whether the principle of chemical divides is applicable to the areas studied. These diagrams are also of great help in establishing the homogeneity of the inflow waters.

Konya Basin

In the Konya Basin the brines and salt minerals are mainly of the Na-Mg-SO_4-Cl type. The salt minerals and brines at the Akgöl plain are of the Na-CO_3-SO_4-Cl-type.

Within the basin, no loss of sodium and potassium takes place until the very concentrated stage. The behaviour of the other solutes can be explained by the successive precipitation of calcite, sepiolite, or a related Mg-silicate, and gypsum.

The waters from the Akgöl plain can be distinguished from the other waters and it is concluded that these waters have a different origin. In Akgöl, sodium and potassium are also conservative elements. The congruency of the Ca- and Mg-patterns favours dolomite or magnesium calcite precipitation over sepiolite precipitation. The constancy of the silica concentration is probably controlled by the precipitation of a polymorph of SiO_2 such as opaline silica or silicagel.

Kenya

The waters and salt minerals in Kenya are in general very carbonate-rich. The waters from the Amboseli Basin and those found along Lake Victoria are of the Na-CO_3-SO_4-Cl-type apart from the localities of Sindo and Luanda which are of the Na-SO_4-Cl-type. The waters east of Lake Turkana are also mainly of the Na-SO_4-Cl-type.

The description of the evolution of the brines is restricted to the Amboseli Basin because the homogeneity of the inflow waters in the other districts was not established. In Amboseli Na is a very conservative element as in the Konya Basin. Mg and Si are lost from the solution from a $\log Cl^-$ value of about -1, Ca and alkalinity are removed from a $\log Cl^-$ value of about -0.5 and, finally, K and SO_4 are removed from a $\log Cl^-$ value of about 0.5. The behaviour of these solutes can be described by calcite, sepiolite and aphtithalite precipitation respectively.

7. MINERALOGY

7.1 IDENTIFICATION OF MINERALS

Salt minerals of both the naturally occurring salt efflorescences and the salts precipitated in the evaporation experiments in the laboratory (see section 8.2) were identified by means of X-ray diffraction analysis with a Nonius Guinier camera FR 552 with a high resolving Johansson $K\alpha_1$ monochromator, using $CoK\alpha_1$ radiation (λ = 0.17889 nm). Table 7.1 shows a survey of all identified salt minerals present in the samples of this study and the characteristic d-values of their X-ray patterns. These characteristic line positions are not necessarily the strongest ones.

It happened not infrequently that a salt assemblage showed a number of unidentiable X-ray reflections. Two unknown X-ray diffraction patterns belonging to unknown minerals occurred regularly. Special attention was paid to these two unknown minerals. Both compounds could be synthesized, analysed and their complete X-ray diffraction pattern was determined. One of those, the mineral named "eugsterite", is accepted as a new mineral by the Commission on new minerals and mineral names of the IMA (see section 7.3). The other one, named "konyaite", is submitted to the Commission on new minerals and mineral names of the IMA. For a description of "konyaite", see section 7.4.

7.2 CRYSTALLOGRAPHIC PROPERTIES

The crystallographic properties, such as crystal system, crystal class, space group, unit cell dimensions and the optical properties of all minerals listed in table 7.1 are described extensively in Dana, Volume II (1957) apart from those of the minerals burkeite, darapskite, gaylussite, loeweite and starkeite and of course the new mineral eugsterite. The data of darapskite can be found in Ericksen and Mrose (1970), those of starkeite in Baur (1962), those of loeweite in Fang (1970) and those of gaylussite were described by Maglione (1968). Crystallographic data of eugsterite and konyaite are given in section 7.3 and section 7.4 respectively. Burkeite is a mineral which is very rarely described in literature. A special paper was written about this mineral as it occurs frequently both in Kenya and in the Konya Basin, cf. section 7.5.

Table 7.1 Characteristic d-values of salt minerals. Intensities between brackets

	mineral	d - values (Å)
1.	aphtithalite $K_3Na(SO_4)_2$	4.09(30) 2.940(75) 2.839(100)
2.	arcanite K_2SO_4	4.162(41) 2.997(92) 2.902(100) / 2.886(76)
3.	aragonite $CaCO_3$	3.396(100) 3.273(52) 1.977(65)
4.	bloedite $Na_2Mg(SO_4)_2.4H_2O$	4.56(95) 4.28(30) 3.29(95) 3.25(100)
5.	burkeite $Na_6(CO_3)(SO_4)_2$	3.795(75) 3.526(80) 2.801(100) / 2.777(55)
6.	calcite $CaCO_3$	3.86(12) 3.035(100) 2.495(14)
7.	darapskite $Na_3(NO_3)(SO_4).H_2O$	10.3(100) 3.46(35) 2.871(30)
8.	dolomite $CaMg(CO_3)_2$	3.69(5) 2.886(100) 2.192(30) 2.015(15)
9.	epsomite $MgSO_4.7H_2O$	5.99(22) 5.35(26) 4.21(100) 2.677(24) / 2.659(22)
10.	eugsterite $Na_4Ca(SO_4)_3.2H_2O$	9.20(39) 5.50(64) 4.50(33) 3.428(100)
11.	gaylussite $Na_2CO_3.CaCO_3.5H_2O$	6.41(95) 4.50(45) / 4.43(40) 3.21(100)
12.	glauberite $Na_2Ca(SO_4)_2$	6.22(8) 3.18(75) 3.13(100) 3.11(80)
13.	gypsum $CaSO_4.2H_2O$	7.61(45) 4.28(90) 3.06(55) 2.87(25)
14.	halite NaCl	2.821(100) 1.994(55) 1.628(15)
15.	hexahydrite $MgSO_4.6H_2O$	5.45(50) 5.10(45) 4.39(100)
16.	kainite $KMgClSO_4.3H_2O$	8.115(69) 7.771(83) 7.372(100) 3.08(86)
17.	konyaite $Na_2Mg(SO_4)_2.5H_2O$	12.01(57) 4.541(100) 4.002(88) 3.960(70)
18.	loeweite $Na_{12}Mg_7(SO_4)_{13}.15H_2O$	10.3(80) 9.41(25) 4.29(95) 4.04(95) 3.17(100)
19.	nahcolite $NaHCO_3$	5.91(16) 4.84(25) 3.482(30) 3.082(25) / 3.059(35) 2.956(70) / 2.936(100)
20.	niter KNO_3	4.66(23) / 4.58(11) 3.78(100) / 3.73(56) 2.662(41) / 2.647(55) / 2.632(30)

Table 7.1 Continued

mineral	d. values			
21. northupite $Na_6Mg_2Cl_2(CO_3)_4$	8.08(50)	4.96(30)	2.697(75)	2.473(100)
22. nesquehonite $MgCO_3.3H_2O$	6.48(100)	3.04(30)	2.617(55)	
23. pirssonite $Na_2Ca(CO_3)_2.2H_2O$	5.13(70) / 4.93(60)		2.654(90) / 2.565(80) / 2.506(100)	
24. sodaniter $NaNO_3$	3.89(6)	3.03(100)	2.311(25)	
25. schoenite/ picromerite $K_2Mg(SO_4)_2.6H_2O$	7.14(25)	4.16(85) / 4.06(95)		3.71(100)
26. starkeite (leonhardtite) $MgSO_4.4H_2O$	6.83(45)	5.43(75)	3.951(65)	
27. thenardite Na_2SO_4	4.66(73)	3.178(51)	3.075(47)	2.646(48)

Scanning Electron Microscopy was applied to the salt minerals which are the main constituents of the salt efflorescences in order to reveal the crystal habit and the morphology of these salts (see section 7.6).

7.3 EUGSTERITE, A NEW SALT MINERAL

Occurrence

Eugsterite has been found in Kenya, in the Great Konya Basin and on bricks of Dutch river clays.

- *Kenya*. In Kenya eugsterite has been found along the shore of Lake Victoria, at Sindo and Luanda (see fig. 4.3). There it occurs as a surface mineral in association with thenardite and halite. It is also found at Kalacha, Turkana district, east of the Chalbi Desert in the north of Kenya (see fig. 4.4). In this area vast salt efflorescences occur and eugsterite is found in association with halite and thenardite. The groundwaters at the localities where eugsterite has been found, are of the $Na\text{-}SO_4\text{-}Cl$-type.
- *Konya Basin*. In the Konya Basin eugsterite has been found in association with sulphates and chlorides of sodium and magnesium. It occurs in the following associations: eugsterite, halite, thenardite; eugsterite, bloedite;

eugsterite, halite, gypsum; eugsterite, halite, glauberite; eugsterite, halite, glauberite, thenardite, nesquehonite. This last association was found around the historical medicinal spring of Tiana. Formulae of the minerals are given in table 3.2.

The analyses of the waters at the sites where eugsterite has been found both in Kenya and in the Konya Basin, have been plotted in fig. 7.1.

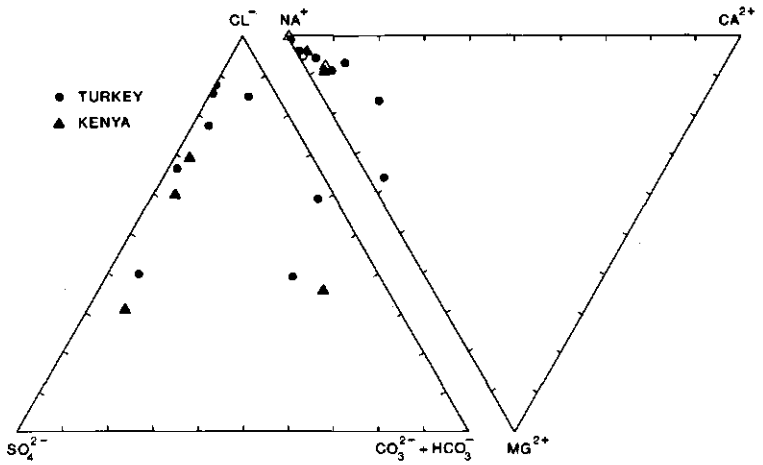

Fig. 7.1 Composition of ground waters at the localities where eugsterite has been found in the Konya Basin in Turkey and in different regions in Kenya plotted in the system Ca-(Na+K)-Mg-Cl-SO_4-(HCO_3+CO_3) expressed in mole per cent.

Type locality is the playa north-east of the village of Karapinar which is situated along the main road from Konya to Eregli. In summer this playa is covered with a flinty white salt crust which consists of halite, thenardite and eugsterite.

- *Bricks*. Eugsterite has been found in salt efflorescences on freshly laid bricks of Dutch river clays in association with gypsum.

Chemical analysis

In order to determine the composition of eugsterite, since the minute amounts of material available precluded conventional chemical analysis, a preliminary investigation was made by DTA.

A natural sample of eugsterite with thenardite and halite shows a sharp endo-

thermic reaction between 165° and 185°. A Mettler TA 2000 B DTA apparatus was used. The reaction product contained glauberite so it seemed likely that eugsterite could be a sodium-calcium-sulphate-hydrate. In addition, qualitative analysis with an electron microscope equipped with an energy-dispersive system established that Na, Ca and S are the major components.

The mineral was synthesized, because the naturally occurring eugsterite always occurs with other minerals and because the grain size was very small (see fig. 7.2). Solutions of sodium sulphate and gypsum were evaporated on a water bath of 60° C and eugsterite formed in considerable amounts in solutions with a molar ratio Na/Ca > 4 together with thenardite and gypsum. Eugsterite did not form from the same solutions at room temperature. Thenardite and gypsum could be separated with a heavy liquid with d = 2.50. Eugsterite occurred both in the heavier fraction together with thenardite and in the lighter fraction together with gypsum because of its sticky character. The tiny eugsterite fluffs were separated from the fraction with gypsum by handpicking under a binocular. The gypsum contamination of the samples (sample size approximately 1 mg) was determined with the aid of a DTA apparatus. These samples showed in addition to the large endothermic peak of eugsterite only very small negligible gypsum peaks. Na- and Ca-content of the samples were analysed by atomic absorption. Sulphate could not be analysed as well because of the small sample size. From the fraction of eugsterite with thenardite, weight loss after heating was determined with a TGA apparatus (Dupont TA 990). In this fraction all Ca and H_2O belongs to eugsterite so the H_2O/CaO ratio of eugsterite could be determined. These samples were large enough to analyse sulphate as well. Results of analyses are given in table 7.2. Combination of these two sets of analyses leads to the ideal formula $Na_4Ca(SO_4)_3.2H_2O$.

X ray crystallography

The X-ray diffraction pattern (table 7.3) was determined for synthetic material as these films were much less complicated than the films of the natural occurrences. Only the pattern of thenardite or gypsum had to be subtracted. The line positions of natural eugsterite agree exactly with those of synthetic eugsterite and comparison of many films showed no shift of lines at all.

It has not been possible to calculate the unit cell by means of the powder data. With a computer program (Visser, 1969) many solutions were obtained but none was very satisfactory. Efforts to grow larger crystals for a single-crystal analysis did not succeed.

Table 7.2 Chemical analyses of synthetic samples

D.T.A. samples	1	2	3
Na mmol	9.15×10^{-3}	9.0×10^{-3}	9.15×10^{-3}
Ca mmol	2.33×10^{-3}	2.25×10^{-3}	2.33×10^{-3}
Na/Ca	3.93	4	3.93

T.G.A. samples	1	2
Na mmol	0.150	0.019
Ca mmol	0.0226	0.0045
SO_4 mmol	0.10	0.0138
H_2O mmol	0.049	0.0087
H_2O/Ca	2.16	1.93

Morphology, crystallograpy and physical and optical properties

The mineral forms clusters of thin fibres. The naturally-occurring fibres have a thickness of 0.5 - 1.5 µm and they are up to 40 µm long. The synthetic fibres are 2 - 6 µm thick and up to 200 µm long (measured on SEM pictures, see fig. 7.2). The mineral is colourless and transparent; its hardness is very low and it is soluble in water. The density could not be measured due to its sticky nature. In the heavy liquid with d = 2.50, the upper fraction consists of mixtures of eugsterite and gypsum, whereas the lower fraction is composed of eugsterite and thenardite.

The SEM picture of the synthetic material shows the symmetry most probably to be monoclinic with $a \hat{} c = 116^{\circ}$.

Optically it is biaxial, but the axial angle could not be determined on account of the fibrous habit. Refractive indices are $1.492 \leq \alpha, \beta, \gamma \leq 1.496$; birefringence = 0.004, n_γ // b, $n_\beta \hat{} c = 27^{\circ}$.

Discussion

Eugsterite is a very common salt mineral which forms during evaporation of nonalkaline waters. The mineral is synthesized easily at 60° while at room temperature it did not form. This may be an indication that it is a metastable

Table 7.3 X-ray diffraction powder pattern of synthetic eugsterite

Line positions measured by Dr. J.W. Visser at the Technisch Fysische Dienst at Delft using a Guinier camera with $CuK_{\alpha}1$ radiation, λ = 0.15406 nm, and a special densitometer for Guinier films.

d(Å)	I	d(Å)	I	d(Å)	I
12.62	1	2.545	5	1.7126	61
9.20	39	2.458	5	1.6999	4
6.32	4	2.291	5	1.6809	5
5.96	1	2.284	2	1.6632	6
5.50	64	2.231	2	1.6530	4
5.35	1	2.214	2	1.6459	<1
4.64	5	2.178	2	1.6198	3
4.60	5	2.170	<1	1.6053	2
4.58	8	2.158	<1	1.5901	1
4.50	33	2.148	2	1.5829	2
4.20	4	2.132	2	1.5523	3
3.860	7	2.112	2	1.5418	<1
3.819	5	2.043	1	1.5318	<1
3.622	3	2.013	7	1.5234	<1
3.590	2	1.9837	2	1.5148	2
3.454	32	1.9546	3	1.5046	<1
3.428	100	1.9431	4	1.4963	3
3.233	4	1.9291	2	1.4645	1
3.211	10	1.9199	<1	1.4599	<1
3.150	4	1.9081	<1	1.4536	1
3.118	<1	1.8935	<1	1.4293	2
3.065	15	1.8835	3	1.4178	3
3.054	6	1.8494	5	1.4021	2
2.973	2	1.8406	1	1.3869	1
2.936	16	1.8313	5	1.3820	<1
2.893	8	1.8125	6	1.3654	1
2.797	19	1.7998	4	1.3555	2
2.763	25	1.7922	2	1.3470	<1
2.746	46	1.7648	1	1.3353	3
2.727	8	1.7619	2	1.3299	<1
2.671	13	1.7273	3	1.3234	2

mineral under natural circumstances.

Hydroglauberite is the only other known sodium-calcium-sulphate-hydrous mineral. However, the X-ray pattern of hydroglauberite differs essentially from that of eugsterite (Slyusareva, M.N., 1969). An unknown sodium-calcium-sulphate-hydrate, called phase X, has been found by L.A. Hardie, Johns Hopkins University, Baltimore, in Saline Valley and by R.C. Erd of the U.S. Geological Survey in the Death Valley salt pan associated with glauberite, thenardite and gypsum (both from L.A. Hardie, unpublished Ph.D. thesis, Johns Hopkins University). This mineral was not chemically analysed but Hardie assumed it to be the same as what is known as "labile salt", a synthetic double salt ($2Na_2SO_4.CaSO_4.2H_2O$) (Hill and Wills, 1938). No X-ray data are available for "labile salt". The X-ray powder diffraction pattern given to "labile salt" by Conley and Bundy (1959) is for thenardite, which is already noted by Braitsch (1971, p. 76). The line positions of the X-ray powder pattern of Hardie's phase X agree fairly well with that of eugsterite. There are, however, some differences in intensities. It is very probable that eugsterite is the same as Hardie's phase X and as "labile salt".

The mineral is called "eugsterite" after Hans P. Eugster, The Johns Hopkins University, Baltimore, Maryland, who has extensively studied the origin and mineralogy of saline lakes.

The mineral and the name were approved by the Commission on New Minerals and Mineral Names, IMA. A revised version of this section will be published in American Mineralogist (in press).

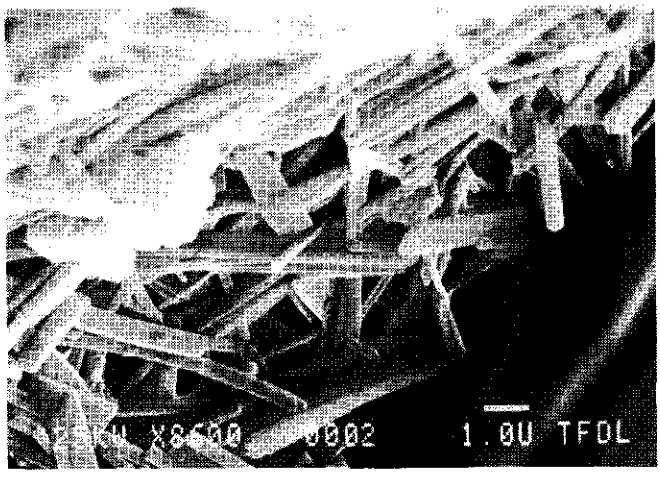

Fig. 7.2 S(canning) E(lectron) M(icroscope) picture of natural eugsterite in association with halite.

7.4 KONYAITE, A NEW SALT MINERAL

(co-authors J.D.J. van Doesburg and L. van der Plas)

Occurrence

Konyaite has been found in salt efflorescences on salt affected soils in the Great Konya Basin in Turkey. It occurs in the following assemblages: konyaite, calcite, gypsum, hexahydrite, bloedite; konyaite, bloedite, hexahydrite, gypsum; konyaite, bloedite, halite, starkeite; konyaite, bloedite, gypsum, halite, calcite; konyaite, calcite, gypsum, hexahydrite; konyaite, loeweite, hexahydrite; (for formulae of these minerals, see table 3.2).

The type locality is in the Great Konya Basin in Turkey along the road from Ereğli to Niğde near the village of Çakmak.

Synthesis and chemical analysis

Because most minerals which occur in association with konyaite contain Na_2SO_4 and/or $MgSO_4$, it was considered likely that konyaite also contains these components. The mineral has been synthesized by evaporation of a solution of Na_2SO_4 and $MgSO_4$ in a molar ratio 1:1 in a watch-glass in the oven at a temperature of 35^{o} C. In this way a white powder consisting of pure konyaite formed. Larger crystals formed by evaporation of a saturated solution using a second larger watch-glass as a cover glass; white powderish salt consisting of pure konyaite crept over the rim of the watch-glass and in the centre transparent single crystals formed.

Table 7.4 shows the chemical analysis of synthetic konyaite. Sodium and magnesium were analysed by means of Atomic Absorption Spectrometry. The sulphate content was determined by means of gravimetric analysis. The water content was determined with a TGA apparatus (Dupont TA 990). The analysis leads to the ideal formula $Na_2Mg(SO_4)_2.5H_2O$.

Table 7.4 Chemical analysis of synthetic konyaite

		1	2	mean value	theoretical
Na	%	13.06	13.14	13.10	13.05
Mg	%	6.99	6.89	6.94	6.90
SO_4	%	53.93	54.14	54.04	54.51
H_2O	%	25.25	25.63	25.44	25.54
				99.52%	100.00%

Table 7.5 X-ray diffraction powder pattern of Konyaite

$d(\text{Å})_{obs}$	$d(\text{Å})_{calc}$	I	hkl	$d(\text{Å})_{obs}$	$d(\text{Å})_{calc}$	I	hkl
12.01	12.010	57	020	2.415	2.416	11	$25\bar{1}$
7.62	7.616	12	011	2.402	2.402	39	220
6.00	6.005	2	040	2.337	2.337	36	$26\bar{2}$
5.76	5.757	19	$10\bar{1}$	2.323	2.323	14	142
5.67	5.670	9	031	2.309	2.309	4	$25\bar{3}$
5.19	5.192	9	$12\bar{1}$	2.300	2.301	5	0101
4.806	4.803	27	110	2.270	2.269	5	$24\bar{0}$
4.677	4.674	2	$13\bar{1}$	2.250	2.250	2	$13\bar{4}$
4.541	4.539	100	120	2.232	2.231	7	152
4.409	4.408	59	$11\bar{2}$	2.222	2.223	8	$09\bar{2}$
4.202	4.201	65	$12\bar{2}$	2.204	2.204	8	$22\bar{4}$
4.180	4.181	17	130	2.183	2.183	14	250
4.017	4.015	9	002	2.158	2.157	8	1100
4.002	4.003	88	060	2.132	2.132	7	$16\bar{2}$
3.960	3.960	70	$01\bar{2}$	2.117	2.117	3	$110\bar{2}$
3.916	3.912	3	$13\bar{2}$	2.101	2.100	1	$24\bar{4}$
3.797	3.797	9	140	2.090	2.090	1	$26\bar{0}$
3.592	3.589	36	032	2.078	2.078	11	$28\bar{2}$
3.448	3.449	10	101	2.060	2.061	4	0102
3.434	3.431	12	150	2.052	2.052	10	$21\bar{1}$
3.413	3.414	33	111	2.038	2.038	5	$19\bar{3}$
3.337	3.338	19	042	2.030	2.029	4	221
3.315	3.315	12	$12\bar{1}$	2.007	2.008	4	004
3.278	3.278	21	$15\bar{2}$	2.000	2.001	23	014
3.156	3.157	22	$10\bar{3}$	1.994	1.994	12	270
3.130	3.131	21	$11\bar{3}$	1.978	1.980	3	024
3.101	3.101	8	160	1.962	1.963	4	$11\bar{1}2$
3.080	3.081	15	052	1.957	1.957	6	$29\bar{2}$
2.988	2.991	31	$14\bar{1}$	1.954	1.954	13	103
2.937	2.937	15	$13\bar{3}$	1.946	1.947	10	$11\bar{3}$
2.881	2.879	1	$20\bar{2}$	1.935	1.936	10	$17\bar{4}$
2.855	2.858	1	$21\bar{2}$	1.928	1.930	4	$18\bar{2}$
2.834	2.835	13	062	1.920	1.919	2	$30\bar{3}$
2.812	2.811	16	170	1.903	1.904	7	044
2.801	2.799	35	$22\bar{2}$	1.897	1.898	12	$13\bar{3}$
2.778	2.776	22	$21\bar{1}$	1.868	1.869	25	$21\bar{5}$
2.724	2.722	35	$22\bar{1}$	1.852	1.853	4	$11\bar{2}0$
2.710	2.709	12	232	1.843	1.843	7	$10\bar{5}$
2.659	2.660	51	$01\bar{3}$	1.825	1.823	10	$31\bar{4}$
2.639	2.638	50	$23\bar{1}$	1.819	1.818	10	$34\bar{2}$
2.611	2.613	10	$02\bar{3}$	1.808	1.807	10	$32\bar{4}$
2.597	2.596	55	$24\bar{2}$	1.800	1.801	2	$01\bar{3}1$
2.572	2.572	9	223	1.790	1.791	3	$01\bar{2}2$
2.558	2.560	2	180	1.782	1.782	11	$33\bar{4}$
2.532	2.533	2	091	1.755	1.756	9	163
2.504	2.506	1	112	1.738	1.739	2	$11\bar{0}2$
2.479	2.479	6	163	1.732	1.731	3	$1\bar{1}21$
2.469	2.466	1	122	1.723	1.722	14	$36\bar{2}$
2.443	2.445	5	043	1.720	1.720	12	212
2.432	2.433	13	171	1.715	1.716	7	$01\underline{4}0$

Table 7.5 continued

$d(Å)_{obs}$	$d(Å)_{calc}$	I	hkl	$d(Å)_{obs}$	$d(Å)_{calc}$	I	hkl
1.707	1.707	10	222	1.578	1.578	9	$01\bar{4}2$
1.691	1.692	3	$01\bar{1}3$	1.564	1.565	6	$22\bar{6}$
1.679	1.679	3	$01\bar{3}2$	1.555	1.556	1	134
1.668	1.669	3	$08\bar{4}$	1.539	1.540	1	0104
1.663	1.663	3	$36\bar{4}$	1.533	1.534	1	$1\bar{4}4$
1.655	1.657	4	$24\bar{2}$	1.522	1.522	1	1150
1.643	1.644	4	$11\bar{4}1$	1.515	1.516	6	$19\bar{5}$
1.636	1.636	4	$33\bar{5}$	1.507	1.508	3	$11\bar{6}$
1.630	1.630	4	291	1.498	1.498	9	2111
1.623	1.623	9	252	1.475	1.476	2	$01\bar{6}1$
1.610	1.610	3	345	1.468	1.469	10	$26\bar{6}$
1.602	1.601	4	330				

X ray Crystallography

About 25 X-ray reflections of naturally occurring konyaite have been obtained by comparison of the X-ray diffraction patterns of the assemblages in which konyaite occurred after subtraction of the reflections of the other known minerals in these assemblages. It was impossible to separate konyaite from its associating minerals. Therefore, the complete X-ray diffraction pattern was determined for synthetic material with a Nonius Guinier camera FR 552 with a high resolving Johansson $K\alpha_1$ monochromator, using $CoK\alpha_1$ radiation (λ = 0.17889 nm). Table 7.5 shows the X-ray diffraction pattern. An X-ray powder photograph of the larger single crystals proved that this X-ray pattern belongs to one pure mineral and not to a mixture of more minerals. The purity of the single crystals was established by means of single crystal photographs. The intensities were measured with a densitometer.

Unit cell data were obtained from the powder data using a computer program (Visser, 1969). The mineral is monoclinic, a = 0.8066 nm, b = 2.4025 nm, c = 05783 nm, beta = 95.375°. From single crystal rotation-, Weissenberg- and precession-photographs the following unit cell data were obtained: monoclinic, a = 0.5783 nm, b = 2.402 nm, c = 0.9474 nm, beta = 122.04°.

These unit cells obtained from the powder data and the single crystal photographs respectively are identical. In a plane perpendicular to the b-axis, the c-axis obtained from the single crystal photographs, which is parallel to the morphological c-axis, forms the diagonal of the unit cell obtained from the powder data. The unit cell obtained from the single crystal photographs is proposed because orientation of the crystallographic c-axis parallel to the morphological c-axis is favourable. The space group is $P2_1/n$, Z = 4 (number

of molecules per unit cell).

Morphology, crystallography, physical and optical properties

The white powderish konyaite consists of clusters of flakes with a thickness of about 3 μm and a diameter of about 50 μm (measured on SEM pictures). If konyaite grows in larger single crystals these crystals are prismatic, transparent, 2 mm long and 0.4 mm thick. The hardness of konyaite is very low and it is soluble in water. The density measured by means of heavy liquids is 2.088. The density calculated on the basis of 4 molecules per unit cell is 2.097. Optically the mineral is biaxial positive. n_α = 1.464, n_β = 1.468, n_γ = 1.474. Birefringence = 0.10. 2V = 74^o ($2V_{calculated}$ = 79^o). n_α // b; $n_\gamma \hat{} c$ = 30^o.

Chemical stability

Konyaite is a very instable mineral. It was identified in the samples taken from the Konya Basin within three months after sampling. Two years later in some samples konyaite was still present but in others it could no longer be identified. Synthetic konyaite could neither be conserved in the oven at the temperature of synthesis 35^o C nor at room conditions. In both cases it transformed between one and five days to bloedite.

Grinded samples of synthetic konyaite were conserved in different exsiccators at room temperature with 0%, 20%, 50%, 80% relative humidity respectively, a few samples per exsiccator. After six weeks all exsiccators contained samples which were completely or partly transformed to bloedite. In addition at 20% and 80% relative humidity samples were present which consisted still of pure konyaite. Ungrinded samples transformed more slowly. The large single crystals did not transform after six weeks.

It can be concluded that konyaite is metastable with respect to bloedite at room temperature. Minor factors such as grainsize determine whether it transforms to bloedite.

The mineral is named for the locality.

It is submitted to the Commission on New Minerals and Mineral Names of the IMA.

7.5

MINERALOGICAL MAGAZINE, SEPTEMBER 1979, VOL. 43, PP. 341-5

Two new occurrences and the Gibbs energy of burkeite

LIDEKE VERGOUWEN

Department of Soil Science and Geology, Agricultural University, PO Box 37, Wageningen, The Netherlands

SUMMARY. Burkeite ($Na_6CO_3(SO_4)_2$) is found as a surface mineral in the north of Kenya associated with thenardite and halite and in the Konya basin in Turkey associated with trona and halite. The cell dimensions of a natural burkeite are $a = 7.070$, $b = 9.220$, $c = 5.173$ Å. The Gibbs energy of burkeite is estimated in relation to other sodium carbonates and sulphates. $\Delta G^{\circ}_{f,298.15}$ (burkeite) = 3594.2 ± 3 kJ.

TWO new occurrences of the salt mineral burkeite ($Na_6CO_3(SO_4)_2$) were found in Kenya and in Turkey as a surface mineral on saline soils. Up till now burkeite has only been found in Searles Lake California (Haines, 1957, 1959). There burkeite is found in a drillhole from a depth of 28 ft to 465 ft always associated with trona ($Na_2CO_3 \cdot NaHCO_3 \cdot 2H_2O$) and in association with one or more of the following minerals: halite (NaCl), hanksite ($9Na_2SO_4 \cdot 2Na_2CO_3 \cdot KCl$), borax ($Na_2B_4O_7 \cdot 10H_2O$), thenardite ($Na_2SO_4$), pirssonite ($Na_2CO_3 \cdot CaCO_3 \cdot 2H_2O$), gaylussite ($Na_2CO_3 \cdot CaCO_3 \cdot 5H_2O$), and northupite ($Na_2CO_3 \cdot MgCO_3 \cdot NaCl$).

Geological setting and paragenesis

a. Kenya. Burkeite was found during a sampling trip in summer 1977 in the north of Kenya along the eastern shore of Lake Turkana (the former Lake Rudolf) near the small village of Loiengalani. Most of the area east of the lake is covered with Miocene and Pliocene basalts. Some spectacular eruption centres can be seen.

Along the shore a lacustrine laminated clay loam occurs, which was deposited when the level of the lake was a few metres higher. In some places this impermeable clay is covered by a very permeable gravelly basaltic material. Water which infiltrates the gravelly basaltic material cannot penetrate the underlying clay and moves on the interface of the gravel and the clay. This water flowing down the surface of the clay evaporates and forms a salt crust. The salt crust consists of halite and thenardite. Around some cracks in the clay the salt looks a bit more glassy. This salt contains burkeite. S(canning) E(lectron) M(icroscope) pictures show rosettes of thenardite needles on burkeite. Halite occurs both in cubes and in patches with no crystalline form on burkeite and between the needles of the thenardite. Sometimes the thenardite needles are overgrown with a layer of halite. Fig. 1 is a SEM of pure burkeite from Kenya.

b. Turkey. In Turkey burkeite was found during a sampling trip in summer 1978 in the Konya basin, which is a lacustrine plain in Central Anatolia. The Uplands of the basin are mostly formed of limestone formations but in some places also of andesitic volcanics. In the basin itself some stratovolcanoes occur. The plain consists of salt-affected clayey marl soils. From the edges some alluvial fans spread into the basin. Huge areas are covered with powdery and crusty salt, especially near the lower edges of the alluvial fans. These salts are mainly chlorides and sulphates of sodium and magnesium, but in the centre of the basin near Ak Göl sodium carbonates can be found. This is the only place where the pH of the ground water was found to be higher than 8. Here burkeite was found associated with halite and trona. They form a white salt crust, which formed as a result of evapotranspiration and seals the surface.

Chemical analysis

Due to the small grain-size of the burkeite (a few micrometres measured on a SEM picture) and to its intimate intergrowth with other salt minerals, it is impossible to separate burkeite from its associated salt minerals. Therefore, no quantitative analysis could be performed and only some qualitative analyses have been made by means of an electron microscope equipped with an energy-dispersive system. In this way it was established that Na, S, and C are the major components.

Crystallographic properties

X-ray powder diffraction data of the natural burkeites were obtained with a Nonius Guinier

FIG. 1. Scanning Electron Micrograph of burkeite from Kenya (made by TFDL, Wageningen).

camera using Co-$K\alpha_1$ radiation, $\lambda = 1.7889$ Å. The data are listed in Table I. The calculated d-values show reasonable agreement with the measured ones. The cell dimensions were calculated using a program written by Visser (1969). From powder diffraction data the space group is determined to be either $Pmm2$ or $P222$.

Stability and thermodynamic properties of burkeite

Eugster and Smith (1965) constructed an $a_{CO_2} - a_{H_2O}$ diagram for mineral reactions involving sodium carbonates and sodium sulphates. They labelled the fields of stable associations under the assumption that burkeite (a mixed carbonate–sulphate) occurs with carbonates. This restriction is valid in the Searles Lake environment, as well as for the locality in Turkey, where burkeite has been found with trona and halite (see fig. 2*a*). The burkeite in Kenya is found with thenardite and halite only, so for the Kenya environment the labels of the stability fields have to be changed accordingly (see fig. 2*b*). Comparison of the two diagrams shows that the association burkeite + trona occurs under more restricted conditions than the association burkeite + thenardite.

There are no thermodynamic data available for

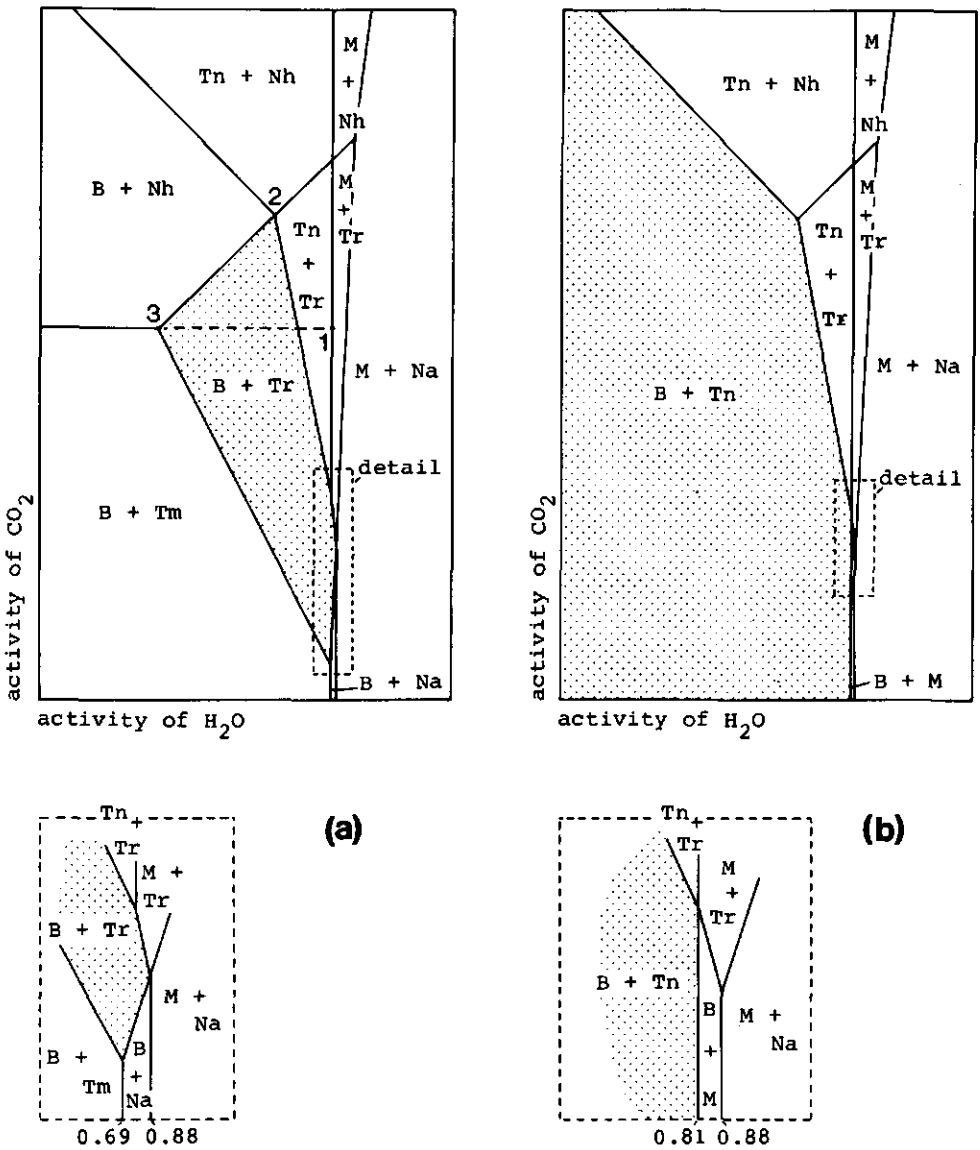

FIG. 2*a* and *b*. $a_{H_2O}-a_{CO_2}$ diagrams for the system Na_2CO_3–Na_2SO_4–H_2O. For abbreviations see Table II. B = burkeite. In fig. 2*a* fields are labelled assuming that burkeite occurs with carbonates. In fig. 2*b* fields are labelled assuming that burkeite occurs with sulphates. The coordinates of points 1, 2, and 3 in fig. 2*a* are: $1P_{CO_2} = 10^{-4}$ atm., $a_{H_2O} = 0.81$; $2P_{CO_2} = 10^{-2.6}$ atm., $a_{H_2O} = 0.29$; $3P_{CO_2} = 10^{-4}$ atm., $a_{H_2O} = 0.01$. In the enlargements of the details the slopes of the field boundaries are arbitrary but their relative steepness has been maintained.

TABLE I. *X-ray data for burkeite*

Burkeite from Kenya			NBS synthetic burkeite		
d_{obs}	d_{calc}	*hkl*	*d*	*hkl*	I/I_1
9.199	9.220	010	9.215	010	8
4.609	4.610	020	4.607	020	5
4.510	4.512	011	4.507	011	17
4.175	4.175	101	4.172	101	4
3.862	3.862	120	3.854	120	40
3.804	3.803	111	3.795	111	75
3.537	3.535	200	3.526	200	80
3.440	3.442	021	3.439	021	19
3.300	3.301	210	3.307	210	3
3.075	3.073	030	3.072	030	17
2.806	2.805	220	2.801	220	100
2.778	2.783	211	2.777	211	55
2.643	2.642	031	2.640	031	75
2.588	2.587	002	2.583	002	75
2.490	2.490	012	2.488	012	5
2.347	2.349	112	2.345	112	6
2.305	2.305	040	2.305	040	11
2.283	2.283	310	2.279	310	4
2.191	2.192	140	2.191	140	3
2.150	2.149	122	2.147	122	14
2.145	2.145	301	2.142	301	11
2.106	2.105	041	2.105	041	6
1.980	1.979	032	1.978	032	12
1.925	1.931	240	1.929	240	30
1.906	1.906	132	1.904	132	25
1.899	1.902	222	1.898	222	30
			1.784	150	2
1.768	1.768	400	1.764	400	17
1.737	1.737	051	1.735	051	8
			1.722	003	3
1.680	1.675	103	1.673	103	2
1.647	1.648	113, 340	1.645	113, 340	3
1.635	1.635	250	1.635	250	4
			1.627	322	4
1.616	1.615	023	1.614	023	4
1.559	1.559	251	1.557	251	5
1.549	1.550	203	1.548	203	6
1.546	1.547	242	1.545	242	5
1.537	1.537	060	1.536	060	6
1.529	1.528	213	1.526	213	5
a 7.070 *b* 9.220 *c* 5.173 Å			*a* 7.055 *b* 9.215		
*Pmm*2 or *P*222			*c* 5.167 Å		

burkeite, but an approximate Gibbs energy of burkeite can be calculated from the Gibbs energies of the other minerals plotted in fig. 2 (see Table II). The equilibrium f_{CO_2} between thermonatrite and nahcolite can be calculated as follows:

$$Tm + CO_2 \leftrightarrows 2Nh \qquad (1)$$

$$\Delta G_R = -RT\ln K = +RT\ln f_{CO_2};$$

at 298.15 K $\quad f_{CO_2} = 10^{-4}$bar.

In fig. 2*a* it can be seen that at this f_{CO_2} and at an a_{H_2O} where thenardite and mirabilite are in equilibrium with each other (point 1 in fig. 2*a*) burkeite is unstable with respect to the assemblage thenardite + trona, which means that at these conditions the ΔG_R of the following reaction must be positive:

$$6Tn + 2Tr \leftrightarrows 3B + CO_2 + 5H_2O; \qquad (2)$$

at $f_{CO_2} = 10^{-4}$bar $\quad \Delta G_R > 0$

$$3G_B > 6G_{Tn} + 2G_{Tr} - G^\circ_{CO_2} - RT\ln f_{CO_2} - 5G^\circ_{H_2O} - 5RT\ln a_{H_2O}. \qquad (3)$$

a_{H_2O} can be calculated from the equilibrium:

$$Tn + 10H_2O \leftrightarrows M \qquad (4)$$

$$\Delta G_R = +10RT\ln a_{H_2O};$$

at 298.15 K $\quad a_{H_2O} = 0.81$.

Substituting this value as well as $f_{CO_2} = 10^{-4}$ in the inequality (3), the following result is obtained:

$$G_B > -3596.02 \text{ kJ}. \qquad (5)$$

In fig. 2*b* it can be seen that the equilibrium between burkeite and natron + mirabilite is situated at a higher a_{H_2O} than the equilibrium between thenardite and mirabilite (where $a_{H_2O} = 0.81$).

$$B + 30H_2O \leftrightarrows Na + 2M \qquad (6)$$

at $a_{H_2O} = 0.81 \quad \Delta G_R > 0$

$$G_B < G_{Na} + 2G_M - 30G^\circ_{H_2O} - 30RT\ln a_{H_2O}$$

$$G_B < -3592.40 \text{ kJ}. \qquad (7)$$

From (5) and (7) it follows:

$$-3596.02 \text{ kJ} < G_B < -3592.40 \text{ kJ}.$$

The accuracy of these values depends on the accuracy of the Gibbs energies of the individual minerals which take part in the reaction equations (1, 2, 4, and 6). As there are no uncertainties given

TABLE II. *Gibbs energies of the minerals*

Name	Formula	$\Delta G^\circ_{f,298.15}$ kJ/mol	Reference
Nahcolite (Nh)	$NaHCO_3$	−851.86	1
Natron (Na)	$Na_2CO_3 \cdot 10H_2O$	−3428.98	1
Thermonatrite (Tm)	$Na_2CO_3 \cdot H_2O$	−1286.55	1
Trona (Tr)	$NaHCO_3 \cdot Na_2CO_3 \cdot 2H_2O$	−2386.55	1
Thenardite (Tn)	Na_2SO_4	−1269.985	2
Mirabilite (M)	$Na_2SO_4 \cdot 10H_2O$	−3646.540	2
Carbon dioxide (g)	CO_2	−394.375	2
Water (liq.)	H_2O	−237.141	2

References: 1. Garrels (R. M.) and Christ (C. L.), 1965. (1 cal. = 4.184 J).
2. Robie (R. A.), Hemingway (B. S.), and Fisher (J. R.), 1978.

for the Gibbs energies of the sodium carbonates, we cannot give an exact uncertainty for the Gibbs energy of burkeite. Therefore, we estimated:

$$\Delta G_{f,\,298.15}\ \text{(burkeite)} = 3594.2 \pm 3\ \text{kJ}.$$

The Gibbs energy of burkeite is calculated from equilibrium relationships with respect to other minerals. As soon as the values of the Gibbs energies of the other minerals change, the Gibbs energy for burkeite has to be changed accordingly. Once the Gibbs energy of burkeite is known, the positions of all other equilibria in the diagrams can be calculated. It can be seen that burkeite can form under the atmospheric condition $f_{CO_2} = 10^{-3.5}$ atm and that during formation the solution must be rather concentrated (activity of H_2O less than 0.88), a stage which is easily reached during evaporation.

Acknowledgements. I thank Dr E. L. Meijer for helping me with the unit-cell computer program and for his helpful discussions.

REFERENCES

Eugster (H. P.) and Smith (G. I.), 1965. *J. Petrol.* **6**, 473.

Garrels (R. M.) and Christ (C. L.), 1965. *Solutions, Minerals and Equilibria.* Harper and Row edn., New York, 450 pp.

Haines (D. V.), 1957. *Geol. Surv.*, open-file report.

—— 1959. *US Geol. Surv. Bull.* **1045-E**, 139.

Robie (R. A.), Hemingway (B. S.), and Fisher (J. R.), 1978. Ibid. **1452,** US Government Printing Office, Washington.

Visser (J. W.), 1969. *J. Appl. Cryst.* **2**, 89.

[*Manuscript received 30 October 1978*]

7.6 SCANNING ELECTRON MICROSCOPY APPLIED TO SALINE SOILS FROM THE KONYA BASIN IN TURKEY AND FROM KENYA

This section is part of
Vergouwen, L., 1981, Scanning Electron Microscopy applied to saline soils from the Konya Basin in Turkey and from Kenya. In: E.B.A. Bisdom (ed.): Submicroscopy of soils and weathered rocks. Ist workshop of Undisturbed Soil Materials (IWGSUSM), Wageningen, 1980. Pudoc, Wageningen, the Netherlands, in press.

Summary

Salts of the Konya Basin in Turkey and from different regions in Kenya were investigated by Scanning Electron Microscopy. This technique was used to examine the crystallographic properties of the individual salt crystals, to investigate their morphology and their influence on the morphology of the salt assemblages in which they are present and to study the relations between the different salt crystals.

The difficulties are described which arise when this very friable material is handled. An analysing equipment is essential for identification of the different minerals. Backscattered electron scanning images and X-ray images are also of great help.

Halite forms a smooth crust sealing the soil; trona, bloedite and hexahydrite make the salt crust very fluffy. Thenardite occurs in two crystal forms.

Procedure

Samples were selected with different salt associations. From each sample a piece was used for X-ray diffraction analysis, to determine the exact mineralogical content of the salt piece, using a Guinier camera with Co $K_{\alpha}1$ radiation; a corresponding piece was used for SEM analysis.

The type of material was very complicated to handle. Only coherent material which did not break into pieces on touching could be used. This is in fact already a preselection. For example it was not possible to handle the thenardite crystals from the puffed solonchaks because of their fragility. Many thermonatrite samples disintegrated as well on handling.

The samples were glued with silverpaint with toluene as solvent on a small aluminium stub. Alcohol as solvent is not suitable because the salts dissolve

in it. This silverpaint has the advantage over normal glue that it is conductive at the same time. The samples were prepared at the same day of using them. Preparation a few days before use appeared to be useless because the samples disintegrate easily. The material was coated first with a carbon layer and then with a gold layer. A carbon coating is required because otherwise the gold does not adhere sufficiently to the material. The gold was evaporated thermally. With this method the distance between the hot spot and the sample is larger than with the sputtering method. The temperature of the sample must be kept as low as possible because some minerals contain crystal water. Thermal evaporation has the additional advantage that the gold layer becomes thicker which is favourable because of the irregular surface of the samples. A disadvantage of this coating method is that the vacuum in the chamber must be higher (10^{-4} torr) than in the case of sputtering (0.1 torr).

The samples very often show charging. This is caused by the fact that the side which is fixed on the aluminium stub is usually very irregular. Therefore not every part of the specimen is in contact with the aluminium stub but only some local spots are fixed. This problem is usually less severe on the rim of the specimen. There the nicest images could be seen.

To reduce the effect of charging we tried to coat the specimen with osmium which has a higher conductivity than gold. This was not very suitable because osmium is first dissolved in distilled water and then the solution is evaporated in a covered petribowl in which the specimen is also placed. The distilled water with the dissolved osmium precipitated on the sample and dissolved the salt material. Small holes could clearly be observed with the SEM.

Some specimens were investigated with the SEM before coating them to see whether the coating procedure would cause mineral transformations. This seemed not to be the case.

The SEM pictures were made with a JEOL JSM - 35 c equipped with EDAX PV 9100 with an ECON windowless detector. Polaroid film was used to obtain direct results because of the difficult material. The mineral-content of the sample is known from the X-ray diffraction analysis. All minerals were chemically identified with EDAX. Although this analysing system is not quantitative, at least not with samples coated with gold, it appeared to be indispensable. Wrong identifications could be prevented in this way for minerals which often showed different crystal habits than expected. In other cases minerals were identified which were present in such small amounts that they could not be detected by X-ray diffraction.

Results

The mineralogy and morphology of halite, thenardite, bloedite, hexahydrite, eugsterite, trona and burkeite were investigated. The crusts were 1/2 - 3 mm thick. No zoning could be detected, neither macroscopically nor microscopically with a light microscope.

Eugsterite is a new salt mineral which occurs both in Kenya and in Konya. The constituting elements of eugsterite could only be determined by means of EDAX because the mineral could not be separated from its associated minerals. This qualitative indication made it possible to synthesize the mineral and to analyse this synthesized material quantitatively (the mineral has been approved by the Commission on New Minerals and Mineral Names of the IMA). From SEM pictures the monoclinic nature of the mineral could be deduced and the angle between the a- and c-axis could be measured.

Fig. 7.3a shows thenardite crystals with bloedite and eugsterite. Thenardite was expected to grow in needle-type crystals as can be seen macroscopically in puffed solonchaks. In association with other salt minerals, thenardite has the tendency to grow in the crystalline form as shown in fig. 7.3. In evaporation experiments in beakers thenardite grows as needles. In fig. 7.3b it can be seen that the small bloedite crystals have precipitated on the thenardite in a later stage. The eugsterite (fig. 7.3c) has crystallized at the expense of the thenardite. Fig. 7.3 is an example of the necessity of an analysing equipment. Without such an equipment the eugsterite needles would have been attributed to either gypsum or thenardite and the thenardite would not have been recognized. Figs. 7.4a and 7.4b show the difference in analysis between the eugsterite needles and the thenardite crystals. Fig. 7.4c is an example of thenardite growing in its needle-type form.

Figs. 7.5a and 7.5b are an example of halite. The smooth surface is continuous with only few pores. This is the type of crust which seals the surface, preventing further evaporation. The small particles on the smooth surface are calcite and quartz.

Fig. 7.6a shows well crystallized halite cubes in equilibrium with bloedite. Both minerals seem to have crystallized at the same time. They have completely intermingled with each other. The bloedite crystals have a somewhat smaller size and are packed somewhat looser than the halite. Fig. 7.6b is an enlargement of the bloedite.

Figs. 7.7a and 7.7b show trona minerals. Trona crystallizes as bars, both criss-cross in all directions and in radiating fans. These trona bars cause the

salt association to become very fluffy.

Figs. 7.8 and 7.9 show the application of different techniques.
In fig. 7.8a the topology of a salt crust mainly consisting of trona bars with different irregularities can be observed.
Fig. 7.8b is a backscattered electron scanning image (BESI) of the same spot. With BESI, the difference in contrast is caused by the difference in chemical composition and not by the topology as in the case of secondary electron images. A comparison of figs. 7.8a and 7.8b indicates that the irregularities on the tops of the trona crystals correspond with the lighter parts of BESI. Spot analyses show that the small grains that occur throughout the sample are quartz grains and that burkeite replaces the trona crystals. The presence of these minerals is confirmed by X-ray diffraction analysis. Si and S X-ray images of the same spot show the distribution of the silica and the burkeite (figs. 7.9a and 7.9b).

Figs. 7.10a and 7.10b is an example of the association hexahydrite and bloedite. Hexahydrite constitues the main part and the small bloedite crystals are deposited on the hexahydrite. This crust has a very large porosity. Identification with EDAX was again indispensable in this case. The middle of fig. 7.10a shows clearly the phenomenon of charging.

Discussion and conclusions

Scanning electron microscopy in combination with an analysing equipment is a very useful technique to evaluate the submicroscopical properties of salt minerals. The morphological properties of the salts, which were determined macroscopically, could be established with the SEM.

The surface of halite crusts is indeed a very sealing smooth crust with many pores.
Bloedite is present in crusts as small rounded crystals which are loosely packed. Especially in association with hexahydrite these crusts are very fluffy.
Driessen & Schoorl (1973) assumed bloedite crystals to be responsible for the sealing of the soil surface but detailed investigation of many crusts containing bloedite contradict these assumptions.
Trona minerals seem to increase the porosity of the salt crust as well.

When saline soils are irrigated, the soils covered with halite crusts need ploughing to avoid runoff of the irrigation water. The porosity of the other types of crusts is usually such that the irrigation water can penetrate the crust easily.

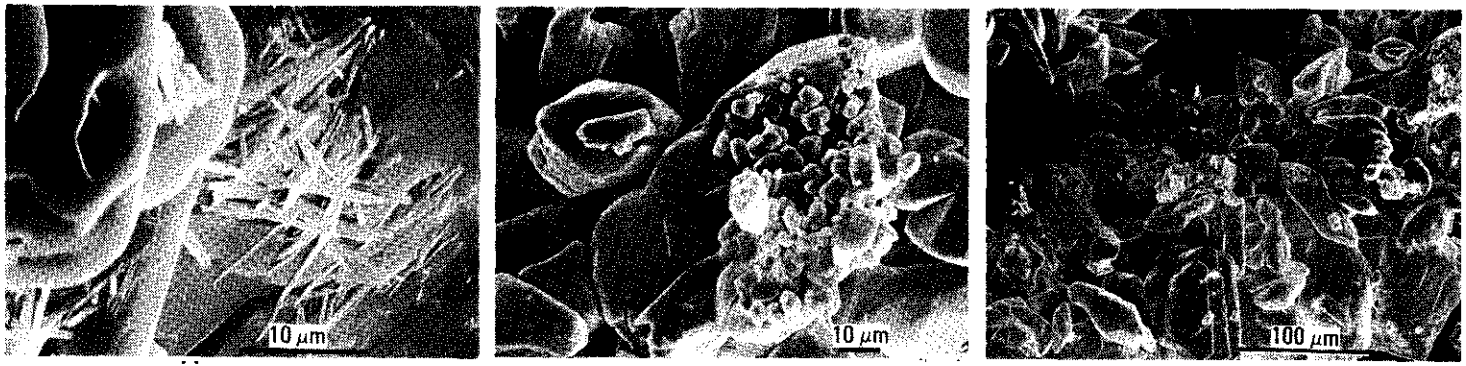

Fig.7.3 a.Thenardite crystals with bloedite and eugsterite. b.Enlargement of the bloedite crystals. c. Enlargement of eugsterite.

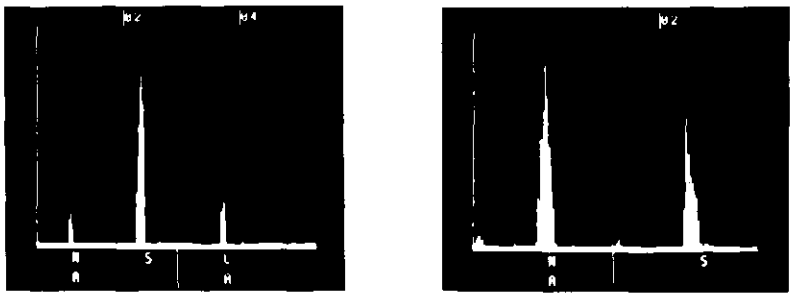

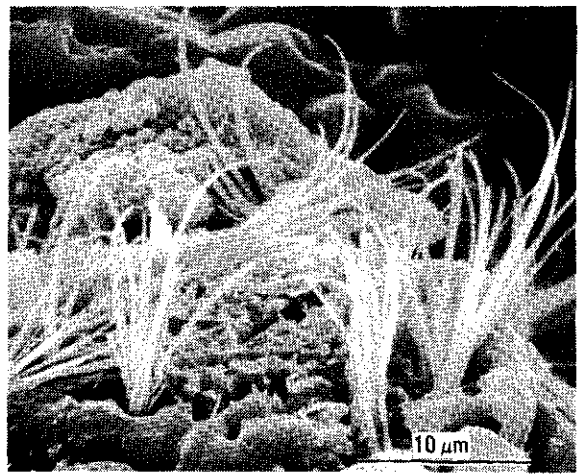

Fig.7.4 a.Analysis of eugsterite. b. Analysis of thenardite. c. Thenardite in needle-type crystals.

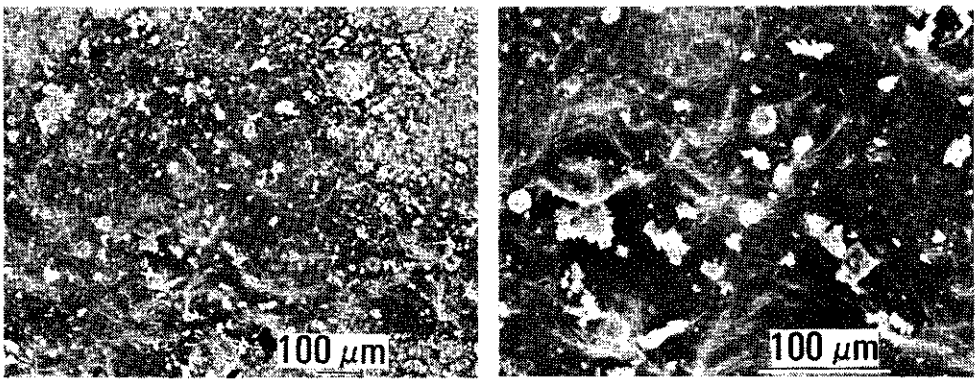

Fig.7.5 a. Smooth halite crust with quartz and calcite grains. b. Enlargement.

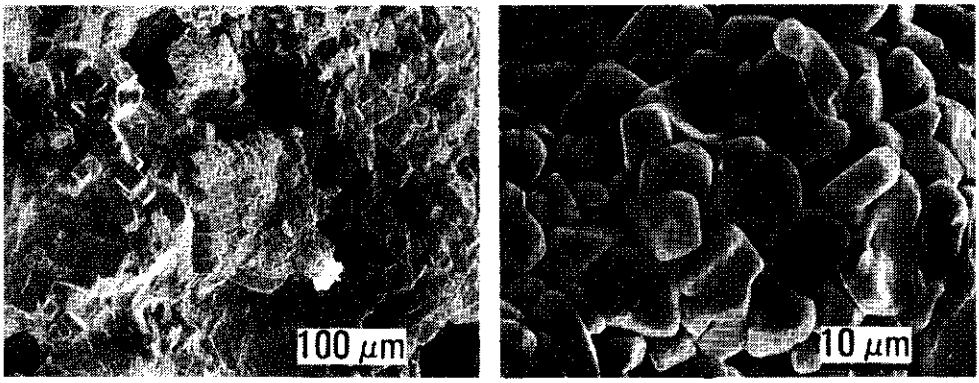

Fig.7.6 a. Halite cubes intermingled with bloedite. b. Enlargement of bloedite

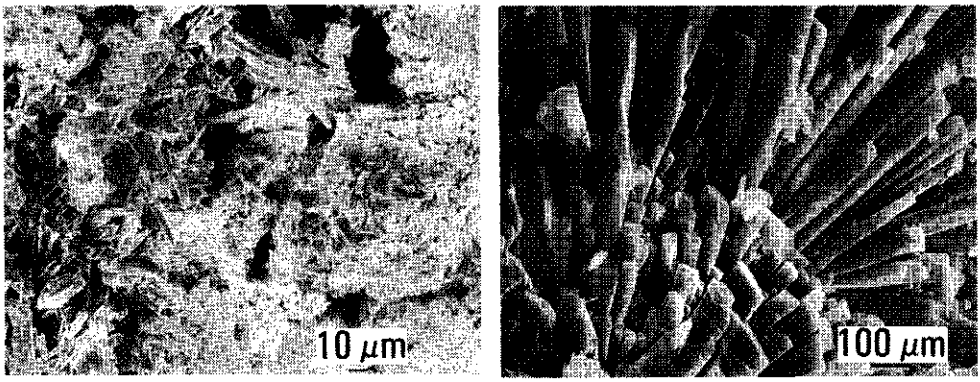

Fig.7.7 a. Trona crystals between aphtithalite. b. Fan of trona crystals.

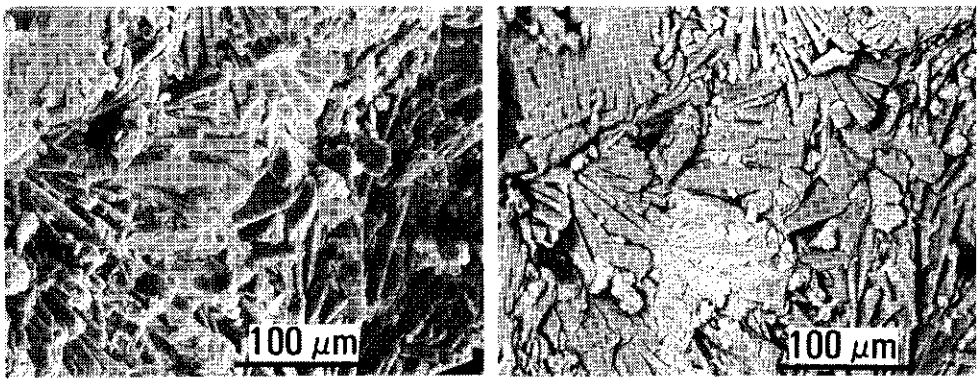

Fig.7.8 a. SE-image of trona, locally transformed into burkeite with scattered quartz grains. b. BESI-image of the same spot.

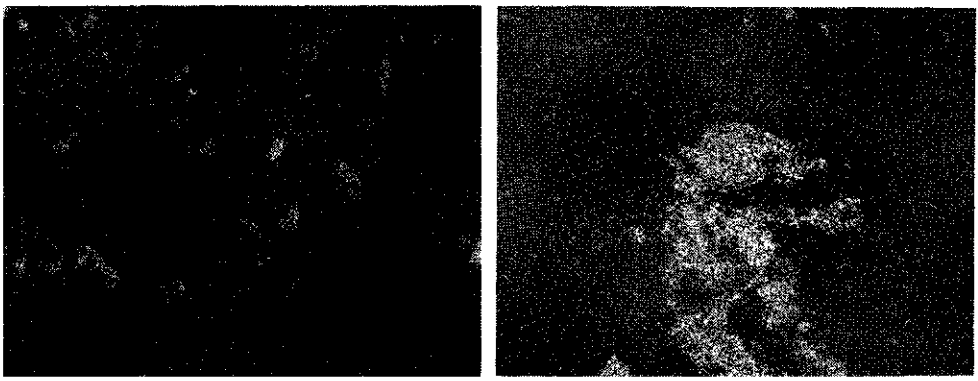

Fig.7.9 a. Si X-ray image of the same spot as fig.7.8. b. S X-ray image of this spot.

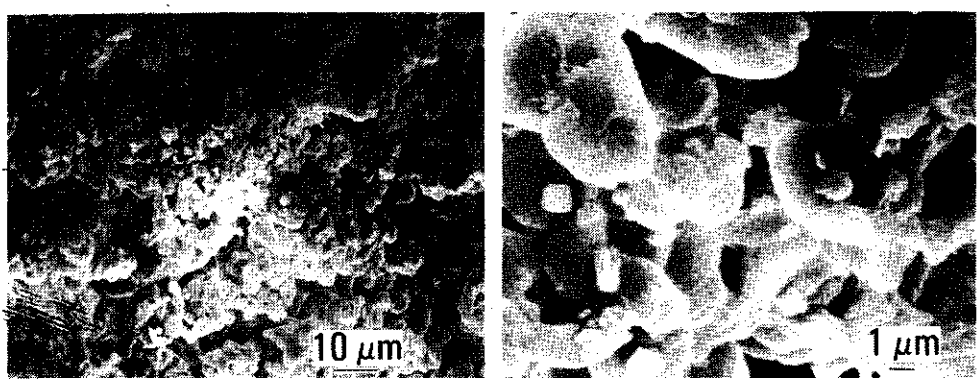

Fig.7.10 a. Hexahydrite with small bloedite crystals. b. Enlargement of hexahydrite.

All SEM pictures were made at TFDL, Wageningen.

8. SALT ASSEMBLAGES AND EVAPORATION EXPERIMENTS

8.1 INTRODUCTION

In this chapter a description is given of the different salt associations, in order to examine the conditions under which the salts precipitated, to test whether the associations represent equilibrium assemblages and to consider the processes that operated during evaporation and precipitation. In order to solve some of these problems, the waters which were sampled in the field were evaporated in the laboratory. A comparison was then made between the salts precipitated from these waters in the laboratory and the assemblages found in the field.

The chapter is divided into three parts. In the first part the results of the evaporation experiments will be given. In the second part the assemblages in the system Na-Ca-SO_4-CO_2-H_2O will be examined. Salt assemblages belonging to this system occur mainly in the visited localities in Kenya and only in a few localities in the Konya Basin.

It is impossible to calculate which minerals will theoretically precipitate from specific waters in this system during evaporation because until now no activity-coefficients for carbonate-ions in concentrated solutions have been available. Therefore, the assemblages in this system have been investigated with the aid of log p_{CO_2} - log a_{H_2O} diagrams. In the third part the salt associations in the system Na-K-Ca-Mg-SO_4-Cl_2-H_2O will be considered. Salt assemblages belonging to this system occur mainly in the Konya Basin.

8.2 EVAPORATION EXPERIMENTS

The ground- and surface waters which have been sampled in the Great Konya Basin in Turkey and in different localities in Kenya were evaporated in evaporating dishes in the laboratory. The water samples were first filtered through a 0.2 µm micropore filter. The amount of water which evaporated from each sample varied between 150-300 ml depending on the amount of water left after analysis of each sample. The relative humidity was approximately 40% and the room temperature 20° C $\pm$ 2°. The samples evaporated in about two weeks. Fig. 8.1 shows a photograph of such an experiment.

During such experiments fractional crystallization occurs because the salts precipitate against the sides of the dishes and during further evaporation of

Table 8.1 Salt Assemblages precipitated from the water samples from Kenya in the laboratory compared with natural assemblages

Loc.	Type of water	log P_{CO_2} 1)	Salt assemblages found in the field 2)	Salt assemblages found in the laboratory 3)
Amboseli waters				
Am 3	groundwater	-1.30		tr, tm, hal, tn
				tm, hal, $KNaSO_4$
				tm, aph, hal
Am 4	groundwater	-2.72	tr	tr, tm, hal
			tm, tr, cal	hal, cal
			tr, cal, prs, tm	
			tr, tm, gay	
Am 5	pond	-3.05	tr, cal, gay, tm	tm
			cal, ar	tr, hal, tm
				tr, tm, hal
Am 6	groundwater	-1.67	tr, cal, gay, tm, aph	tr, hal, syl, $KNaSO_4$
Am 8	groundwater	-0.98	tr, tm, gay	syl, hal, tm
			tr, aph	hal, syl
			tr, aph, gay, prs	
Am 11	river water	-2.60		hal, syl, cal
Am 14	river water	-1.82		cal, hal
Turkana waters				
Maikona	groundwater	-2.79	hal, tn	pth, kai, hal
			hal, gps	hal, kai, gps
				kai, hal, gps
Kalacha I	groundwater	-2.44	hal, tn, eug	hal, tn, ntp
				hal, cal
Kalacha II	groundwater	-2.35	hal, tn	dpsk, ntr, tn, hal
				tn, hal, ntr, dpsk
North Horr	groundwater	-2.89	hal, tr, brk	tr, hal, brk
				tr, hal, brk
				brk, hal
Furaful	river water	-3.59	tn, hal	tn, hal
Loyengalani	spring	-2.78	tn, hal	ntp, hal, cal
			tn, hal, brk	

1) log P_{CO_2} calculated from HCO_3^--concentration and pH measured in the field. Equilibrium constants from Stumm and Morgan (1970).

2) These are the salt assemblages formed in the immediate vicinity of the site of sampling of the groundwater.

3) The salts deposited in the evaporating dishes. The sequence of the different assemblages is the same as in the dishes, from the upper rim till the bottom.

4) b.r. before rains

5) a.r. after rains

Table 8.1 cont'd

Loc.	Type of water	log P_{CO_2} [1]	Salt assemblages found in the field [2]	laboratory [3]
Lake Victoria Waters				
Simbi 1	spring	-2.17	tm, tr	sdn
Simbi 2	groundwater	-1.51	tr, tm, gay	sdn, gps
Miti Bili 1 b.r. [4]	spring	-0.10	tr, cal, gay, nah	sdn, dpsk, tm, tr, hal
				sdn, dpsk, tm, tr, hal
Miti Bili 1 a.r. [5]	spring	-0.16	tr, cal, gay, nah	tm, tr, hal, brk
				tm, tr, hal, brk
				tm, tr, hal, brk
Miti Bili 2 a.r.	groundwater	-1.95	tr	tr, tm, hal
			tr, tm	tr, tm, hal
Miti Bili 3 a.r.	groundwater	-2.08	tr, gay	tr, tm, hal, brk
				tr, tm, hal, brk
				tm, hal, brk
				tr, tm, hal, brk
Miti Bili 4 a.r.	groundwater	-2.05	tr, tm, hal, brk	tr, tm, hal, sdn, dpsk
			tr, hal	tr, tm, brk, hal, sdn
			tr, nah, gay	brk, tr, hal, tm, sdn
			tr, gay	
			tr, hal, brk	
Miti Bili 5 a.r.	surface water	-3.71		tm, hal, brk
				tr, tm, hal
Lake Victoria	lake water	-3.32		cal, hal, syl, tm
Kanam 1 b.r.	groundwater	-1.30	tr, nah	sdn, dpsk, hal
			tr, tm, gay	sdn, dpsk, hal
			tr, hal, gay	
Kanam 1 a.r.	groundwater	-1.38	tr, hal, tm, gay	tm, tr, hal, brk
			tr, gay	tm, tr, hal, brk
Kanam 2 a.r.	groundwater	-2.45		tm, hal, brk
				tr, tm, hal, brk
Luanda	groundwater	-1.0	eug, gps	bl, tn, kon
				tn, hal, bl, kon
				tn, hal
Sindo	groundwater	-0.83	hal, tn	kai, hal
			gps	tn, lw, hal, kon
				lw, hal, kon

For abbreviations of the minerals, see table 2.2 and 3.2. In addition darapskite (dpsk), $Na_3(NO_3)(SO_4).H_2O$; pentahydrite (pth), $MgSO_4.5H_2O$; kainite (kai), $KMgClSO_4.3H_2O$; northupite (ntp), $Na_6Mg_2Cl_2(CO_3)_4$.

Table 8.2 Salt assemblages precipitated from the water samples from the Konya Basin compared with natural assemblages

Loc.	Type of water	log p_{CO_2} [1]	Salt assemblages found in the field [2]		laboratory [3]
T1	pond	-2.53	bl, hxh, gps		eps, hal, hxh
T4	groundwater	-1.28	tn, gl		hal, bl, hxh, kon, lw
			tn, aph		hal, bl, hxh, lw, kon
			bl, hal, gl		
			bl, gps		
			bl, hal, hxh, sch		
T5[a]	irrigation channel	-0.97		T4	hal, hxh, gps, lw
					hal, hxh, gps
T5[b]	groundwater	-2.27	eps, bl, gps	T5	hal, hxh, gps
					hal, hxh, gps
T6	groundwater	-1.18	bl, hxh, gps		hal, hxh
					hal, hxh, ar
T8	crater lake	-2.64	hal, tn, nsqh, eug		hal, eps
					hal, eps
T9	groundwater	-1.75	hal, gl, gps		hal, hxh
			hal, tn, eug		hal
			tn		hal
T10	groundwater	-1.46	tn, aph		lw, hal
					hal
T11	groundwater	-1.79	bl, eug		pth, hal
					pth, gps, hal
T13	groundwater	-1.57	hal, gps, eug		tn, hal, lw, hxh
			tn, eug		gps, hal, hxh, tn
					gps, hal, hxh, tn, kon
T14	groundwater	-1.08	hal, gps		gps, lw, hal, kon
					gps, hxh, lw, hal, kon
					gps, hal, hxh, bloed, kon
T15[a]	groundwater	-1.76	hal, gps, brk		hal, tn
			hal, tn		
T15[b]	irrigation channel	-3.19			hal, cal, lw
					hal, cal
T16	spring	-0.23	hal, tn, eug		hal, tn
			gps, cal		

Table 8.2 cont'd

Loc.	Type of water	log P_{CO_2} [1]	Salt assemblages found in the field [2]	laboratory [3]
T17	groundwater	-1.86	bl, eug	gps, hal, hxh, kon, lw
				gps, hal, hxh, kon, lw
				gps, hal, lw, hxh, kon
T22	groundwater	-1.71	bl, hxh, gps, kon	gps, hxh, lw, hal
				eps, gps, lw, hxh, hal
				eps, gps, hal
T23	groundwater	-1.87	bl, hal, gps	pth, hal, gps
			bl, hal, gl	gps, hxh, pth, hal
T24	groundwater	-2.22	hal, gl	hal, gps
			hal, gl, tn, gps, eug	hal, $MgCO_3.3H_2O$
T25	spring	+0.03	hal, tn, nsqh, gl, eug	hal, tn, $Na_6Mg_2Cl_2(CO_3)_4$
				hal, gps
				brk, tn, hal
T26	groundwater	-0.53	hal, tr, brk	brk, $Na_6Mg_2Cl_2(CO_3)_4$
T27	river	-1.97		hal
T28	groundwater	-1.28	hal, tn, aph	hal, gps, cal, hxh
			tn, aph	
T29	groundwater	-1.74	hal, tn	tn, hal
			hal, eug	cal, hal
T31	groundwater	-2.51	hal, tr, brk	tr, tm, hal, brk
				hal, brk, tr
T32	groundwater	-2.84	hal, tr, brk	hal, brk, tr
T33	groundwater	-1.99	tn, hal, eug	hal, hxh, kon
			tn, eug	hal, hxh, kon
			tn	hal
T35	groundwater	-2.05	bl, hxh, gps, kon	hal, hxh, kon
			bl, gps, lw	hxh, hal, lw
				hxh, hal
				lw, hxh, kon
T36	groundwater	-1.30	hal, bl	hal, hxh, pth
			hal, bl, stk, kon	hal, pth, hxh, gps
T37	groundwater	-1.76	hal, bl, gps, kon	hal, hxh
				gps, hal, hxh

1), 2), 3) see table 8.1

For abbreviations of the minerals see table 3.2 and 4.2.

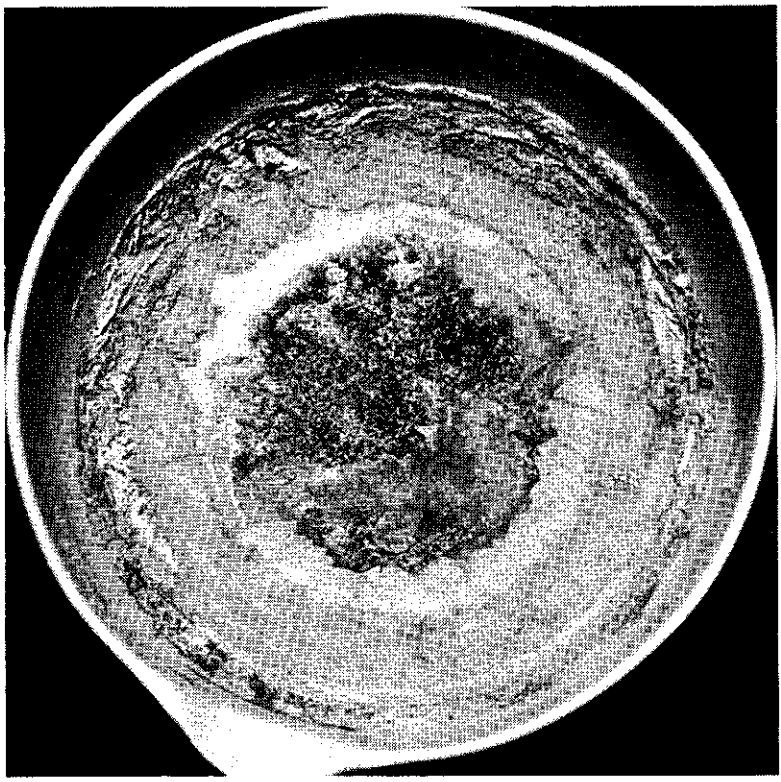

Fig.8.1 An example of an evaporation experiment.

the solution, the salt minerals are no longer in contact with the solution.

The salts at the upper rim have precipitated first. The salt at the bottom is a mixture of the last-formed crystals and of crystals which sink to the bottom during the whole process of evaporation. Usually only well crystallized halite cubes sank to the bottom. Evaporation in evaporating dishes in the laboratory closely reproduces the process which takes place during evaporation of ground water in nature because in the latter case fractional crystallization also occurs.

The salt minerals produced in the dishes were analysed by X-ray diffraction. Enough salt precipitated from the more concentrated waters to enable different analyses of the salt association, beginning with the precipitate of the upper rim and going downwards towards the precipitate in the centre. The less concentrated waters, such as river water, formed a very thin salt film against the side of the dishes permitting only one analysis to be made.

Table 8.1 and 8.2 show the minerals which formed in the dishes from the

waters from Kenya and Konya respectively. For comparison, the natural salt assemblages found in the immediate vicinity of the sampling site are also given together with the equilibrium log p_{CO_2} of the waters (calculated using the analysed HCO_3^--concentrations), the pH measured in the field (see table 3.1 and 4.1) and the equilibrium constants at 25° C and 1 bar, taken from Stumm and Morgan, 1970. The equilibrium log p_{CO_2} of the waters containing CO_3^{2-} calculated using the analysed CO_3^{2-}-concentration and the pH measured in the field appears to be in general a factor 0.5 higher than that calculated by means of the HCO_3^--concentration. This may be due to the fact that activity coefficients have been neglected, which has a greater effect in the case of bivalent than monovalent ions.

8.3 PHASE DIAGRAMS IN THE SYSTEM $Na-Ca-SO_4-CO_2-H_2O$

The system $Na-CO_2-H_2O$

The stability fields of the minerals trona, thermonatrite, nahcolite and natron in the system $Na-CO_2-H_2O$ can be studied with a log p_{CO_2} - log a_{H_2O} diagram at constant P and T in which p_{CO_2} is the partial CO_2-pressure and a_{H_2O} is the water-activity. It would be more rigourous to use f_{CO_2}, the fugacity of CO_2, instead of P_{CO_2}, but, because P_{CO_2} is a measurable quantity and because the difference between p_{CO_2} and f_{CO_2} is negligibly small, it is convenient to use p_{CO_2}.

The slope of the field boundaries between the stability fields of minerals in such a plot is determined by the ratio of H_2O to CO_2 molecules in the reaction equation (Garrels & Christ, 1965). The reaction equations and their corresponding slopes are (for abbreviations and formulae of the minerals, see table 8.3):

$2tr \leftrightarrows 3tm + CO_2 + 2H_2O$	slope	-2	(1)
$tr + CO_2 \leftrightarrows 3nah + H_2O$	"	1	(2)
$2tr + 25H_2O \leftrightarrows 3nat + CO_2$	"	25	(3)
$tm + 9H_2O \leftrightarrows nat$	"	∞	(4)
$tm + CO_2 \leftrightarrows 2nah$	"	0	(5)
$2nah + 9H_2O \leftrightarrows nat + CO_2$	"	9	(6)

If the Gibbs energy of formation of these minerals is known, the position of these lines in a log p_{CO_2} - log a_{H_2O} diagram can be calculated.
For example for reaction (1):

$$\Delta G_R^o = - RT \ln K = - 2RT \ln a_{H_2O} - RT \ln p_{CO_2}$$

in which

$$\Delta G_R^o = 2\Delta G_{f(H_2O)}^o + \Delta G_{f(CO_2)}^o + 3\Delta G_{f(tm)}^o - 2\Delta G_{f(tr)}^o$$

If ΔG_R^o can be calculated, the position of the field boundary between the stability fields of trona and thermonatrite is fixed. The same procedure can be applied to the other minerals in the system Na_2O - CO_2 - H_2O. It is clear that the resultant diagram is dependent upon the values of the Gibbs energies of the individual minerals, and many different values are reported in the literature. Fig. 8.2 and fig. 8.3 show the diagram calculated with two different sets of Gibbs energies of formation - those selected by Al-Droubi (1976) and those selected by Garrels and Christ (1965) (see table 8.3).

Table 8.3 Gibbs energies of formation of minerals and other species in the system Na_2O-CaO-SO_3-CO_2-H_2O at 25° C and 1 bar (ΔG_f^o)

Species	Chemical formula	Gibbs energy of formation $\frac{\Delta G_f^o}{kJ/mol}$	
nahcolite (nah)	$NaHCO_3$	- 851.68	(1)
		- 851.86	(2)
natron (nat)	$Na_2CO_3.10H_2O$	-3429.58	(1)
		-3428.98	(2)
trona (tr)	$NaHCO_3.Na_2CO_3.2H_2O$	-2381.7	(1)
		-2386.55	(2)
thermonatrite (tm)	$Na_2CO_3.H_2O$	-1289.59	(1)
		-1286.55	(2)
gaylussite (gay)	$Na_2CO_3.CaCO_3.5H_2O$	-3384.04	(1)
		-3372.64	(3)
pirssonite (prs)	$Na_2CO_3.CaCO_3.3H_2O$	-2661.79	(1)
		-2661.79	(3)
thenardite (tn)	Na_2SO_4	-1269.99	(4)
mirabilite (mb)	$Na_2SO_4.10H_2O$	-3646.54	(4)
burkeite (brk)	$Na_6CO_3(SO_4)_2$	-3594.2	(5)
calcite (cal)	$CaCO_3$	-1129.40	(6)
$CO_{2(g)}$		- 394.37	(4)
H_2O (l)		- 237.14	(4)

(1) Al-Droubi (1976). These values have been calculated from pK values and from values for the species in solution from Robie et al. (1978).
(2) Garrels & Christ (1965). (3) Hatch (1972). (4) Robie, Hemingway and Fisher (1978). (5) Vergouwen (1979). (6) Helgeson (1969).

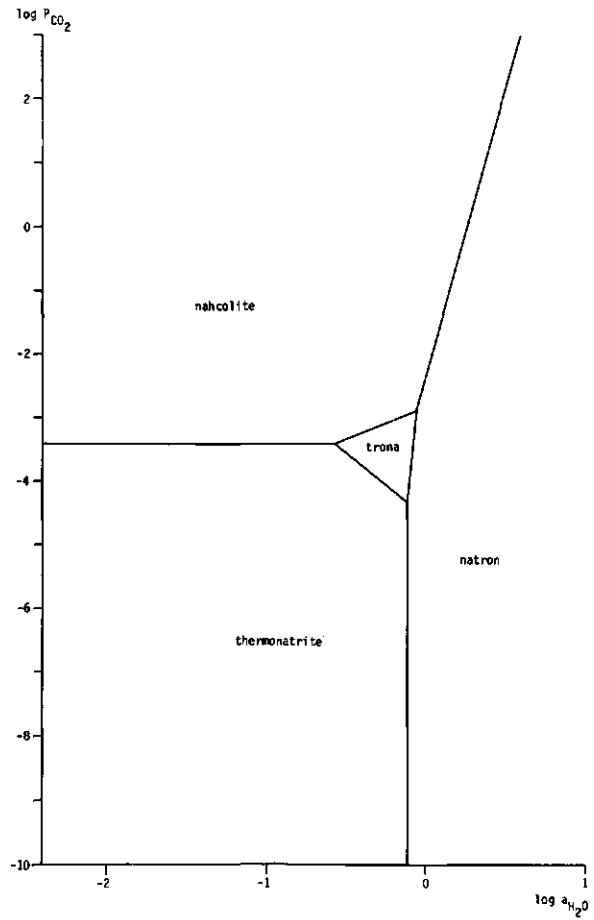

Fig. 8.2 Log p_{CO_2} - log a_{H_2O} - diagram of minerals in the system Na-CO_2-H_2O calculated by means of thermodynamic data selected by Al-Droubi (1976).

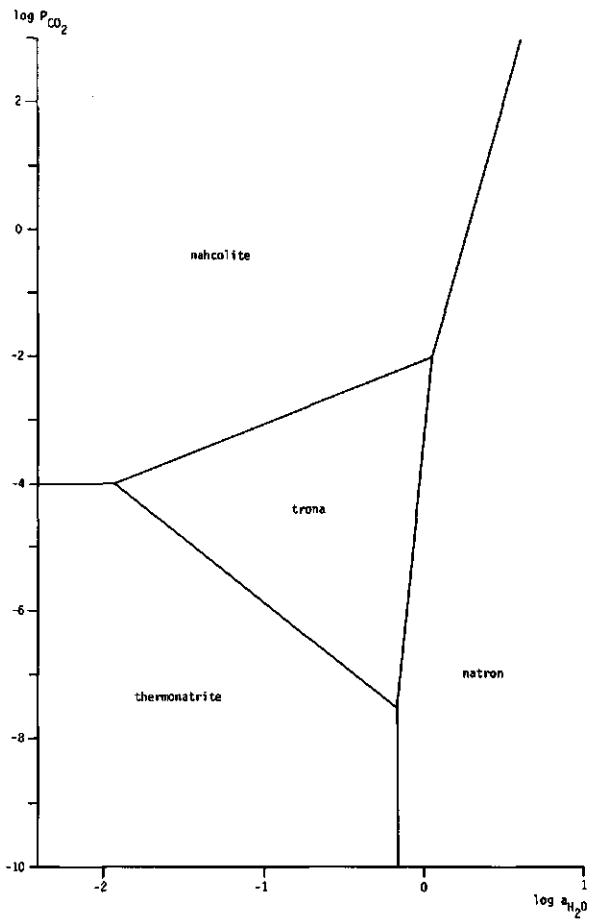

Fig. 8.3 Log P_{CO_2} - log a_{H_2O} - diagram of minerals in the system Na-CO_2-H_2O calculated by means of thermodynamic data selected by Garrels & Christ (1965).

In the diagram calculated with the values of Garrels & Christ, the stability field of trona is considerably enlarged at the expense of the other three carbonates in comparison with the diagram calculated with the values of Al-Droubi. This demonstrates the dependence of the calculated mineral stability fields on the choice of thermodynamic data.
In the following considerations the values of Garrels & Christ have been used because, contrary to Al-Droubi's values, these are more consistent with the observations made in the field and in the experiments.

The system Na-Ca-CO_2-H_2O

The stability fields of the minerals gaylussite and pirssonite can be superposed on the sodium carbonate diagram, assuming calcite or a $CaCO_3$-containing mineral to be stable over the whole log p_{CO_2} - log a_{H_2O} range. Gaylussite and pirssonite are related according to the reaction:

$$prs + 3H_2O \rightleftharpoons gay \qquad \text{slope } \infty \qquad (7)$$

Once more, the Gibbs energies of formation determine the a_{H_2O} at which these two minerals are in equilibrium with each other. The Gibbs values selected by Al-Droubi (1976) yield an equilibrium water activity between pirssonite and gaylussite that is completely different from that calculated with the values of Hatch (1972) (see table 8.3). The equilibrium water activity calculated with Hatch's values is greater than 1, which means that gaylussite would always be metastable with respect to pirssonite. As gaylussite occurs much more frequently than pirssonite, Hatch's values are probably not realistic.
The stability fields of gaylussite and pirssonite are delineated by the following reactions:

$$prs \rightleftharpoons tm + cal + H_2O \qquad \text{slope } \infty \qquad (8)$$

$$prs + CO_2 \rightleftharpoons cal + 2nah + H_2O \qquad \text{slope } 1 \qquad (9)$$

$$3\,prs + CO_2 \rightleftharpoons 2tr + 3cal + H_2O \qquad \text{slope } 1 \qquad (10)$$

$$3\,gay + CO_2 \rightleftharpoons 2tr + 3cal + 10H_2O \qquad \text{slope } 10 \qquad (11)$$

$$gay + CO_2 \rightleftharpoons cal + 2nah + 4H_2O \qquad \text{slope } 4 \qquad (12)$$

$$gay + 5H_2O \rightleftharpoons cal + nat \qquad \text{slope } \infty \qquad (13)$$

In fig. 8.4 these calcium-containing minerals are superposed on the sodium-carbonate diagram calculated with Garrels & Christ values for the Gibbs energies of the sodium carbonates. The gaylussite and pirssonite stability-fields are bounded by reactions (8), (10), (11), (12) and (13) (see fig. 8.4). From this diagram it is concluded that both pirssonite and gaylussite can form in equilibrium with trona. The same diagram calculated with the Gibbs energy

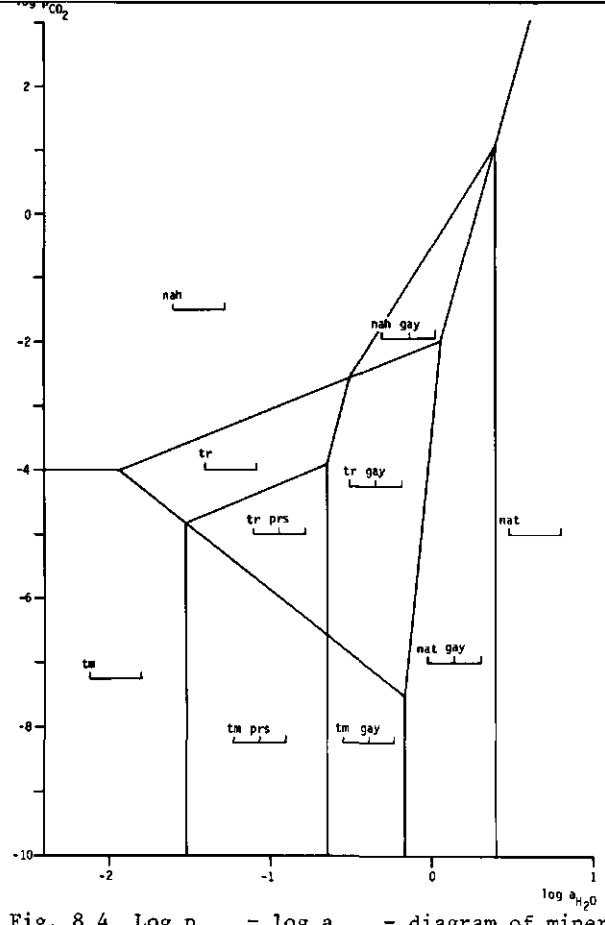

Fig. 8.4 Log p_{CO_2} - log a_{H_2O} - diagram of minerals in the system Na-Ca-CO_2-H_2O assuming calcite or a $CaCO_3$-containing mineral to be present over the whole log p_{CO_2} - log a_{H_2O} - range.

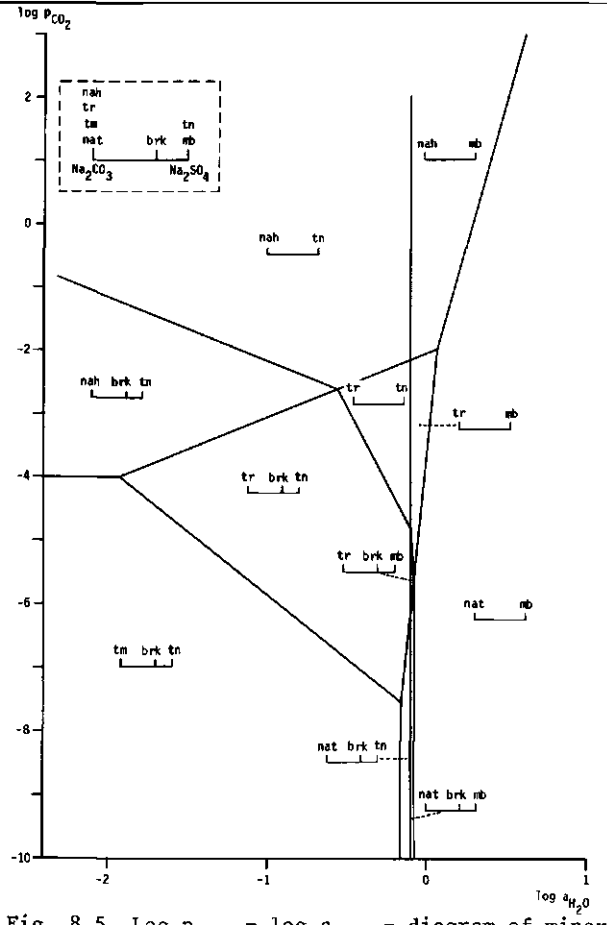

Fig. 8.5 Log p_{CO_2} - log a_{H_2O} - diagram of minerals in the system Na-SO_4-CO_2-H_2O assuming a Na_2SO_4-containing mineral to be present over the whole log p_{CO_2} - log a_{H_2O} - range.

values of the sodium carbonates selected by Al-Droubi shows that pirssonite cannot form in equilibrium with trona. Because pirssonite and trona often occur in the same mineral assemblages in nature, preference is given to the values selected by Garrels & Christ.

Al-Droubi (1976) states that at high CO_2-pressures the association calcite + nahcolite is unstable with respect to gaylussite and that the latter is favored by high p_{CO_2}. It is clear from both fig. 8.4 and from reaction (12) that this statement is incorrect.

The system Na-SO_4-CO_2-H_2O

The minerals burkeite, thenardite and mirabilite can be represented in the system Na-SO_4-CO_2-H_2O in addition to the sodium carbonates mentioned in section 8.3. Thenardite and mirabilite are related via the reaction:

$$Tn + 10H_2O \rightleftharpoons Mb \qquad \text{slope} \backsim\!\!\!\!\infty \qquad (14)$$

The stability field of burkeite in relation to the sodium carbonates can be determined assuming either thenardite or mirabilite (depending on the water activity) or a sodium sulphate containing mineral to be stable over the whole $\log CO_2$ - $\log H_2O$ - range. The Gibbs energy of burkeite as determined in section 7.5 is used to calculate its stability field (fig. 8.5). The Gibbs energy of burkeite was found using Garrels' values of the Gibbs energies of the sodium-carbonates and it is, therefore, consistent to use this value to determine a stability field of burkeite in a diagram constructed with the Garrels & Christ Gibbs energy values of the sodium carbonates.

The following reactions delineate the stability field of burkeite:

$$brk + CO_2 + H_2O \rightleftharpoons 2nah + 2tn \qquad \text{slope } -1 \qquad (15)$$

$$3brk + CO_2 + 5H_2O \rightleftharpoons 6tn + 2tr \qquad \text{"} \quad -5 \qquad (16)$$

$$3brk + CO_2 + 65H_2O \rightleftharpoons 6mb + 2tr \qquad \text{"} \quad -65 \qquad (17)$$

$$brk + 30H_2O \rightleftharpoons 2mb + nat \qquad \text{"} \quad \backsim\!\!\!\!\infty \qquad (18)$$

The system Na-Ca-SO_4-H_2O-CO_2

Fig. 8.6 shows a log p_{CO_2} - log a_{H_2O} -diagram of the system Na-Ca-SO_4-H_2O-CO_2. This figure is a combination of fig. 8.4 and fig. 8.5 and is constructed under the assumption that both a $CaCO_3$-containing and a Na_2SO_4-containing mineral is present over the whole log p_{CO_2} - log a_{H_2O} - range. With this assumption, minerals such as eugsterite, glauberite and gypsum, which also belong to the system Na-Ca-SO_4-H_2O-CO_2 are not stable, which is consistent

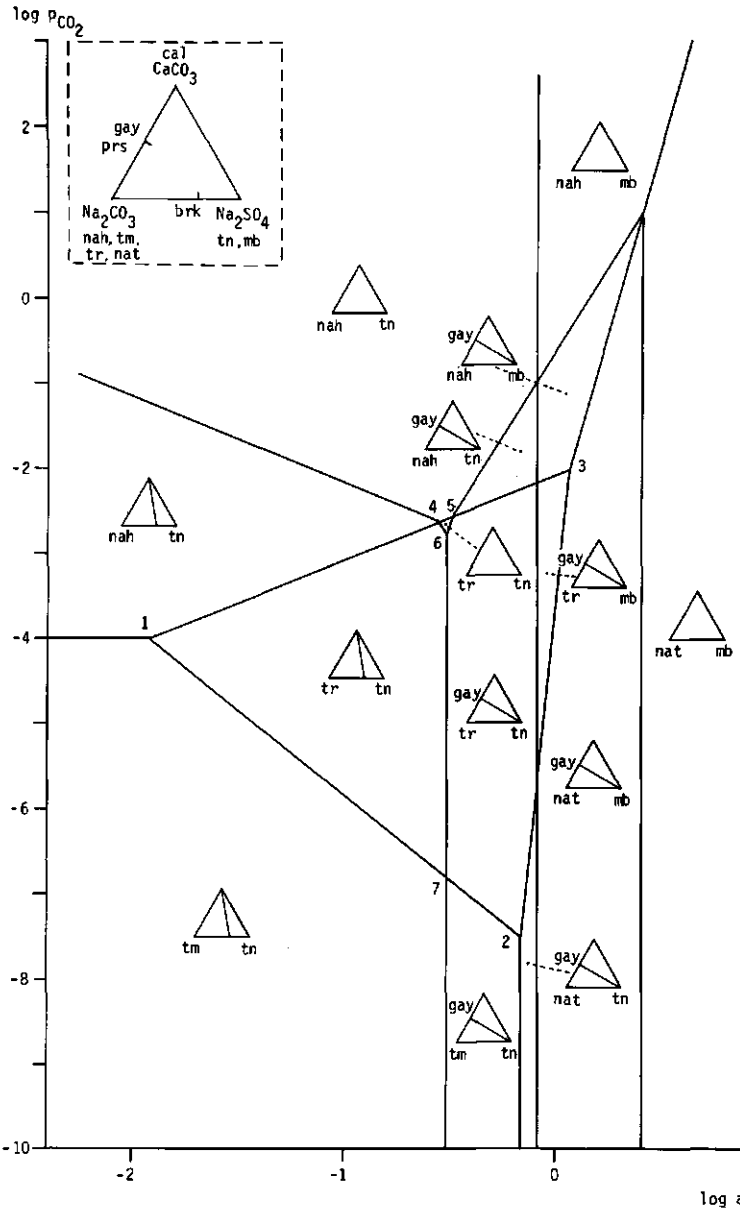

Fig. 8.6 Log p_{CO_2} - log a_{H_2O} - diagram of minerals in the system Na-Ca-SO_4-CO_2-H_2O assuming a $CaCO_3$- and a Na_2SO_4-containing mineral to be present over the whole log p_{CO_2} - log a_{H_2O} - range.

with the absence of these minerals from natural assemblages containing sodium carbonates.

Fig. 8.6 shows that the burkeite and gaylussite stability field contract in comparison with those in the Na-Ca-CO_2-H_2O (fig. 8.4) and the Na-SO_4-CO_2-H_2O (fig. 8.5) systems. Their bounding reaction is:

gay + 2tn $\rightleftarrows$ brk + cal + $5H_2O$ slope ∞ (19)

Whenever the sulphate concentration permits the formation of burkeite, pirssonite is metastable with respect to burkeite + calcite.

In general, if trona occurs in association with thermonatrite, the conditions of formation must have been somewhere along line 1-2 (fig. 8.6), which means a p_{CO_2} below atmospheric conditions ($10^{-3.5}$ atm.) if equilibrium has been maintained during the process of precipitation. The assemblage trona-nahcolite must have formed under equilibrium conditions described by line 1-3, at a p_{CO_2} around or higher than atmospheric CO_2-pressure.

The larger the number of minerals formed in equilibrium with each other, at constant P and T and with a definite number of components, the more restricted are the possible conditions of formation. For example the assemblage trona, thermonatrite, burkeite, can only form at conditions described by line 1-7; trona, thermonatrite, gaylussite by line 7-2; trona, nahcolite, gaylussite by line 5-3, etc. (see fig. 8.6).

Explanation of symbols used in fig. 8.4, fig. 8.5 and fig. 8.6

The minerals occurring in fig. 8.4 contain the components Na_2CO_3 and $CaCO_3$ in addition to CO_2 and H_2O. If the composition of the minerals is represented by a line with Na_2CO_3 on one side and $CaCO_3$ on the other side, all sodium carbonates plot on the Na_2CO_3-side of this line and calcite plots on the $CaCO_3$-side of the line. Gaylussite and pirssonite plot in the middle of the line as one mole of gaylussite or pirssonite is composed of one mole Na_2CO_3 and one mole $CaCO_3$ in addition to H_2O (see inset in fig. 8.4). Where more minerals coincide at the same point along the line, the one that appears in a certain stability field is named. For example tm ⌊——⌋ means: in this field thermonatrite is stable in association with calcite.

tm prs ⌊——⌋ means: in this field pirssonite is stable either with thermonatrite or with calcite. Thermonatrite and calcite cannot coexist here since at the boundary between these two fields the thermonatrite plus calcite react to give pirssonite.

The minerals occurring in fig. 8.5 contain the components Na_2CO_3 and Na_2SO_4 in addition to CO_2 and H_2O. If the composition of the minerals is represented

on a line with Na_2CO_3 on one side and Na_2SO_4 on the other, burkeite plots at a distance 2/3, because one mole of burkeite is composed of two moles of Na_2SO_4 and one mole Na_2CO_3 (see inset in fig. 8.5). The minerals of fig. 8.6 can be represented in the compositional triangle Na_2CO_3, Na_2SO_4 and $CaCO_3$ (see inset fig. 8.6).

For example:

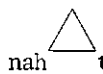

means: in this field, the association nahcolite, thenardite and calcite is a stable association.

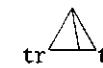

means: in this field burkeite is stable either with trona and calcite or with thenardite and calcite; trona and thenardite cannot coexist.

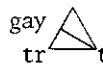

means: in this field gaylussite is stable either with thenardite and trona or with thenardite and calcite; trona and calcite cannot coexist.

At the boundary between the stability fields of the last two examples, the reaction burkeite plus calcite gives gaylussite plus thenardite (crossing of the two joins in the triangle) takes place.

This method of representing stable associations of minerals and their compositions along lines or in triangles is extensively described in Korzhinskii (1959).

Salt assemblages in the system Na-Ca-SO_4-CO_2-H_2O

The aim of this section is to investigate whether the assemblages belonging to the system Na-Ca-SO_4-CO_2-H_2O which have been found in the field and in the evaporating dishes are equilibrium assemblages and whether these assemblages can be explained by means of the log p_{CO_2} - log a_{H_2O}-diagrams previously discussed. In table 8.4 the agreements and differences between the two sets of salt assemblages have been given.

Lake Victoria. The samples along Lake Victoria at Simbi, Miti Bili and Kanam all contain trona.

At Miti Bili the calculated equilibrium CO_2-pressure of the groundwater originating from the spring decreases downstream but is always higher than atmospheric CO_2-pressure (see table 8.1). The salts sampled at locality Miti Bili 1 (see fig. 4.3) precipitated from surface water. Water coming from a spring flows over the soil surface and evaporates. The CO_2-pressure lies somewhere between the calculated value of the spring water ($10^{-0.16}$ bar) and atmospheric CO_2-pressure ($10^{-3.5}$ bar). If the salt association found around the spring (trona, calcite, gaylussite, nahcolite) has formed in equilibrium at p_{CO_2} of $10^{-2.57}$ bar

Table 8.4 Differences and similarities of salt assemblages belonging to the system $Na-Ca-SO_4-CO_2-H_2O$ found in Kenya and those in evaporating dishes precipitated from waters sampled in Kenya.

Kenya (see table 4.3)	Evaporation experiments (see table 8.1)
Lake Victoria	*Lake Victoria*
- trona is present in all assemblages	- trona does not occur in all assemblages
- thermonatrite is not always present	- thermonatrite occurs in all assemblages
- nahcolite occurs	- nahcolite does not occur
- burkeite occurs	- burkeite occurs
- gaylussite occurs, not in association with burkeite	- gaylussite does not occur
- pirssonite does not occur	- pirssonite does not occur
- nitrates do not occur	- nitrates occur
Amboseli	*Amboseli*
- trona occurs in all assemblages	- trona does not occur in all assemblages
- nahcolite does not occur	- nahcolite does not occur
- aphtithalite occurs, no sylvite	- both aphtithalite and sylvite occur
- burkeite does not occur	- burkeite does not occur
- both pirssonite and gaylussite occur	- pirssonite and gaylussite do not occur

(point 5, fig. 8.6), degassing must have taken place before precipitation according to:

$$2HCO_3^- \rightleftarrows CO_3^{2-} + CO_2 + H_2O \qquad (20)$$

At the other localities at Miti Bili, the salt efflorescences precipitated from water which was brought to the soil surface by capillary rise. Again the CO_2-pressure of these waters must be somewhere between atmospheric CO_2-pressure and the calculated CO_2-pressure of the groundwater which is higher than atmospheric CO_2-pressure. The salt associations formed in this way show assemblages characteristic for low CO_2 pressures, if they represent equilibrium assemblages of minerals. For example, the assemblage trona, thermonatrite, gaylussite would have formed under conditions described by line 7-2 in fig. 8.6 which means at CO_2-pressures between $10^{-6.8}$ and $10^{-7.5}$ bar. Such a drop in p_{CO_2} under natural circumstances is highly improbable. Therefore, these associations (formed under conditions of capillary rise) must be assumed to be non-equilibrium assemblages. The formation of nahcolite is apparently inhibited although this is a stable sodium carbonate under the calculated CO_2-pressures in the waters.

The presence of burkeite at Miti Bili explains the absence of pirssonite in the assemblages. Burkeite does not occur in samples in which gaylussite is present and these two minerals can only coexist at one specific water activity at

which reaction (19) takes place (see fig. 8.6).

Amboseli. The salts sampled at Amboseli (see table 4.3) originated by evaporation of groundwater. The partial CO_2-pressures of the Amboseli groundwaters vary from $10^{-0.74}$ to $10^{-3.05}$ bar (see table 8.1), well above atmospheric CO_2-pressure. Just as along Lake Victoria, trona is present in all samples containing sodium carbonates. Nahcolite has not been found and thermonatrite is widespread. Once more, many assemblages occur which could only have formed under much lower CO_2-pressures - if they precipitated under equilibrium conditions.

Because some of the waters at Amboseli contain significant amounts of potassium, aphtithalite is formed both in association with pirssonite and with gaylussite. The aphtithalite controls the activity of sulphate in such a way that burkeite does not form. The absence of burkeite in these samples explains the presence of pirssonite.

Konya Basin. In the Konya Basin in Turkey sodium carbonates occur only in a restricted area around Akgöl, at localities T15, T26, T31 and T32. The carbonate associations are very simple, mainly trona, burkeite. This association is stable over a very large log p_{CO_2} - log a_{H_2O} range below log p_{CO_2} = -2.61 bar (fig. 8.5). The CO_2-pressures of the waters at these localities vary between $10^{-0.53}$ and $10^{-3.19}$ bar. Some of these CO_2 pressures fall within the trona, burkeite stability range. In case of the higher values degassing will have taken place before precipitation of the salt assemblage.

Evaporating dishes. A few water samples taken in the Lake Victoria area produced nitrates upon evaporation in the laboratory. The nitrate concentration of the waters was not determined at the time of analysis but the high nitrate content explains in some cases the great difference between anion- and cation concentration of the analysed ions (see table 4.1). For example the waters from Simbi appeared to be very nitrate-rich after evaporation in the laboratory. In the field, however, only carbonates - no nitrates - were found.

The waters from the spring at Miti Bili show another remarkable feature. From a water sample taken before the rainy season, nitrates precipitated in the evaporation dishes in association with carbonates. No nitrates formed at all from a water sample from the same spring collected one month later after abundant rainfall. The same phenomenon was observed in groundwater samples taken in a dry river bed at Kanam (fig. 4.3).

In the evaporation experiments it was observed that thermonatrite is the

first sodium carbonate to precipitate, sometimes in association with trona, in most dishes in which any sodium carbonates precipitated. From the rim downwards towards the centre of the dishes the ratio of trona to thermonatrite increases. The initial CO_2-pressure of the waters lies somewhere between the calculated CO_2-pressure (see table 8.1) and atmospheric CO_2-pressure. Apparently, the same process takes place in the dishes as under natural circumstances. Thermonatrite forms in the experiments although nahcolite or trona are the stable sodium carbonates at CO_2-pressures that are higher than the atmospheric value. The same is observed in the field. This can be explained as follows: Once thermonatrite precipitates, two processes occur simultaneously:

1. Evaporation causes all concentrations in solution to rise and therefore also the CO_2-content. It is well known that the diffusion of CO_2 through the solution-air interfase is a slow process and the CO_2-pressure of the solution, therefore, will increase.
2. The sodium concentration is higher than the alkalinity in most water samples from which the sodium carbonates precipitated. In the case of thermonatrite precipitation the same process will take place as in the case of calcite precipitation which was explained in section 5.4. During precipitation of thermonatrite and further evaporation, the sodium concentration will increase and the alkalinity will decrease causing the CO_2-pressure of the water to decrease.

These two processes counteract each other and, therefore, it is impossible to predict whether the CO_2-pressure of the solution will increase or decrease during thermonatrite precipitation. An increasing CO_2-pressure favours the formation of trona over themonatrite.

Gaylussite and pirssonite did not form in the evaporation experiments. In those cases where gaylussite formed under natural conditions from carbonate-rich samples taken from the Lake Victoria area, burkeite formed in the evaporating dishes. This might be due to the following two reasons:

1. Degassing of CO_2 causes the Ca-concentration to become too low for the formation of gaylussite. During fractional crystallisation calcite is no longer in contact with the solution and cannot react to form gaylussite as it would do under equilibrium conditions.
2. The activity of H_2O reaches a lower value in the evaporating dishes than under natural circumstances. At low water activities gaylussite is metastable with respect to burkeite (see fig. 8.6), provided that sufficient sulphate is present.

It must be emphasized that the conclusions in this section, which have been drawn on the basis of thermodynamic data, are valid only if the latter are valid. Thus, thermonatrite precipitates either as a metastable phase with respect to trona and nahcolite. or the thermodynamic data on which this conclusion is based are not valid.

8.4 SOLUBILITY CALCULATIONS IN THE SYSTEM Na-K-Mg-Ca-Cl-SO_4-H_2O

Most salt minerals in the Konya Basin in Turkey belong to the system Na-K-Mg-Ca-Cl-SO_4-H_2O, the so-called "seawater system". Much experimental work has been done in this system in order to explain salt sequences in marine evaporite deposits. Especially van 't Hoff and coworkers (1905, 1909, 1912) determined many phase diagrams in an effort to elucidate the seawater problem. Phase diagrams are useful as long as the system is not too complicated. For multicomponent systems however, phase diagrams have their limitations and mineral solubility predictions in such systems require a theory which describes the behaviour of electrolyte solutions in an accurate way. First a short review of the development of the theory describing such solutions will be given.

The activity of a species i is defined as:

$$a_i = \gamma_i m_i \tag{22}$$

where a_i = activity of species i
γ_i = activity coefficient of species i
m_i = molality of species i.

For an electrolyte $A_{\nu+}B_{\nu-}$ which dissociates in $\nu+$ kations A and $\nu-$ anions B ($\nu+ + \nu- = \nu$), the mean ionic activity coefficient $\gamma_{\pm}$ is used, which is defined as:

$$\gamma_{\pm} = \sqrt[\nu]{\gamma_+^{\nu+} \cdot \gamma_-^{\nu-}} \tag{23}$$

In dilute solutions the mean ionic activity coefficient can be calculated using the Extended Debye-Hückel equation:

$$\log \gamma_{\pm} = \frac{-A|z_+z_-|\sqrt{I}}{1+Ba\sqrt{I}} \tag{24}$$

where A and B are constants which involve the temperature and the dielectric constant in a different way

a = distance of closest approach of the ions

I = ionic strength, defined as $I = \frac{1}{2} \Sigma m_i z_i^2$ where m_i is the molality of every different ionic species i and z_i is the charge of ion i

z_+ = electric charge of the kation

z_- = electric charge of the anion.

The Extended Debye-Hückel equation is valid for solutions with an ionic strength less than 0.1. Scatchard (1936) describes the deviation at higher ionic strengths between the experimental mean ionic activity coefficient and the activity coefficient calculated from the Extended Debye-Hückel equation. The new equation becomes:

$$\log \gamma_{\pm} = \frac{-A|z_+z_-|\sqrt{I}}{1+Ba\sqrt{I}} + B_i^{\cdot} I \qquad (25)$$

The first term is the normal Extended Debye-Hückel equation and the second term is called the "Scatchard deviation function". Scatchard found that the function $B_i^{\cdot}$ appears to be either constant over a wide range of ionic strengths or is a slowly varying function of I.

Harned (1935) did many experiments with mixed electrolytes and he found the following relation, known as "Harned's rule", between the activity coefficient of an electrolyte B and the molality of another electrolyte C.

$$\log \gamma_B = \log \gamma_{B(o)} - \alpha_B m_C \qquad (26)$$

where $\gamma_{B(o)}$ is the activity coefficient of B in a solution which contains only salt B and α_B is a mixing parameter, called "Harned's coefficient" (Harned, 1935; Robinson & Stokes, 1970).

Wood (1972, 1975) combined the Scatchard deviation function with Harned's rule resulting in an equation which appeared to be applicable to concentrated brines and which agreed rather well with experimental data. His equation is as follows:

$$\log \gamma_{\pm} = \frac{-A|z_+z_-|\sqrt{I}}{1+Ba\sqrt{I}} + \frac{2\nu_+\nu_-}{\nu} (B_i + \sum_{j=1}^{n} \alpha_{ij} y_j) I \qquad (j \neq i) \qquad (27)$$

where α_{ij} is a constant mixing parameter characterizing the interaction of the i and j components

y_j is the ionic strength fraction of the j^{th} component.

Pitzer and coworkers (1973, 1974, 1975) describe the thermodynamic properties of brines to high ionic strengths by a virial expansion of the activity coefficient using second, third and higher virial coefficients. Reference is given to Pitzer et al (1973, 1974, 1975) and Harvie & Weare (1980) as the equations are rather complicated. Scatchard (1968) and Pitzer (1973) indicated that the use of only a second virial coefficient is not sufficient to predict thermodynamic properties of solutions above a ionic strength of 4. Third or higher virial coefficients are required. Recently Harvie & Weare (1980) developed the method of Pitzer and coworkers (1973, 1974, 1975) for mineral solubility calculations. Harvie & Weare (1980) objected against the Wood model as this is only a second virial coefficient model. Another objection against the Wood model is that the Harned's coefficients which are used in the model are not internally consistent (de Rooij, personal communication). Harvie & Weare (1980) demonstrated that second and third virial coefficients are sufficient to perform mineral solubility calculations. They derived chemical potentials and third virial coefficients from ternary experimental phase diagrams. Unfortunately, their calculations did not yet include parameters for systems with carbonates.

The computerprogram of Harvie & Weare permits the prediction of precipitation of mineral sequences from solutions, for example the sequences in marine evaporites (Eugster et al, 1980; Harvie et al, 1980). With the program both sequences formed under equilibrium conditions and sequences formed during fractional crystallisation can be traced. Precipitation under equilibrium conditions allows backreaction of previously formed minerals with the solution. During fractional crystallisation a mineral which once precipitated is no longer in contact with the solution.

The system Na-Mg-SO_4-H_2O

Minerals precipitating from a solution in the ternary system Na-Mg-SO_4-H_2O can be depicted in a $m_{Na_2SO_4}$ - m_{MgSO_4} -diagram, which is shown in fig. 8.7. This diagram has been calculated by Harvie and Weare (1980) from experimental data at 25^{o} C.

Such diagrams indicate which mineral(s) are in equilibrium with the saturated solution as well as the composition of the saturated solution. If, for example, a solution with an initial composition P evaporates, mirabilite will be the first precipitate in equilibrium with a solution with composition Q. During further evaporation and precipitation of mirabilite, the composition of the solution will change along the saturation line of mirabilite until the solution becomes

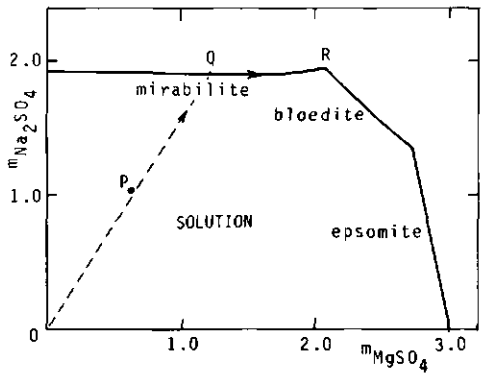

Fig. 8.7 Calculated mineral solubilities in the system Na-Mg-SO_4-H_2O at 25° C (from Harvie & Weare, 1980)

also saturated with respect to bloedite at composition R. The phase rule shows that R is an invariant point at constant temperature and pressure. Therefore, the composition of the saturated solution no longer changes once it has reached composition R. At this point both mirabilite and bloedite will precipitate. It is evident that the $Na_2SO_4/MgSO_4$ ratio in the initial solution determines whether the final precipitate will consist of mirabilite + bloedite or of epsomite + bloedite.

The system Na-Mg-SO_4-Cl-H_2O

Addition of chlorine to the ternary system of the preceding paragraph results in the quaternary reciprocal system Na-Mg-Cl-SO_4-H_2O. Fig. 8.8 is a Jänecke diagram of this system at 25° C, as calculated recently by Harvie & Weare (1980). These authors claim a better agreement with experimental data than any earlier effort. On the chlorine-free righthand side of the square, the same sequence mirabilite-bloedite-epsomite appears as in the ternary diagram of fig. 8.7.

In this Jänecke type of diagram only the ratio of the components in a saturated solution can be found and not their absolute concentrations as in fig. 8.7. The labels in the fields indicate the first mineral species with which a solution, plotting in that field, becomes saturated. For example, thenardite will be the first mineral to precipitate when a solution with initial composition P evaporates. During further evaporation and thenardite precipitation the composition of the solution will move away from the saltpoint of thenardite (the point at which solid thenardite plots) along a line through the initial composition P (see

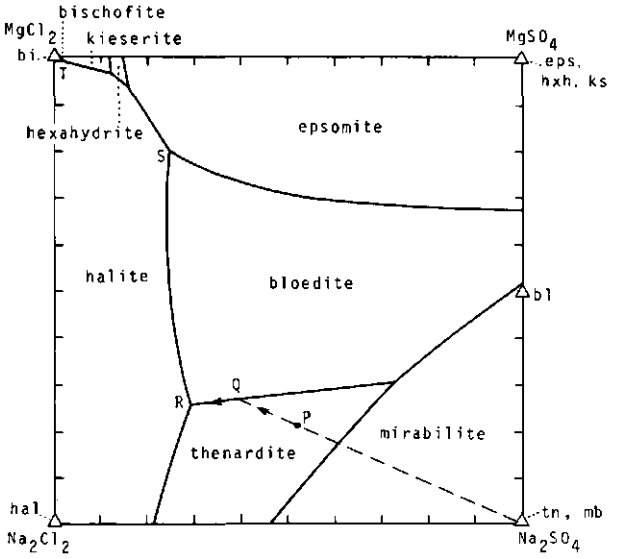

Fig. 8.8 Jänecke diagram of the reciprocal system Na-Mg-SO_4-Cl-H_2O at 25° C from Harvie & Weare (1980). For abbreviations of salt points, see table 3.2. In addition, bi: bischofite ($MgCl_2.6H_2O$); ks: kieserite ($MgSO_4.H_2O$)

arrow in fig. 8.8) until the composition of the solution reaches the field labelled bloedite. At this composition Q both thenardite and bloedite will precipitate and the composition of the solution will change along the boundary between the thenardite and bloedite fields until the invariant point R is reached, where thenardite, bloedite and halite are in equilibrium with a saturated solution with composition R. The final precipitate will consist of these three minerals.

The square can be divided in three subtriangles (see fig. 8.8). All initial solutions plotting in subtriangle Na_2Cl_2-Na_2SO_4-bloedite will terminate at invariant point R; all initial solutions plotting in subtriangle Na_2Cl_2-bloedite-$MgSO_4$ will terminate at invariant point S and all initial solutions plotting in subtriangle Na_2Cl_2-$MgCl_2$-$MgSO_4$ will terminate at invariant point T. At each invariant point three minerals are in equilibrium with a saturated solution.

The system Na-K-Mg-Cl-SO_4-H_2O

The quinary system Na-K-Mg-Cl-SO_4-H_2O cannot be represented in a two dimensional diagram unless an additional restriction is made. Fig. 8.9 is a Jänecke projection of this quinary system at 25° C with the restriction that all mineral

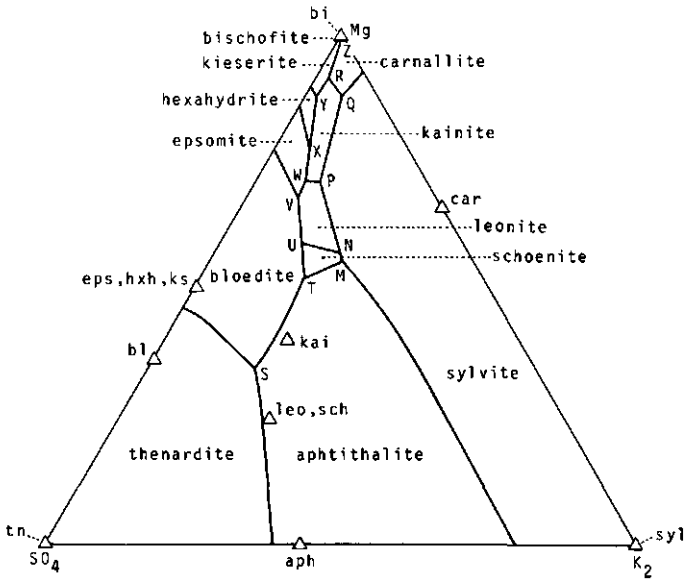

Fig. 8.9 Jänecke projection at 25° C of the system Na-K-Mg-Cl-SO_4-H_2O calculated by Harvie & Weare (1980). All mineral zones denoted are saturated with respect to halite. Abbreviations of salt points, see fig. 8.7. In addition, leo: leonite ($K_2Mg(SO_4)_2.4H_2O$); kai: kainite ($KMgClSO_4.3H_2O$); car: carnallite ($KMgCl_3.6H_2O$).

zones are also saturated with respect to halite. Along the potassium-free Mg-SO_4 side of the triangle the same mineral sequence can be seen (thenardite, bloedite epsomite, hexahydrite, kieserite, bischofite) as the sequence along the boundary of the halite field in fig. 8.8.

The labels of the fields have the same meaning as the labels in fig. 8.8 and the evolution of a solution which is saturated with respect to certain minerals is also derived in the same way. For a detailed description of the use of Jäneck diagrams, the reader is referred to Braitsch (1971). Both the ratio of the compo nents in the saturated solution and the ratio of the quantity of minerals which have precipitated from this solution can be derived from this diagram.

The diagram can be divided in subtriangles by joining the saltpoints of the different minerals. The subtriangle in which an initial solution plots determine the invariant point at which the evaporation will end. For example, initial compositions plotting in subtriangle thenardite-aphtithalite-bloedite will terminat at invariant point S at which point thenardite, aphtithalite and bloedite coprecipitate with halite in equilibrium with a saturated solution with composition S Three minerals are in equilibrium with a saturated solution in addition to

halite at an invariant point in this system.

The system Na-K-Ca-Mg-Cl-SO_4-H_2O

The phase relations in the senary system Na-K-Ca-Mg-Cl-SO_4-H_2O can be represented in a tetrahedron with Mg, K, Ca and SO_4 at the corners and all mineral zones saturated with respect to halite. This tetrahedron can be subdivided into subtetrahedra formed by four saltpoints of minerals. Evaporation of an initial solution plotting in a certain subtetrahedron must terminate at the invariant point at which the four minerals forming the corners of the subtetrahedron co-precipitate. Four minerals are in equilibrium with a saturated solution in addition to halite at an invariant point in this system.

It is evident that the phase relations are too complicated to visualize in two dimensions. The program of Harvie & Weare (1980), which has been developed for this system, permits the calculation of the mineral sequences that precipitate from a solution in this senary system.

Salt assemblages in the system Na-K-Mg-Ca-Cl-SO_4-H_2O

Some striking differences become apparent by comparing the salt assemblages found in the Konya Basin and the assemblages in the evaporating dishes precipitated from the waters sampled in the Konya Basin. Table 8.5 shows the similarities and differences between the two sets of salt assemblages. The assemblages containing sodium carbonates have not been taken into account in this table (see table 8.3).

The analyses of five carbonate-poor samples, T9, T8, $T5^b$, T11 and T13 from Turkey (for chemical analyses, see table 3.1) and the carbonate-poor Luanda sample from Kenya (see table 4.1) were selected and run with the computerprogram of Harvie & Weare in San Diego, California by Nancy Möller-Weare. The calculation was done assuming that equilibrium precipitation takes place. Before running the samples, the water analyses were all charge balanced within the stated per cent deviation. The necessary concentration changes were made on the major ion (if obvious) or on all the major ions if their concentrations were similar. The carbonate-ions were subtracted from the solutions by assuming calcite precipitation.

In all selected samples gypsum was the first mineral to precipitate. Glauberite formed in the next stage by backreaction of gypsum. Halite was the third mineral with which the solutions became saturated, followed by thenardite and/or bloedite. The potassium-bearing minerals formed in a later stage. According to

Table 8.5 Differences and similarities of salt assemblages belonging to the system Na-K-Mg-Ca-Cl-SO_4-H_2O found in the Konya Basin and those in evaporating dishes precipitated from waters samples in the Konya Basin. For abbreviations of minerals, see table 3.2.

Konya Basin (see table 3.3)	Evaporation experiments (see table 8.2)
- bloedite occurs in many assemblages in the following associations: bl-hxh-gps -hal-gl -eps-gps -hxh-sch-hal -eug -hal-gps -gps-lw -hal-stk-kon -hal-gps-kon -hxh-gps-kon	- bloedite occurs in only two dishes in the following associations: bl-hal-hxh-kon-gps -hal-hxh-kon-gps
- thenardite occurs in the following associations: tn-gl -aph -hal-eug -gps-hal-eug-gl -hal-aph thenardite does not occur with Mg-bearing minerals	- thenardite occurs in the following associations: tn-gps-hal-hxh -gps-hal-hxh-kon -hal -hal-lw-hxh thenardite occurs with Mg-bearing minerals, not with bloedite
- loeweite occurs only once in the following association: lw-gps-bl	- loeweite occurs very often in the following associations: lw-hal-bl-hxh-kon -gps-hal-hxh -hal-hxh-tn -gps-hal-kon -gps-hxh-hal-kon -hal-cal -gps-eps-hxh-hal -hxh-hal
- aphtithalite is the only potassium bearing mineral, no polyhalite	- no potassium bearing minerals
- glauberite occurs	- no glauberite
- eugsterite occurs	- no eugsterite
- not always halite	- always halite
- konyaite occurs rarely	- konyaite occurs often

the computer calculations the following minerals precipitate from the selected samples under the assumption of equilibrium precipitation:

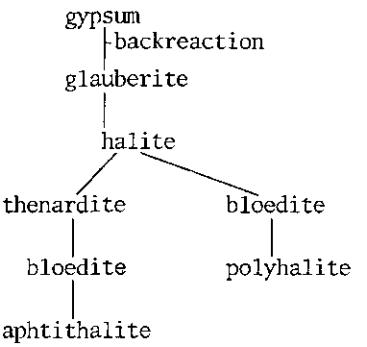

The samples were run until a_{H_2O} reached a value of about 0.70. At this water-activity two samples (T9 and the Luanda sample) ended at an invariant point (bloedite, thenardite, aphtithalite, glauberite, halite).

It must be concluded from a comparison of both the natural salt assemblages and the salt assemblages formed in the laboratory with the equilibrium sequences calculated with the program of Harvie & Weare, that the assemblages formed in the field, mainly due to evapotranspiration of groundwater, approach much better precipitation under equilibrium conditions than the assemblages formed in the evaporating dishes.

There is some evidence for the non-equilibrium conditions in the dishes. Eugsterite can, as glauberite, be regarded as a mineral which forms at the expense of gypsum during equilibrium precipitation, although it is a metastable mineral contrary to glauberite. Eugsterite and glauberite are both absent in the evaporating dishes. The minerals loeweite and konyaite, both being metastable minerals at ambient conditions, formed often in the dishes. Furthermore, thenardite and either hexahydrite or epsomite cannot form in equilibrium with each other in the same assemblage (see fig. 8.9). In the dishes thenardite occurs often in association with hexahydrite. This association can only have formed during a process of fractional crystallisation.

In the field equilibrium conditions predominate. Both eugsterite and glauberite, which precipitate by backreaction of gypsum with the solution, have formed widespread under natural circumstances. Apparently all thenardite, if it has formed in Mg-rich solutions, has backreacted with the solution to Mg-bearing minerals because thenardite does not occur in association with a Mg-bearing mineral in the field, not even with bloedite. Not all assemblages found in the field

have formed under equilibrium conditions. The coexistence of thenardite and gypsum and the presence of eugsterite and konyaite prove that also during evapotranspiration both fractional crystallization and formation of metastable minerals takes place. Konyaite even had disappeared in some samples two years after sampling, which proves the metastability of this mineral. Such non-equilibrium processes occur on a less extensive scale than in the evaporating dishes.

Prediction of mineral assemblages in salt efflorescences and in evaporating dishes is difficult, even if accurate activity coefficients for brines are available. In both cases the processes are a mixture of equilibrium conditions, fractional crystallization and formation of metastable minerals. The salt assemblages in natural salt efflorescences are best predicted by assuming precipitation under equilibrium conditions, whereas the mineral assemblages in evaporating dishes in the laboratory are best predicted by assuming the formation of metastable minerals and fractional crystallization.

9. STABLE ISOTOPES IN WATERS FROM THE KONYA- AND AMBOSELI BASINS; A RECONNAISSANCE STUDY

9.1 INTRODUCTION

In recent years the stable isotope composition of natural waters has increasingly been used to trace the origin of these waters, and their subsequent history during evaporation and/or interaction with soils and rocks. This study is primarily concerned with the evolution of evaporating solutions and the precipitation of salt minerals from these solutions.

It was felt that the stable isotopic composition of the water samples from the Konya Basin in Turkey and from the Amboseli Basin in Kenya could give additional information on the processes involved such as the evolution of the evaporating solutions and the precipitation of salt minerals from these solutions. The opportunity to determine the isotopic composition of the water samples arose during the present study but because the samples were not taken with this aim in mind, only those samples could be used which fulfilled the requirements for isotopic analysis.

9.2 THE STABLE ISOTOPES OF HYDROGEN AND OXYGEN

Hydrogen and oxygen, both constituents of water, occur as mixtures of different isotopes, namely hydrogen with mass 1 (99.984%), deuterium with mass 2 (0.016%) and three isotopes of oxygen with masses 16 (99.76%), 17 (0.04%) and 18 (0.20%). The different masses of these isotopes cause them to behave in slightly different ways in chemical reactions, although their chemical properties are identical. Consequently, the isotopic compositions of two oxygen and/or hydrogen bearing compounds which are in equilibrium will, in general, be slightly different. This difference, defined as the equilibrium isotope fractionation, increases as the equilibrium temperature is lowered. In general the heaviest isotope is concentrated in the phase in which it is most strongly bound.

The isotopic composition of a sample is measured with a mass spectrometer. Unknown samples are measured relative to a standard of known isotopic composition. The standard used for water analyses is the so-called SMOW (Standard

Mean Ocean Water). Isotopic values are commonly reported in the δ-notation, in which the isotopic composition of an unknown sample (x) is related to the isotopic composition of a standard sample (st) in the following way:

$$\delta_x = \frac{R_x - R_{st}}{R_{st}} . 1000$$

In this formula R denotes the isotope ratios D/H or $^{18}O/^{16}O$. Consequently $\delta^{18}O$ and δD of SMOW are 0. The δ-value is expressed in °/oo (per mil) and has an analytical precision which is in general of the order of 1 °/oo for δD and 0.1 °/oo for $\delta^{18}O$. Positive values of δ indicate that the sample is enriched in D or ^{18}O relative to the standard and is, therefore, heavier; negative values indicate that the sample has less of the heavy isotope than the standard and is, therefore, lighter.

9.3 FACTORS AFFECTING THE ISOTOPIC COMPOSITION OF NATURAL WATERS

The oceans are the largest reservoir of water on the earth's surface. All meteoric waters and the lakes, rivers and groundwaters originating from them are directly or indirectly derived from the ocean reservoir.

The isotopic compositions of many meteoric waters ranging from tropical rainwater to Antarctic ice and snow have been measured (Craig, 1961; Epstein et al, 1965, 1970). For these waters there is a linear relationship between δD and $\delta^{18}O$ given by:

$$\delta D = 8\ \delta^{18}O + 5$$

This line, called the Meteoric Water Line (MWL), determines the isotopic composition of almost all precipitations as a function of geographic latitude, topography, and local climatic conditions.
In older papers this equation is also given as $\delta D = 8\ \delta^{18}O + 10$ because at that time the Antarctic precipitations had not yet been analysed.

The linear relationship between the hydrogen and oxygen isotopic compositions is caused by the fact that the condensation of waters from the earth's atmosphere in the form of rain or snow is essentially an equilibrium fractionation process, and that all of these waters derive ultimately from a single source of water, namely ocean water. The fractionation of D/H is proportional to the $^{18}O/^{16}O$ fractionation in the ratio of 8:1. As temperature decreases, both fractionations increase proportionally.

Some deviations from the linear relationship given above do occur. In the Eastern Mediterranean, which is relevant to the discussion of the isotopic

results of the Konya Basin, the precipitations follow a line given by (Gat, 1966):

$$\delta D = 8\ \delta^{18}O + 22$$

Other exceptions to the normal linear relationship are the isotopic compositions of waters from closed basins. Waters in closed basins are usually concentrated saline waters which form by evaporation of precipitation waters. The isotopic compositions of such waters also show a linear relationship, but have a slope of 4-6, instead of 8 as for normal waters. Such lines, which are characteristic for evaporation processes, intersect the MWL at the point of the mean of the precipitations in that particular area.

Another type of waters which do not follow the MWL are the (usually hot) spring waters, that have had a measurable degree of interaction and exchange with solid rocks. Rocks constitue a large reservoir of oxygen, because almost all minerals can be considered as compounds of oxides, but only a small reservoir of hydrogen, as most minerals contain no, or at most only a small amount of hydrogen. Water, on the contrary, is a large reservoir both of oxygen and hydrogen. If a certain amount of water interacts with a rock body, with which it is not in isotopic equilibrium under the given conditions, the isotope exchange with the rock will cause a significant shift of the oxygen isotopic composition of the water. The hydrogen isotopic composition remains virtually unchanged during this process, because there is relatively little hydrogen to exchange with. These effects are essentially caused by the relative sizes of the exchanging reservoirs. If, for example, hydrogen and oxygen isotopes are exchanged between 1 kg of water and 1.6 kg of kaolinite, a mineral certainly richer in hydrogen than most minerals, the final oxygen isotope composition would be for 50% determined by the contribution of the kaolinite whereas the hydrogen isotopic composition would only be determined for less than 3% by the kaolinite contribution. This means that the original D/H ratio of the water would hardly change by the water-rock interaction. Fig. 9.1 shows the Meteoric Water Line (MWL), the East Mediterranean Water Line (EMWL), and the evolution of the isotopic composition of a specific precipitate during evaporation and water-rock interaction respectively in a δD-$\delta^{18}O$ diagram.

Not only the isotopic composition of a natural water changes during evaporation, but also its chemical composition changes as a linear function of its degree of evaporation as long as it is not saturated with respect to one or more salt minerals. On the other hand, a water can also change its chemical com-

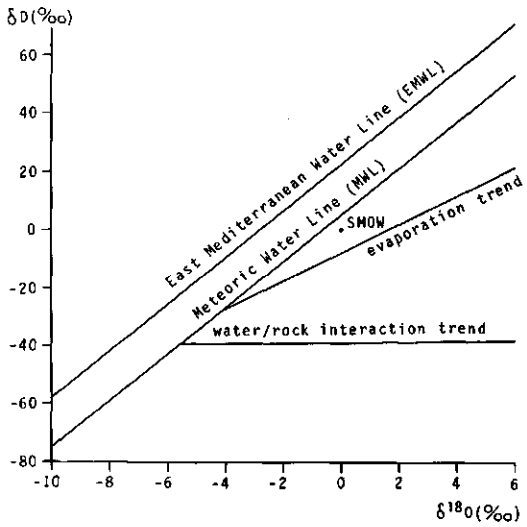

Fig. 9.1 East Mediterranean Water Line (EMWL) $D = 8\delta^{18}O + 22$. Meteoric Water Line (MWL) $D = 8\delta^{18}O + 5$. Evaporation trend, slope 5. Water-rock interaction trend, slope ± 0.

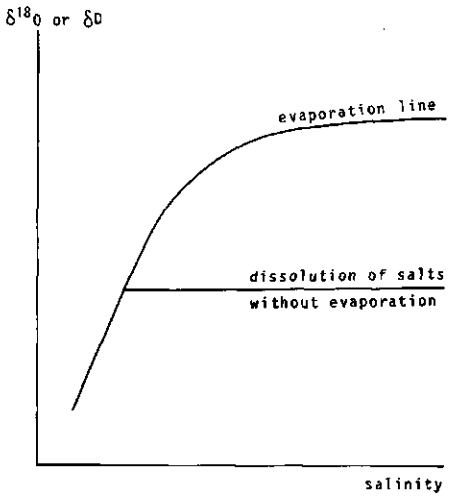

Fig. 9.2 The isotopic composition of an evaporating water body under natural circumstances with a given relative humidity reaches a steady state. Dissolution of salts increases the salinity without changing the isotopic composition.

position by dissolution of salts without changing its isotopic composition.

The simple case of evaporation of a single batch of water in a completely dry atmosphere (relative humidity 0) is, of course, never realized in nature. Examples which closely approach this situation have been described by Fontes & Gonfiantini (1967). In most cases of evaporation under natural conditions, with a given humidity, in which the vapor has a defined isotopic composition, the isotopic composition of the evaporating body of water reaches a steady state. The process is complicated by the fact that there is usually a continuous inflow of new water into the evaporating body. The mathematics of such situations become rather complicated and are beyond the scope of this study.
The evolution of the isotopic composition of an evaporating body in which no evaporation, but only dissolution of salts takes place, is shown schematically in a δD or $\delta^{18}O$ versus salinity diagram in fig. 9.2.

It can be concluded that the history of a natural water can be traced by measuring its chemical and its isotopic composition. It becomes possible to determine the isotopic composition of the precipitation in a specific area and

to distinguish between effects of evaporation and of interactions between water and rocks or specific minerals.

9.4 ANALYTICAL PROCEDURES AND DATA

For the δD determination, the waters were reduced to hydrogen gas prior to analysis by reacting the water with uranium metal at 800° C. For the $\delta^{18}O$ measurement, the waters were equilibrated with small amounts of CO_2 of known isotopic composition at 25° C; the fractionation between water and CO_2 is accurately known. Analyses were performed by Dr. R. Kreulen and J. Meesterburrie of the department of Geochemistry, Vening Meinesz Laboratory, Rijks Universiteit, Utrecht, on a mass spectrometer Micro-mass 602.

From the analytical methods used, it is clear that in the case of the oxygen isotope compositions activity ratios are in fact measured instead of concentration ratios (the sample and the standard are equilibrated with small amounts of CO_2), whereas in the case of D/H ratios concentration ratios are measured (all the hydrogen of the water sample and standard is converted to hydrogen gas). In dilute solutions the difference between concentrations and activities is negligible. For some of the highly concentrated brines this salt effect becomes measurable.

Sofer & Gat (1975) determined that the Mg-concentration has the largest effect on the activity of the isotopes. Therefore, the δD of the sample with the highest Mg-concentration has been recalculated, using the formula given by Sofer & Gat (1975), to show the difference between the δD expressed in concentration ratios and the δD expressed in activity ratios. This difference, calculated for sample 37 from the Konya Basin, is -1.5°/oo, i.e. around the analytical precision. Because the corrections are smaller for the other samples, the corrections have not been applied in the discussion of the results.

Table 9.1 summarizes the data obtained. In addition, the Cl-concentrations have been given as an indication of the relative salinities. The data have been plotted on fig. 9.3 and 9.4 (Konya samples and Amboseli samples respectively). The localities of sampling can be seen on fig. 3.2 and fig. 4.2. Tables 3.1 and 4.1 show the chemical analyses of the water samples. The data on precipitation in the Konya Basin, as well as two samples from the Çarşamba river as reported by Şentürk et al (1970) have been included in fig. 9.3.

Table 9.1 $\delta^{18}O$ and δD values of water samples from the Konya Basin in Turkey and from the Amboseli Basin in Kenya

locality	$\delta^{18}O$ °/oo (SMOW)	δD °/oo (SMOW)	log Cl (mol/m^3)
Konya			
1	+ 4.7	+12	1.1
2	- 5.8	-37	0.3
5a	-11.0	-65	0.6
5b	-11.1	-65	0.6
6	- 4.2	-24	0.5
8	+ 2.3	- 3	2.9
9	- 1.7	-35	3.2
12	-11.4	-71	-1.1
13	-10.5	-70	2.3
14	- 9.9	-67	2.1
16	+10.0	- 9	2.7
17	- 9.6	-64	1.5
22	- 9.8	-64	1.4
26	- 9.3	-65	1.5
27	- 7.8	-45	-0.1
28	- 9.6	-62	0.8
29	-10.3	-66	0.9
31	-11.6	-80	1.4
32	-11.0	-74	0.9
33	- 2.3	-35	3.2
37	- 6.5	-44	3.0
Amboseli			
3	- 0.4	- 9	0.6
4	- 4.8	-24	0.5
5	+14.1	+63	1.8
6	- 5.3	-25	-0.2
8	- 4.0	-17	1.1
11	- 5.0	-18	-0.6
13	- 1.9	- 8	0.2
14	- 4.8	-23	-0.5

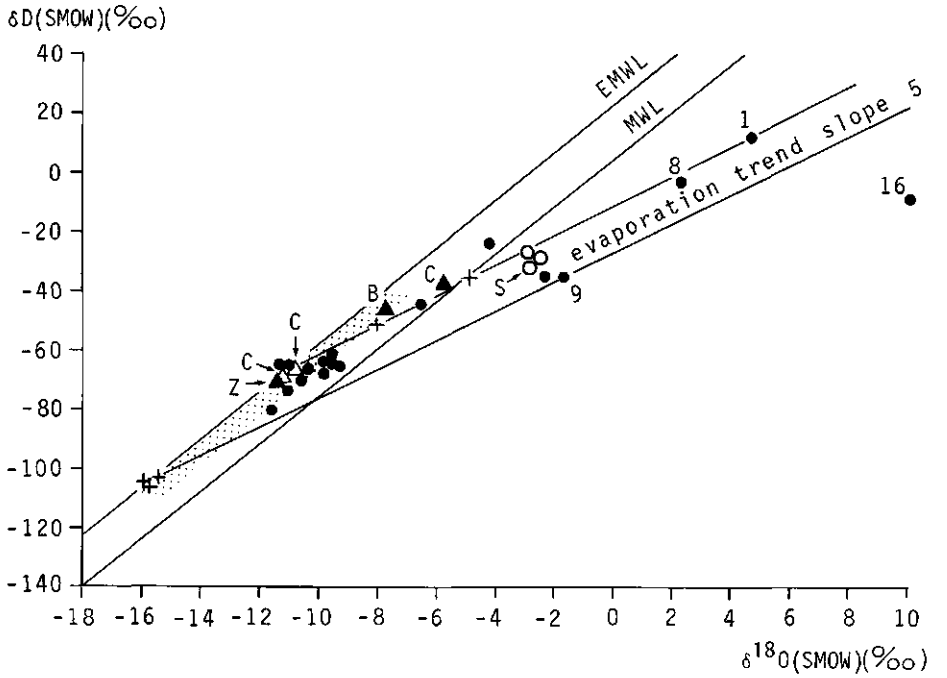

Fig. 9.3 Isotopic composition of waters from the Konya Basin. Symbols: +, precipitation waters from Şenturk et al. (1970). ▲ and Δ; Riverwaters from this study and Şenturk et al. respectively. C: Çarsamba river; Z: Zanopa river; B: Bor river. ● and O other waters from this study and Şenturk et al. respectively. S: Sugla Lake. Figures are described in the text.

9.5 DISCUSSION

Konya

As can be seen from fig. 9.3, most precipitation samples as well as the river samples in the Konya Basin plot well above the MWL ($\delta D = 8\ \delta^{18}O + 5$), and are close to the East Mediterranean Water Line ($\delta D = 8\ \delta^{18}O + 22$). The spread of the individual values is considerable. Therefore, no single combination of δD and $\delta^{18}O$ for a particular water can be considered as the starting composition for groundwaters in the Konya Basin. A range of possible precipitations is indicated in fig. 9.3. Although the Çarşamba river is the most important single source of water for the Basin, other small rivers like the Zanopa and the Bor rivers contribute also to its water budget, as does local rainfall in the basin. Crater Lake (no. 8), within the mouth of an extinct volcano, derives all of its water from local rainfall.

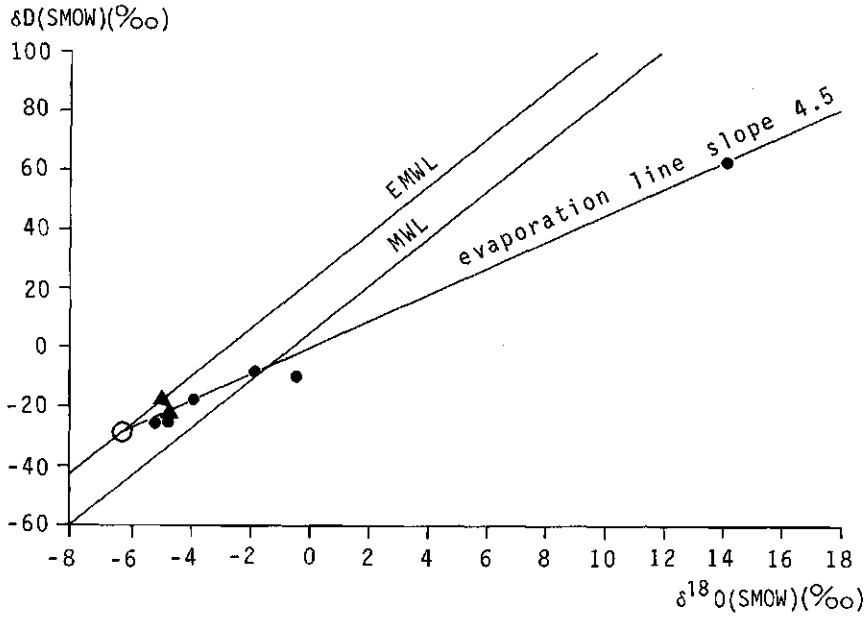

Fig. 9.4 Isotopic composition of waters from the Amboseli Basin in Kenya. Symbols: ▲, riverwaters; ● other waters; ○ inferred composition of local precipitation.

From the spread of the possible precipitations it seems evident that a considerable scatter of the isotopic composition of the evaporated waters is to be expected. Therefore, we have to limit the discussion to some general remarks, which can be made on this basis.

Gat (1979) discusses different hydrologic models in which evaporation takes place. In his terminology most of the hydrologic situations in the Konya Basin which gave rise to salt formation can be considered as "terminal groundwater lakes" (type A_1) (see fig. 9.5), or "groundwater lakes with low waterstand" (type B_2). Crater Lake (no. 8) comes closes to type C, a "perched lake" without connection with the regional groundwater system. The Kaşinhani sample (no. 1) is a "terminal surface flow lake", type A_2. Lakes such as type A_2 or type C, characterized by high evaporation, show highly enriched isotopic compositions, a fact born out by the data obtained in this study. The Kaşinhani sample shows in fact the largest enrichment in heavy isotopes of any of the normal ground- and surface waters listed in table 9.1.

The lake samples Kaşinhani (no. 1), Crater Lake (no. 8) and Playa (no. 9) show a large shift in isotopic composition following an evaporation trend with slope 5 (see fig. 9.3). In the groundwaters belonging to type B_2-waters (groundwater

lakes with low water stand), the evolution of the waters through capillary evaporation results in an increasing salinity, without large changes in the δ-values. Fig. 9.3 shows indeed that the isotopic compositions of most waters, even of those that show a considerable salinity (see table 9.1), have not shifted far from the isotopic composition of the precipitations.

A single sample is unique, as it cannot conceivably be derived exclusively by evaporation processes from any of the available sources. This is the sample of the springs at Akhüyük (no. 16) which has an extremely high $\delta^{18}O$-value of + 10 °/oo. Most probably this water originated by evaporation from local rainwaters, bringing it first to a hypothetical composition of roughly δD = -10 °/oo, $\delta^{18}O$ = + 2 °/oo, thereby greatly increasing its salinity. After this evaporation step, the water infiltrated into the substratum to considerable depth and underwent rock-water interaction at elevated temperatures, thereby shifting the oxygen isotope composition from the hypothetical value of +2 to its present level of $\delta^{18}O$ = + 10 °/oo, after which the waters found their way upwards along a fault zone on which the hot springs are situated. The geological setting of the springs at Akhüyük makes this hypothesis acceptable.

Amboseli Basin (Kenya)

The Amboseli basin in Kenya most closely corresponds to the terminal surface flow lakes (type A_1) in Gat's classification. The groundwaters in such a situation show moderate enrichment in the heavy isotopes (see fig. 9.4), whereas the surface samples can be highly enriched. This is exactly as has been found, the most enriched sample at δD = + 63°/oo, and $\delta^{18}O$ = + 14.1 °/oo being the surface sample of the lake in an advanced stage of evaporation, whereas the other samples represent the local groundwaters.

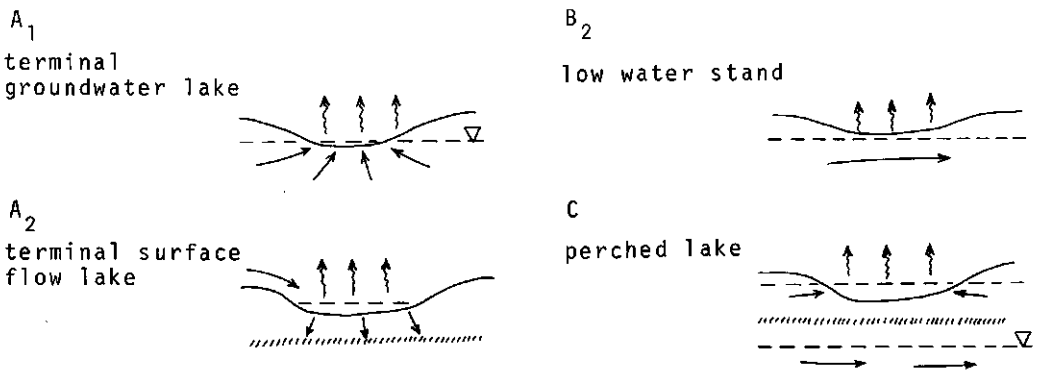

Fig. 9.5 Different hydrological models which give rise to salt formation. Type numbers and figures from Gat (1979).

The most consistent explanation of the isotope data of the Amboseli basin seems to be that the local precipitation is not lying on the MWL, but is in fact lying on a line similar to the East Mediterranean Water Line; this could well be the case as the Amboseli basin is, like the Eastern Mediterranean, characterized by a semi-arid climate. The estimated composition of the local precipitation has been indicated in fig. 9.4.

The use of the isotopic composition of waters in order to obtain quantitative information on the source and development of the groundwaters in closed basins would require a more detailed sampling program, preferably with sampling carried out over a period of time. In addition humidity measurements should be made, both in and above the soil profile.

10. SUMMARY

This study deals with the relation between the mineralogical composition of salt assemblages and the composition of groundwaters from which these salts precipitated. A comparison was made between salts and waters sampled in the Konya Basin in Turkey and waters sampled in three different regions in Kenya.

The chemical composition of waters from rivers entering the Konya Basin is different from the composition of those from rivers in Kenya. The initial composition of these rivers determines the type of minerals that will precipitate during evaporation of these river waters. The ratio of calcium to carbonate at the moment the solution becomes saturated with respect to calcite, usually the first mineral to precipitate, determines whether the final solution will become carbonate-rich or carbonate-poor. The ratio of magnesium to silica and the ratio of calcium to sulphate at the moment the solution becomes saturated with respect to sepiolite and gypsum respectively, determine the magnesium and sulphate content of the final solution. In this way six different types of concentrated brines originate and six different types of salt assemblages precipitate from these brines during evaporation.

The concentrated waters and the salt assemblages in the Konya Basin belong mainly to the Na-Mg-SO_4-Cl-type. The evolution of the groundwater composition and the type of minerals which precipitated from these groundwaters can be explained by assuming successive precipitation of calcite, sepiolite and gypsum.

The concentrated waters and the salt assemblages from Kenya belong mainly to the Na-CO_3-SO_4-Cl-type. The behaviour of the dissolved species and the type of salt minerals can be explained by assuming calcite and sepiolite precipitation only.

The crystallographic properties of some salt minerals were determined by means of X-ray diffraction analysis and the morphological properties by Scanning Electron Microscopy. The presence of halite causes a salt crust to become dense and sealing. The porosity of a salt crust increases when bloedite or trona is present.

Prediction of the sequence of salt minerals which will precipitate from a concentrated solution requires an accurate knowledge of the thermodynamic properties of concentrated electrolyte solutions. Unfortunately, these properties are still unknown for carbonate-rich solutions. Only recently a theory was developed

for carbonate-poor solutions.

The watersamples were evaporated in the laboratory in evaporating dishes under ambient conditions. The mineralogical composition of the precipitates was compared with the assemblages that occur in the field.

The carbonate-containing salt assemblages both from the field and from the laboratory experiments were investigated by means of log p_{CO_2} - log a_{H_2O} - diagrams. It appeared that neither the field nor the laboratory salt assemblages were in equilibrium with the CO_2-pressures of the solutions from which they precipitated. These CO_2-pressures were calculated from the analytical data.

The carbonate-free salt assemblages from the Konya Basin were investigated by means of Jänecke-diagrams. For a few selected samples the theoretical mineral sequences were calculated under the assumption of equilibrium precipitation with the help of the computerprogram of Harvie & Weare (1980). It appeared that prediction of mineral assemblages in salt efflorescences is difficult even with a sound thermodynamic theory. Salt assemblages in natural salt efflorescences could best be predicted assuming precipitation under equilibrium conditions, whereas mineral assemblages in evaporating dishes in the laboratory could best be predicted assuming both metastable mineral formation and fractional crystallization. This conclusion is supported by the presence of the two new minerals, konyaite and eugsterite, which have been discovered in this study. Both are metastable minerals under ambient conditions.

The oxygen and hydrogen isotopic composition of some waters from the Konya Basin in Turkey and of the watersamples from the Amboseli Basin in Kenya were determined. The isotope fractionation caused by evaporation is different in groundwater and surface water. Processes of evaporation and water-rock interaction could be distinguished.

11. SAMENVATTING

Zoute gronden zijn niet geschikt voor landbouw. Daarom is het van het grootste belang te voorkomen dat geschikte landbouwgronden verzouten. Bovendien moet veel aandacht geschonken worden aan de verbetering van reeds verzoute gronden.

Zoute gronden komen voor in semi-aride en aride gebieden. Door de hoge verdamping in zulke gebieden nemen de concentraties van de opgeloste stoffen in het oppervlaktewater en in het grondwater toe. Wanneer deze stoffen niet voldoende afgevoerd worden, zullen ze als zouten in of op de bodem neerslaan. Natuurlijk gevormde zoute gronden ontstaan veelal door verdamping van grondwater in hydrografisch afgesloten bekkens. Ook door menselijke invloed kunnen gronden verzouten wanneer in aride gebieden irrigatie wordt toegepast zonder zorg te dragen voor voldoende drainage.

Bodemkundigen die zich met zoute gronden bezighouden, zijn over het algemeen niet geïnteresseerd in de mineralogische samenstelling van de zouten. Gewoonlijk lossen zij de zouten op en bepalen de concentraties van de verschillende ionen in oplossing. Vanuit landbouwkundig oogpunt is dit begrijpelijk omdat planten lijden van te hoge concentraties zouten in opgeloste vorm. In dit proefschrift is een verband gelegd tussen de mineralogische samenstelling van de zouten en de chemische samenstelling van het grond- en oppervlaktewater waaruit ze neerslaan.

Monsters uit drie verschillende streken in Kenya en uit het Konya bekken in Turkije werden met elkaar vergeleken. De twee verschillende gebieden werden om de volgende redenen uitgezocht:

1. De zouten uit Kenya zijn van een geheel ander type dan die uit Konya.
2. Beide gebieden waren reeds eerder bestudeerd door Nederlandse bodemkundigen van de Landbouwhogeschool in Wageningen en van de Kenya Soil Survey in Nairobi. Hierdoor was voldoende bodemkundige kennis aanwezig en bestond de mogelijkheid voor deskundige begeleiding.

Naast monsters van de zoutuitbloeiingen werden ook monsters van het grond- en oppervlaktewater genomen.

De samenstelling van de rivierwaters die het Konya bekken binnenstromen verschilt van de Kenyaanse rivierwater samenstelling. De verhouding van de opgeloste stoffen in het rivierwater bepaalt uiteindelijk het type mineralen dat bij verdamping zal neerslaan.

Calciet is gewoonlijk het eerste mineraal dat tijdens verdamping neerslaat. De verhouding tussen calcium en carbonaat in de verdunde oplossing bepaalt of de geconcentreerde oplossing carbonaat-arm of -rijk zal worden. Wanneer de oplossing verzadigd raakt aan sepioliet is de magnesium-silica verhouding bepalend of de uiteindelijke oplossing magnesium-rijk of -arm zal zijn; de calcium-sulfaat verhouding op het moment dat de oplossing verzadigd raakt aan gips bepaalt het sulfaat-gehalte van de geconcentreerde oplossing. Zo ontstaan zes verschillende hoofdtypes geconcentreerde oplossingen waaruit zes verschillende types zouten neerslaan. Deze types bevatten alle chloride.

In het Konya-bekken behoren de geconcentreerde waters en de zoutmineralen grotendeels tot het Na-Mg-SO_4-Cl-type. De ontwikkeling van de grondwatersamenstelling en het bijbehorende type mineralen kan verklaard worden wanneer uitgegaan wordt van de opeenvolgende precipitatie van calciet, sepioliet en gips. De geconcentreerde waters en de zoutmineralen uit Kenya behoren hoofdzakelijk tot het Na-CO_3-SO_4-Cl-type. Het gedrag van de ionen in oplossing en het voorkomen van dit type zoutmineralen kunnen verklaard worden door de opeenvolgende precipitatie van calciet en sepioliet.

De kristallografische en morfologische eigenschappen van een aantal zoutmineralen werden met behulp van röntgendiffractie analyse en elektronenmicroscopie bepaald. Wanneer haliet in voldoende mate aanwezig is in een zoutassociatie, vormt deze een dichte, afsluitende korst. Bloediet en trona vergroten de porositeit van een zoutkorst.

Wanneer we willen voorspellen welke zoutmineralen uit geconcentreerde oplossingen zullen neerslaan, moeten we de thermodynamische eigenschappen van electrolytoplossingen kennen. Tot op heden zijn deze eigenschappen voor carbonaatrijke oplossingen niet bekend. Zeer recent is een theorie voor carbonaat-arme oplossingen ontwikkeld.

Alle watermonsters werden in indampschalen onder laboratoriumomstandigheden verdampt. De mineralogische samenstelling van het neerslag is vergeleken met de mineraalgezelschappen die in het veld onder natuurlijke omstandigheden zijn neergeslagen.

Zowel de natuurlijke carbonaathoudende mineraalgezelschappen als de gezelschappen die zich in het laboratorium gevormd hebben, werden onderzocht met behulp van log p_{CO_2} - log a_{H_2O}-diagrammen. Het bleek dat deze beide groepen mineraalgezelschappen niet in evenwicht waren met de CO_2-druk van de oplossingen waar ze uit neersloegen. Deze CO_2-druk werd berekend uit de analytische gegevens.

De carbonaatvrije mineraalgezelschappen uit het Konya-bekken werden onder-

zocht met behulp van Jänecke diagrammen. Van een aantal monsters is met behulp van het computerprogramma van Harvie & Weare (1980) berekend in welke volgorde de zouten onder evenwichtsomstandigheden zouden neerslaan. Het bleek, dat zelfs met een gedegen thermodynamische theorie het moeilijk is een goede voorspelling te doen omtrent de zouten die gevormd zullen worden. De gezelschappen die onder natuurlijke omstandigheden door evapotranspiratie van grondwater ontstaan zijn, blijken beter verklaard te kunnen worden wanneer precipitatie onder evenwichtsomstandigheden wordt aangenomen. De gezelschappen die in de verdampingsexperimenten onder laboratoriumomstandigheden ontstaan zijn, kunnen beter verklaard worden onder de aanname dat metastabiele vorming van mineralen en fractionele kristallisatie plaats heeft gevonden. Deze conclusie is mede gebaseerd op het voorkomen van de mineralen eugsteriet en konyaiet. Dit zijn twee nieuwe mineralen die tijdens deze studie ontdekt zijn. Beide mineralen zijn metastabiel bij 1 atmosfeer druk en kamertemperatuur.

De zuurstof- en waterstofisotoop-samenstelling van een aantal watermonsters uit het Konya-bekken en van de watermonsters uit het Amboseli-bekken in Kenya werden bepaald. De isotoop-fractionering in grondwater en in oppervlaktewater onder invloed van verdamping is verschillend. Er kon een onderscheid gemaakt worden tussen water dat verdamping had ondergaan en water waarbij intensieve interactie met gesteenten had plaatsgevonden.

12. REFERENCES

Al-Droubi, A., 1976. Géochimie des sels et des solutions concentrées par évaporation. Modèle thermodynamique de simulation. Application aux sols salés du Tchad. Thèse, Université Louis-Pasteur, Strasbourg, France, 177 p.

Aubert, G., 1967. Classification des Sols. Edition 1967. Trav. CPSS, Grignon.

Beek, C.G.E.M. van, Breemen, N. van, 1973. The alkalinity of alkali soils. J. Soil Sci., 24, p. 129-136.

Begheyn, L.Th., 1980. Methods of chemical analyses for soils and waters. Agricultural University, Wageningen, the Netherlands.

Braitsch, O., 1971. Salt deposits, their origin and composition. Springer-Verlag, New York, 297 p.

Brinkman, R., 1979. Ferrolysis, a soil-forming process in hydromorphic conditions. Pudoc, Wageningen, the Netherlands.

Brinkmann, R., 1976. Geology of Turkey. Elsevier, Amsterdam, Oxford, New York, 158 p.

Conley, R., and Bundy, W.M., 1959. Mechanism of gypsification. Geochim. Cosmochim. Acta, 15, p. 57-72.

Craig, H., 1961. Isotopic variations in meteoric waters. Science, 133, p. 1702-1703.

Dana, J.D., 1951. System of Mineralogy, vol. II. John Wiley & Sons, New York.

Drever, J.I. and Smith, C.L., 1978. Cyclic wetting and drying of the soil zone as an influence on the chemistry of ground water in arid terrains. Am. Jour. Sci., 278, p. 1448-1454.

Driessen, P.M., 1970. Soil salinity and alkalinity in the Great Konya Basin, Turkey. Pudoc, Wageningen, the Netherlands, 99 p.

Driessen, P.M.,and Schoorl, R., 1973. Mineralogy and morphology of salt efflorescences on saline soils in the Great Konya Basin, Turkey. J. Soil Sci. 24, no. 4, p. 436-442.

Epstein, S., 1970. Antarctic ice sheet: stable isotope analyses of Byrd station cores and interhemispheric climatic implications. Science, 168, p. 1570-1572.

Epstein, S., Sharp, R.P., and Gow, A.J., 1965. Six-year record of oxygen and hydrogen isotope variations in South Pole firn. Journ. Geophys. Research, 70, p. 1809.

Ericksen, G.E., and Mrose, M.E., 1970. Mineralogical studies of the nitrate deposits of Chile. II. Darapskite, $Na_3(NO_3)(SO_4).H_2O$. Am. Min., 55, p. 1500-1517.

Eswaran, H., and Carrera, M., 1980. Mineralogical zonation in salt crust. International Symposium on salt-affected soils, Karnal. p. 237-293.

Eugster, H.P., 1970. Chemistry and origin of the brines of Lake Magadi, Kenya. Mineral. Soc. Amer. Spec. Paper 3, p. 215-235.

Eugster, H.P., and Hardie, L.A., 1978. Saline Lakes. In: Lerman, A., ed., Lakes: Chemistry, Geology and Physics. New York, Springer-Verlag, p. 237-293.

Eugster, H.P., Harvie, C.E., and Weare, J.H., 1980. Mineral equilibria in a six-component seawater system, $Na-K-Mg-Ca-SO_4-Cl-H_2O$, at 25° C. Geochim. Cosmochim. Acta, 44, p. 1335-1347.

Eugster, H.P., and Jones, B.F., 1977. The behaviour of potassium and silica during closed basin evaporation. 2nd IAGC Symposium Water-Rock Interaction, Strasbourg, II, p. 1-12.

Eugster, H.P., and Jones, B.F., 1979. Behaviour of major solutes during closed basin brine evolution. Am. J. Sci., 279, p. 609-631.

Eugster, H.P., Smith, G.I., 1965. Mineral Equilibria in Searles Lake Evaporites, California. J. Petr., 6, p. 473-522.

Eugster, H.P., and Surdam, R.C., 1973. Depositional Environment of the Green River Formation of Wyoming: A Preliminary Report. Geol. Soc. Amer. Bull., 84, p. 1115-1120.

Fang, J.H., and Robinson, P.D., 1970. Crystal Structures and mineral chemistry of double-salt hydrates: II the crystal structure of loeweite. Am. Min., 55, p. 378-386.

FAO/Unesco, 1973. Irrigation, drainage and salinity: an international source book. Unesco, Paris. 510 p.

FAO/Unesco, 1971-1978. Soil Map of the World, 1 : 5.000.000. Unesco, Paris. In two of the four following languages: English, French, Russian and Spanish. Vol. I-10.

Fauck, R., Lamouroux, M., Perraud, A., Quantin, P., Roederer, P., Vieillefon, J., and Ségalen, P., 1979. Projet de classification des sols. O.R.S.T.O.M., Paris.

Fontes, J.C., and Gonfiantini, R., 1967. Comportement isotopique au cours de l'évaporation d'eaux bassin Sahariens. Earth Plan. Sci. lett., 3, p. 258-266.

Gac, J.Y., Al-Droubi, A., Fritz, B., and Tardy, Y., 1977. Geochemical behavior of silica and magnesium during the evaporation of water in Chad. Chem. Geol., 19, p. 215-228.

Garrels, R.M., and Christ, C.L., 1965. Solutions, Minerals and Equilibria. Harper and Row, New York, 450 p.

Garrels, R.M., and Mackenzie, F.T., 1967. Origin of the chemical composition of some springs and lakes. In: Equilibrium concepts in natural water systems. American Chemical Society, Washington, D.C., p. 222-242.

Gat, J.R., 1966. The isotopic composition of atmospheric water in the Mediterranean Sea area and their interpretation in terms of air-sea interactions, presented at the 20th Congress of the Comité International de l'Exploration Scientifique de la Mer Méditerranée, Bucharest.

Hardie, L.A., 1965. Phase equilibria involving minerals of the system $CaSO_4$-Na_2SO_4-H_2O. Ph.D. Thesis, The Johns Hopkins University, Baltimore.

Hardie, L.A., 1967. The gypsum-anhydrite equilibrium at 1 atm. pressure. Am. Min., 52, p. 121-200.

Hardie, L.A., 1968. The origin of the recent non-marine evaporite deposit of Saline Valley, Inyo County, California. Geochim. Cosmochim. Acta, 32, p. 1279-1301.

Hardie, L.A., and Eugster, H.P., 1970. The evolution of closed-basin brines. Mineral. Soc. Am. Spec. Paper 3, p. 273-290.

Harned, H.S., 1935. Some thermodynamic properties of univalent halide mixtures in aqueous solution. J. Amer. Chem. Soc., 57, p. 1865.

Harvie, C.E., and Weare, J.M., 1980. The prediction of mineral solubilities in natural waters: the Na-K-Mg-Ca-Cl-SO_4-H_2O system from zero to high concentration at 25° C. Geochim. Cosmochim. Acta, 44, p. 981-997.

Harvie, C.E., Weare, J.H., Hardie, L.A., and Eugster, H.P., 1980. Evaporation of seawater: calculated mineral sequences. Science, 208, p. 498-500.

Hatch, J.R., 1972. Phase relationships in part of the system sodium carbonate-calcium carbonate-CO_2-H_2O at 1 atm. pressure. Ph.D., Univ. of Illinois, Urbana-Champaign.

Helgeson, H.C., 1969. Thermodynamics of hydrothermal systems at elevated temperatures and pressures. Am. J. Sci., 267, p. 729-804.

Hill, A.E., and Wills, J.H., 1938. Ternary systems XXIV. Calcium sulfate, sodium sulfate and water. J. Am. Chem. Soc., 60, p. 1647-1655.

Jacks, G., 1973. Chemistry of groundwater in a district in Southern India. J. Hydrol., 18, p. 185-200.

Jones, B.F., Eugster, H.P., and Rettig, S.L., 1977. Hydrochemistry of the Lake Magadi basin, Kenya. Geochim. Cosmochim. Acta, 41, p. 53-72.

Jung, D., and Keller, J., 1972. Die jungen Vulkanite im Raum zwischen Konya und Kayseri (Zentral-Anatolien). Z. Deutsch. Geol. Ges., 123, p. 503-512.

Korzhinskii, D.S., 1959. Physicochemical basis of the analysis of the paragenesis of minerals. Consultants Bureau, Inc., New York, 142 p.

Linke, W.F., 1965. Solubilities of organic and metal organic compounds. Amer. Chem. Soc., Van Nostrand.

Maglione, G., 1968. Présence de gaylussite et de trona dans les "natronières" du Kanem (pourtour nord-est du Lac Tchad). Bull. Soc. Fr. Minéral. Crystallogr., 91, p. 388-395.

Meester, T. de (ed.), 1970. Soil map of the Great Konya Basin. Agricultural University, Wageningen, the Netherlands.

Meester, T. de (ed.), 1970. Soils of the Great Konya Basin, Turkey. Pudoc, Wageningen, the Netherlands, 290 p.

Meester, T. de, 1971. Highly calcareous lacustrine soils in the Great Konya Basin, Turkey. Pudoc, Wageningen, the Netherlands, 169 p.

Mellaart, J., 1964. Early cultures of the South Anatolian Plateau. Anatolian Stud. XIII.

Nesbitt, W.H., 1974. The study of some mineral-aqueous solution interactions: Ph. D. thesis, Johns Hopkins Univ., Baltimore, 173 p.

Pitzer, K.S., 1973. Thermodynamics of electrolytes. I. Theoretical basis and general equations. J. Phys. Chem., 77, p. 268-277.

Pitzer, K.S., 1975. Thermodynamics of electrolytes. V. Effects of higher-order electrostatic terms. J. Solution Chem., 4, p. 249-265.

Pitzer, K.S., and Kim, J.J., 1974. Thermodynamics of electrolytes. IV. Activity and osmotic coefficients for mixed electrolytes. Am. Chem. Soc., 96, p. 5701-5707.

Pitzer, K.S., and Mayorga, G., 1973. Thermodynamics of electrolytes. II. Activity and osmotic coefficients for strong electrolytes with one or both ions univalent. J. Phys. Chem., 77, p. 2300-2308.

Pitzer, K.S., and Mayorga, G., 1974. Thermodynamics of electrolytes. III. Activity and osmotic coefficients for 2-2 electrolytes. J. Solution Chem., 3, p. 539-546.

Richards, L.A., 1954. Diagnosis and improvement of saline and alkali soils. Agriculture handbook no. 60. U.S. Department of Agriculture, 160 p.

Robie, R.A., Hemingway, B.S., and Fisher, J.R., 1978. Thermodynamic properties of minerals and related substances at 298.15 K and 1 bar pressure and at higher temperatures. U.S. Geol. Surv. Bull. 1452, 456 p.

Robinson, R.A., and Stokes, R.H., 1970. Electrolyte solutions. Butterworths, 570 p.

Saggerson, E.P., 1952. Geology of the Kisumu District. Report no. 21. Geological

Survey of Kenya, Nairobi.

Scatchard, G., 1936. Concentrated solutions of strong electrolytes. Chem. Rev., 19, p. 309-327.

Scatchard, G., 1968. The excess free energy and related properties of solutions containing electrolytes. J. Am. Chem. Soc., 90, p. 3124-3127.

Sentürk, F., Bursali, S., Omay, Y., Ertan, I., Güler, S., Yalçin, H., and Onhan, E., 1970. Isotope techniques applied to groundwater movement in the Konya plain. From: Isotope Hydrology 1970. Proceedings of an IAEA syposium, 9-13 march 1970. International Atomic Energy Agency, Vienna, 1970.

Slyusareva, M.N., 1969. Zapiski Vses. Mineralog. Obshch., 98, p. 59-62. (in Russian).

Sofer, Z., and Gat, J.R., 1975. The isotopic composition of evaporating brines; effect of the isotopic activity ratio in saline solutions. Earth Planet. Sci. Lett., 26, p. 179-186.

Soil Survey Staff, 1975. Soil taxonomy: a basic system of soil classification for making and interpretating soil surveys. Soil Conservation Service, U.S. Dept. of Agric., Washington, D.C., Agriculture Handbook No. 436.

Sombroek, W.G., 1980. Legend of the exploratory soil map of Kenya, scale 1 : 1 000 000. Internal communication no.22, Kenya Soil Survey, Nairobi.

Stoessell, R.K., and Hay, R.L., 1978. The geochemical origin of sepiolite and kerolite at Amboseli, Kenya. Contr. Miner. Petr., 65, p. 255-267.

Stoops, G., Eswaran, H., and Abtahi, A.,1978. Scanning electron microscopy of authigenic sulphate minerals in soils. In: M. Delgado (ed.), Proceedings fifth international work meeting on soil micromorphology, Granada, Spain, p. 1093-1113.

Stumm, W., and Morgan, J.J., 1970. Aquatic chemistry. An introduction emphasizing chemical equilibria in natural waters. Wiley. Interscience Ed., New York, 583 p.

Surdam, R.C., and Sheppard, R.A., 1978. Zeolites in saline alkaline lake deposits In: Sand, L.B., and Mumpton, F.A., eds. Natural zeolites: Occurrence, properties, use. Elmsford, New York, Pergamon Press, p. 145-174.

Touber, L. Reconnaissance soil and vegetation survey of the Amboseli-Kibwezi area. In preparation.

United States Department of Agriculture, 1938. Soils and Men, Yearbook of Agriculture, 1938.

Van 't Hoff, J.H., 1905. Zur Bildung ozeanischer Salzablagerungen. Erstes Heft. Vieweg. 85 p.

Van 't Hoff, J.H., 1909. Zur Bildung ozeanischer Salzablagerungen. Zweites Heft

Vieweg, 90 p.

Van 't Hoff, J.H., 1912. Untersuchungen über die Bildungsverhältnisse der ozeanischen Salzablagerungen. Precht and Cohen, eds. Akad. verlags ges., Leipzig, 374 p.

Vergouwen, L., 1979. Two new occurrences and the Gibbs energy of burkeite. Min. Mag., 43, p. 341-345.

Vergouwen, L., 1981. Mineralogical composition and origin of salt efflorescences in the Konya basin, Turkey and in Kenya. N. Jb. Miner. Mh., p. 23-34.

Vergouwen, L., 1981. Scanning electron microscopy applied to saline soils from the Konya Basin in Turkey and from Kenya. In: E.B.A.Bisdom (ed.): Submicroscopy of soils and weathered rocks. Ist workshop of the International Working-Group on Submicroscopy of Undisturbed Soil Materials (IWGSUSM), Wageningen, 1980. Pudoc, Wageningen, the Netherlands, in press.

Vergouwen, L., 1981. Eugsterite, a new salt mineral. Am. Min. , in press.

Visser, J.W., 1969. A fully automatic program for finding the unit cell from powder data. J. Appl. Cryst., 2, p.89.

Williams, L.A.J., 1970. The volcanics of the Gregory Rift Valley, East Africa. Bull. Volcanol., 34, p. 439-465.

Williams, L.A.J., 1972. Geology of the Amboseli Area. Geological Survey of Kenya, Report no. 90, Nairobi, 86 p.

Wood, J.R., 1972. Prediction of mineral solubilities in concentrated brines. A thermodynamic approach. Ph. D. Thesis, Baltimore, Maryland, 121 p.

Wood, J.R., 1975. Thermodynamics of brine-salt equilibria. I- The systems NaCl-KCl-$MgCl_2$-$CaCl_2$-H_2O and NaCl-$MgSO_4$-H_2O at 25°C. Geochim. Cosmochim. Acta, 39, p. 1147-1163.

CURRICULUM VITAE

Na het behalen van het eindexamen gymnasium bèta aan het Stedelijk Gymnasium te Utrecht, begon de schrijfster in 1969 haar studie geologie aan de Rijks Universiteit te Utrecht. In mei 1972 deed zij haar kandidaatsexamen met hoofdvakken geologie en scheikunde en bijvakken wiskunde en natuurkunde. In december 1976 werd het doctoraalexamen geologie afgelegd met als hoofdvak geochemie en de bijvakken algemene en economische geologie en chemische thermodynamica. In januari 1977 trad zij in dienst als promotie-assistente bij de afdeling Bodemkunde en Geologie van de Landbouwhogeschool in Wageningen. Gedurende het promotie-onderzoek werden reizen gemaakt naar Kenya en Turkije waar zoutmineralen verzameld werden.